



182(3), 2020



COMBUSTION ENGINES



INSTYTUT TECHNICZNY WOJSK LOTNICZYCH

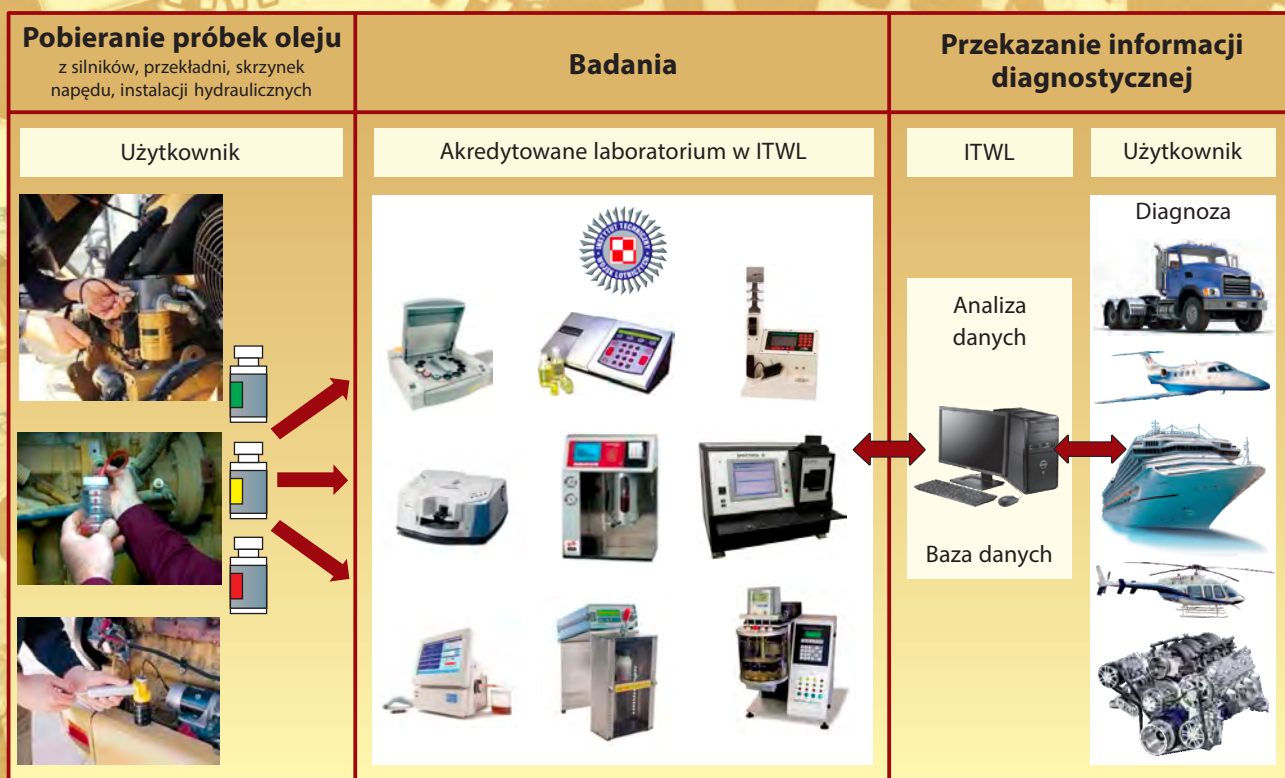
ul. Księcia Bolesława 6, 01-494 Warszawa, skr. poczt. 96

tel.: 261 851 300; faks: 261 851 313

www.itwl.pl

e-mail: poczta@itwl.pl

SYSTEM DIAGNOSTYKI TRIBOLOGICZNEJ



System Diagnostyki Tribologicznej (SDT), opracowany w Instytucie Technicznym Wojsk Lotniczych, przeznaczony jest do wspierania eksploatacji obiektów technicznych.

Na podstawie wyników badań próbek oleju pobranych z układów tribologicznych prowadzi się ocenę i prognozowanie stanu technicznego obiektów technicznych (statki powietrzne, pojazdy mechaniczne, statki wodne, maszyny robocze i inne).



AB 138



9/MON/2017



INSTYTUT TECHNICZNY WOJSK LOTNICZYCH
ZAKŁAD SILNIKÓW LOTNICZYCH
Akredytowane laboratorium:
Laboratorium Diagnostyki Systemów Tribologicznych

PTNSS Supporting Members Członkowie wspierający PTNSS

BOSMAL Automotive Research and Development Institute Ltd

Instytut Badań i Rozwoju
Motoryzacji BOSMAL Sp. z o.o

Motor Transport Institute

Instytut Transportu Samochodowego

Institute of Aviation

Sieć Badawcza Łukasiewicz
– Instytut Lotnictwa

Automotive Industry Institute

Sieć Badawcza Łukasiewicz
– Przemysłowy Instytut Motoryzacji

The Rail Vehicles Institute TABOR

Sieć Badawcza Łukasiewicz
– Instytut Pojazdów Szynowych TABOR

Institute of Mechanised Construction and Rock Mining

Instytut Mechanizacji Budownictwa
i Górnictwa Skalnego

Industrial Institute of Agricultural Engineering

Sieć Badawcza Łukasiewicz
– Przemysłowy Instytut Maszyn Rolniczych

AVL List GmbH

Solaris Bus & Coach S.A.

Air Force Institute of Technology

Instytut Techniczny Wojsk Lotniczych

Toyota Motor Poland Ltd. Sp. z o.o.

Military Institute of Armoured & Automotive Technology

Wojskowy Instytut Techniki Pancernej
i Samochodowej



COMBUSTION ENGINES

A Scientific Magazine

2020, 182(3)

Year LIX

PL ISSN 2300-9896

PL eISSN 2658-1442

Editor:

Polskie Towarzystwo Naukowe Silników Spalinowych

43-300 Bielsko-Biała, Sarni Stok 93 Street, Poland

tel.: +48 33 8130402, fax: +48 33 8125038

E-mail: sekretariat@ptnss.pl

WebSite: <http://www.ptnss.pl>

Papers available on-line: <http://combustion-engines.eu>

Scientific Board:

- Krzysztof Wisłocki – chairman, Poland (*Poznan University of Technology*)
- Yuzo Aoyagi – Japan (*Okayama University*)
- Ewa Bardasz – USA (*National Academy of Engineering*)
- Piotr Bielaczyc – Poland (*BOSMAL Automotive Research and Development Institute Ltd.*)
- Zdzisław Chłopek – Poland (*Warsaw University of Technology*)
- Tadeu Cordeiro de Melo – Brazil (*Petrobras*)
- Jan Czerwinski – Switzerland (*CJ Consulting*)
- Friedrich Dinkelacker – Germany (*Leibniz Universität Hannover*)
- Hubert Friedl – Austria (*AVL*)
- Barouch Giechaskiel – Italy (*European Commission, JRC Italy*)
- Leslie Hill – UK (*Horiba*)
- Timothy Johnson – USA (*Corning Inc.*)
- Kazimierz Lejda – Poland (*Rzeszow University of Technology*)
- Hans Peter Lenz – Austria (*TU Wien*)
- Helmut List – Austria (*AVL*)
- Toni Kinnunen – Finland (*Proventia*)
- David Kittelson – USA (*University of Minnesota*)
- Christopher Kolodziej – USA (*Delphi Automotive Systems*)
- Hu Li – UK (*University of Leeds*)
- Federico Millo – Italy (*Politecnico Torino*)
- Jeffrey D. Naber – USA (*Michigan Technological University*)
- Andrzej Niewczas – Poland (*Motor Transport Institute*)
- Marek Orkisz – Poland (*Rzeszow University of Technology*)
- Dieter Peitsch – Germany (*TU Berlin*)
- Stefan Pischinger – Germany (*FEV Germany*)
- Andrzej Sobiesiak – Canada (*University of Windsor*)
- Stanisław Szwaja – Poland (*Częstochowa University of Technology*)
- Piotr Szymański – Netherlands (*European Commission, JRC*)
- Leonid Tartakovsky – Israel (*Technion – Israel Institute of Technology*)
- Andrzej Teodorczyk – Poland (*Warsaw University of Technology*)
- Xin Wang – China (*Beijing Institute of Technology*)
- Thomas Wallner – USA (*Argonne National Laboratory*)
- Michael P. Walsh – USA (*International Council on Clean Transportation*)
- Mirosław Wendeker – Poland (*Lublin University of Technology*)
- Piotr Wolański – Poland (*Warsaw University of Technology*)
- Mirosław Wyszynski – UK (*University of Birmingham*)

Contents

Trzeciak A.M., Gieras M. Temperature estimating method for exhaust gases in valveless pulsejet engine (CE-2020-301)3

Puzdrowska P. Evaluation of the significance of the effect of the active cross-sectional area of the inlet air channel on the specific enthalpy of the exhaust gas of a diesel engine using statistics F of the Fisher-Snedecor distribution (CE-2020-302).....10

Marszałek N. The impact of thermodynamics parameters of turbofan engine with ITB on its performance (CE-2020-303).....16

Polak F. Energy balance comparison of small unmanned vehicle equipped with electric and hybrid propulsion system (CE-2020-304).....23

Kozak M., Siejka P. Soot contamination of engine oil – the case of a small turbocharged spark-ignition engine (CE-2020-305)28

Stepanenko D., Kneba Z. ECU calibration for gaseous dual fuel supply system in compression ignition engines (CE-2020-306)33

Michalak P., Merkisz J., Stawecki W., Andrzejewski M., Daszkiewicz P. The selection of the engine unit – main engine generator during the modernization of the 19D/TEM2 locomotive (CE-2020-307)38

Tomaszewski S., Medwid M., Andrzejewski M., Cierniewski M., Jakuszko W. New rail-road tractor with a combustion engine and an alternative electric drive (CE-2020-308)47

Ziółkowski A., Fuć P., Lijewski P., Rymaniak Ł., Daszkiewicz P., Kamińska M., Szymlet N., Jagielski A. Analysis of exhaust emission measurements in rural conditions from heavy-duty vehicle (CE-2020-309)54

Cieślik W., Szwajca F., Golimowski J. The possibility of energy consumption reduction using the ECO driving mode based on the RDC test (CE-2020-310)59

Declaration of the original version
The original version of the Combustion Engines journal is the printed version.

Editorial:

Institute of Combustion Engines and Powertrains
 Poznan University of Technology
 60-965 Poznan, Piotrowo 3 Street
 tel.: +48 61 2244505, +48 61 2244502
 E-mail: papers@ptnss.pl
 Prof. Jerzy Merkisz, DSc., DEng.
 (Editor-in-chief)
 Miłosław Kozak, DSc., DEng.
 Prof. Jacek Pielecha, DSc., DEng.
 (Editorial Secretary for Science)
 Prof. Ireneusz Pielecha, DSc., DEng.
 Wojciech Cieślik, DEng.
 (Technical Editors)
 Joseph Woodburn, MScI
 (Proofreading Editor)
 Wojciech Serdecki, DSc., DEng.
 (Statistical Editor)
 and Associate Editors

Editor
Polish Scientific Society
of Combustion Engines
 43-300 Bielsko-Biała, Sarni Stok 93 Street, Poland
 tel.: +48 33 8130402, fax: +48 33 8125038
 E-mail: sekretariat@ptnss.pl
 WebSite: <http://www.ptnss.pl>

The Publisher of this magazine does not endorse the products or services advertised herein. The published materials do not necessarily reflect the views and opinions of the Publisher.

© Copyright by
Polish Scientific Society of Combustion Engines
 All rights reserved.
 No part of this publication may be reproduced, stored in a retrieval system or transmitted, photocopied or otherwise without prior consent of the copyright holder.

Subscriptions
 Send subscription requests to the Publisher's address.
 Cost of a single issue PLN 30 + VAT.

Preparation for print
 ARS NOVA Publishing House
 60-782 Poznań, Grunwaldzka 17/10A Street

Circulation: 100 copies
Printing and binding

Zakład Poligraficzny Moś i Łuczak, sp. j.,
 Poznań, Piwna 1 Street

The journal is registered in the Polish technical journals content database – **BAZTECH** www.baztech.icm.edu.pl



The journal is listed in the international database

IC Journal Master List
 – **Index Copernicus** www.indexcopernicus.com



Papers published in the **Combustion Engines**

quarterly receive 20 points as stated by the Notification of the Minister of Science and Higher Education dated 31 July 2019.

Cover

I – Vetus M3.29 20 kW diesel engine
 (fot. www.vetus.info); background (Monaco – www.goodfreephotos.com)
 IV – Porsche 3D-printed pistons for the 911 GT2 RS
 (fot. www.caranddriver.com)

Temperature estimating method for exhaust gases in valveless pulsejet engine

The article describes the problem of measuring the temperature in a pulse combustion chamber. The object of the study is a valveless pulsejet. The problem is analysed on the example of exhaust gases temperature measurement. The measurement in these conditions requires the use of a sensor resistant to large changes in gas velocity and temperature and at the same time with adequately low inertia. This excludes the use of fast and precise yet thin, resistant wire sensors or ultrafast thin film thermocouples. Finally, a temperature measurement system based on sheathed thermocouples was chosen. During each test the thermocouple has its own temperature which is different from the medium temperature. In order to properly determine the measured temperature of flowing media it is necessary to take the sensor time characteristics into account. In this article the iteration method is proposed to solve this problem.

Key words: pulsating combustion, pulsejet, temperature measurement, periodic flow, combustion chamber

1. Introduction

Combustion driven oscillations were first observed in 1777. When small flame was moving inside a vertical tube in a certain location the sound was generated (so called singing tube) [10].

In the vast majority of combustion chambers currently used in the gas turbines in industry or aviation, in which combustion is carried out under constant pressure, oscillations caused by combustion are unfavorable. Numerous experiments have been carried out in order to find the way to prevent this, because it can lead to significant damage to the combustion chamber or the entire device in which the chamber operates.

There is also a group of pulsating combustion chambers in which combustion occurs periodically in isochoric manner. In those devices pressure pulsations are desirable. High pressure fluctuations in this case intensify combustion process and in consequence combustion efficiency is higher than in isobaric devices. The oldest representant of this group is a pulsejet engine.

First pulsejet engine was patented in 1907 by Russian engineer Karavodin [10]. Later, it was widely used by Germans during the Second World War to propel V-1 "buzz bomb". After the war various tests were conducted on pulsejet engines. Unfortunately, the engines' disadvantages such as high noise, vibration, low propulsive efficiency and narrow throttle ability made pulsejet engines useless for manned aircraft. In consequence pulse combustion research fell into decline.

Despite the complex nature of the pulsating combustion process, which is a result of not fully explained chemical and gasdynamic phenomena interaction, it has remained in the sphere of researcher's interest. In fact, it has been noted for some time now that the interest in pulsed combustion chambers has increased. The advantages of pulsating combustion are widely appreciated as the pulsating combustion chambers are implemented in impingement drying, gas boilers or used for propelling the Unmanned Aerial Vehicles (UAV). According to [4] they can be even used to produce fuels from sewage sludge.

Although their construction is simple, pulsating combustion chambers are considered to be extremely demanding as research objects. Tests conducted by authors of this article proved that even a minor change of geometrical configura-

tion can lead to significant changes in engine behaviour. Moreover, the change in combustion chamber dimension during its work due to thermal expansion as well as high vibration have to be taken into account during the tests.

One of the most important measurements in the pulsed combustion research program is the temperature measurement in characteristic sections. Determining the temperature and fuel flow values allows one to estimate combustion efficiency, especially when an exhaust gas analyser is additionally used. To measure the temperature in pulsations conditions of the combustion process with a frequency exceeding 100 Hz in the tested engine and temperature values exceeding 1000 K, it is necessary to create an appropriate and credible measuring system. An additional difficulty is caused by the explosive, unstable combustion process, during which a medium flow with high speed and temperature variations is generated. This requires the use of a sensor that, apart from the adequate mechanical strength, should be characterized by an appropriate response to rapid changes in the measured parameter.

Despite the difficulties with the selection of sensors that meet the required criteria, the temperature tests of exhaust gases temperature (EGT) in the outlet cross-section of the valveless pulsejet engine were carried out. Average as well as instantaneous values were tested.

Research was conducted on specially designed test bench placed in Institute of Heat Engineering of Faculty of Power and Aeronautical Engineering of Warsaw University of Technology. During the work, a measuring station containing all the modules needed for effective temperature measurement was designed and built. The sensor was verified in terms of its ability to record temperature changes during the engine's operating cycle and then the adequate measurements were made. Test results were analyzed using an application built in the LabView environment as well as by using Matlab software and Excel applications.

2. Description of test stand

The view of the test stand is presented in Fig. 1. The main element of the stand is a valveless pulsejet engine, which was placed on a frame made of aluminum profiles, thanks to which any configuration of its setting was possible, allowing optimal spacing of the sensors.



Fig. 1. The view of the test stand

The engine was attached to the stand at one point only. This was the center of the front wall of the combustion chamber and the point from which the thrust was simultaneously received. The other two supporting elements allowed the engine to move along them during its expansion as a result of the high temperature.

The engine test bench, apart from the standard elements allowing startup and running of the engine, was equipped with ultrafast Kistler pressure transducer assigned for combustion chamber actual pressure measurement. To avoid thermal damage to the sensor, it was equipped with a water cooling system and a temperature control system.

The tested pulsejet engine was fueled by propane gas. Fuel flow measurement was provided by rotameter with 4% accuracy. To increase the accuracy of rotameter readings depending on fuel pressure, two fuel pressure gauges were installed in the system – one at the inlet and one at the outlet of the meter. Additionally, to verify fuel flow readings a precise scale was used to weight the gas container before and after the engine run. To control gas fuel flow as precisely as possible propane bottles were equipped with a heating and temperature monitoring system. The thrust measurement was carried out by means of a tensometric beam connected to the measuring card using the necessary transducer.

To avoid thrust readings distortions a special force transformation system was designed to allow movement of sensor together with the engine horizontal axis when it was increasing its volume due to high temperature.

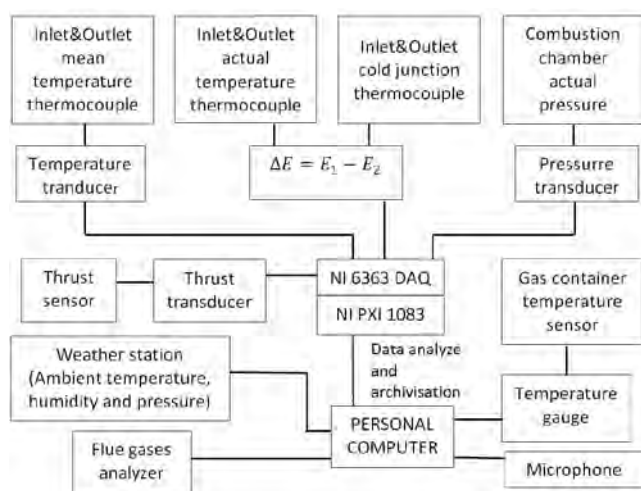


Fig. 2. Measurement system block diagram

To measure mean temperature in the outlet and inlet stations K-type thermocouples were used. A dynamic temperature measurement layout will be described further in this article.

Data acquisition was carried out using a PXI – 1082 computer with a 6363 data acquisition card. The acquisition, archiving and initial analysis of test data took place in the LabView environment. The block diagram of the entire measuring system is shown in Fig. 2.

3. EGT in outlet station measurement

3.1. Selection of measuring method

Temperature measurement in exhaust station of pulsejet engine is one of the pivotal elements of the pulse combustion research program. It not only provides information about combustion quality but it also becomes a significant value when verifying numerical simulations.

Despite the importance of this parameter, authors of this publication found it impossible to come across any work which would refer to the analyzed problem in the field of pulsating combustion research in a satisfactory manner. In works [8, 9], some trials are undertaken but they are only rough measurements of mean EGT without any detailed comments. Authors of [8] also emphasize difficulties during the tests of pulsejet engine.

Some advanced works [5, 6] were conducted by internal combustion engines researchers. In [5] authors pointed out that measurement of crank-angle resolved EGT is a challenging task because modern optical non-intrusive measurement methods requires substantial engine modifications and are consequently in few engine research laboratories. Authors provide precise EGT measurements but also concluded that this is only estimation and further work is needed. Similar work and conclusions were developed in [6]. But in this case there is no crank-angle resolved EGT estimation. It was concluded that further work is necessary to determine the method which ought to allow examination of high frequency cyclic fluctuations.

Other group of researchers was focused on thin film ultrafast thermocouples [1–3]. This kind of sensors seems to be the most promising because the time constant is of the order of ns. Moreover, the sensors are able to withstand temperatures up to 790°C [1]. Unfortunately, their application in harsh environment requires placing them on some surface [3]. This in turn causes increase in the time of reaction because the sensor is measuring the surface temperature, so in consequence the real time constant is dependent of thermal inertia of surface's material.

After taking into account different hardware solutions, a dynamic temperature measurement system based on sheathed thermocouples was chosen. Thermocouples are widely used in all kinds of combustion engines because their small sizes and reasonable time-constant allow for measurement during engine run. Additionally, in the application considered, the sensor could be destroyed easily. With thermocouples, it was possible to keep the cost of frequent sensor replacement at acceptable levels.

The K-type thermocouple used met the criteria for measuring the temperature in the engine outlet station. Its measuring range is from –100°C to 1000°C for long-term

measurements, while with temporary use the measuring range is from -200°C to 1300°C . The thermocouple is suitable for measuring temperature in an inert, reducing, oxidizing and vacuum atmosphere. For accuracy class 1 in the range from -40°C to 375°C , the temperature deviation is equal to 1.5°C , and in the range from 375°C to 1000°C the deviation is 0.4% [14].

The measuring junction of a thermocouple should be grounded to the metal protective sheath. This results in a short time constant. The protective cover is required to provide protection against mechanical damage to the junction.

Proper selection of material of the outer metal cover provides protection against adverse environmental effects. It also affects the time constant. Inconel 600 (75% Ni, 16% Cr, 8% Fe) has been deemed the most suitable. It has the following properties [14]:

- good overall corrosion resistance,
- very good oxidation stability,
- the maximum operating temperature in the air of 1150°C ,
- not recommended for an atmosphere above 750°C containing sodium.

The diameter of the protective cover influences the thermoelement time constant: the larger the protective cover diameter, the longer time constant. The construction of the dynamic temperature measuring thermocouple used in this research had the smallest protective cover diameter available at the manufacturer that is 0.5 mm , which ensures the time constant of about 8 ms .

The thermocouples were placed on a special trolley that enabled them to move with the engine (Fig. 3). Thanks to this, during each test the temperature measurement was carried out in the same position relative to the engine outlet section.

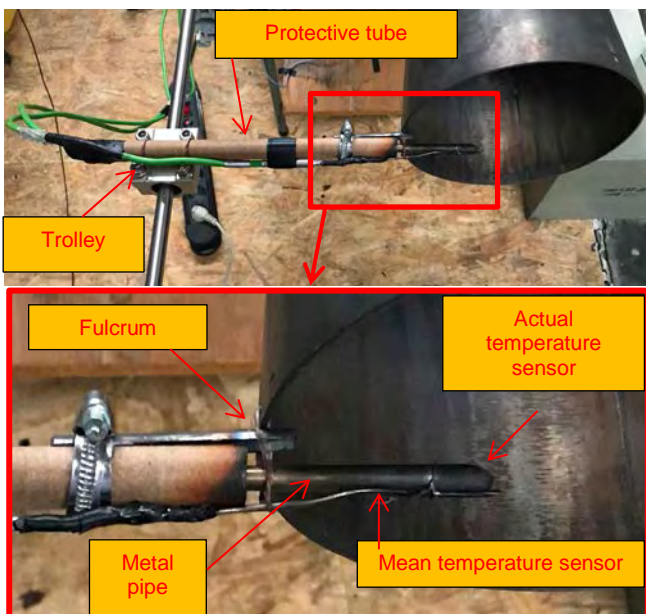


Fig. 3. The view of the system of thermocouples

Due to weak stiffness the actual temperature sensor was routed inside metal pipe of a small diameter to protect

it against bending when engine was running. Only the measuring junction was outside the pipe. The mean temperature sensor was routed outside the metal pipe and mechanically connected to it (Fig. 3).

The method of introducing an additional temperature sensor was used to compensate the temperature in the cold junction of the actual thermocouple. It consisted of a PT 100 sensor with an accurate transducer. The solution diagram is shown in Fig. 4. View of the cold end compensation system of the instantaneous thermocouple is shown in Fig. 5. To ensure greater stability of the cold junction temperature, the reference thermocouples together with the resistance sensor were placed in a thick-walled metal tube filled with foamed polystyrene (Fig. 5). The connection of the reference system with the measuring thermocouple was ensured by means of MT-type "socket-plug" terminals (Fig. 5). Due to its small dimensions, the entire compensation system occupied relatively little space on the test stand.

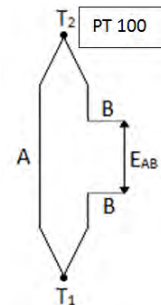


Fig. 4. Schematic diagram of actual temperature measurement system

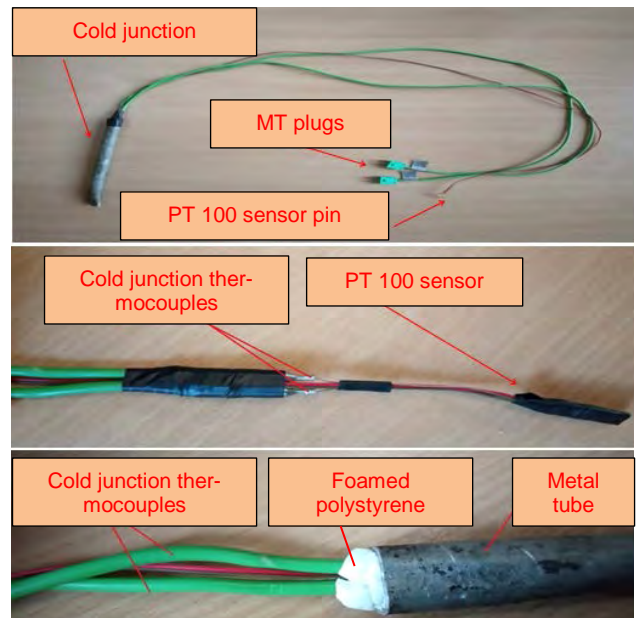


Fig. 5. Construction of actual temperature measurement system

Due to the fact that the thermocouple characteristics are non-linear, the temperature of the cold junction should be converted to Seebeck voltage (E_2) in accordance with PN-EN 60584-1. The potential difference between cold and hot junction ΔE should be summed with Seebeck voltage E_2 . The obtained result – the electromotive force E_1 should

be converted into the tested temperature, using the tables contained in PN-EN 60584-1.

$$E_1 = E_2 + \Delta E \quad (1)$$

Voltage ΔE measurement was carried out in a way to meet the law of Intermediate Metals requirements. For this purpose, voltmeter connectors were plugged in MT socket. This place was located away from heat sources, and the signal was transmitted to the measuring card through a shielded cable with a BNC connector at the end. The role of voltmeter was taken by NI 6363 DAQ. The signal from the mean temperature thermocouple was amplified, converted and averaged by a measuring transducer with electronic cold junction compensation.

3.2. Verification of dynamic temperature measurement system

During tests the signal from the thermocouple was sampled with frequency of 3500 Hz and then logged. To verify the proposed method, a spectral analysis of the recorded signal was carried out (Fig. 6).

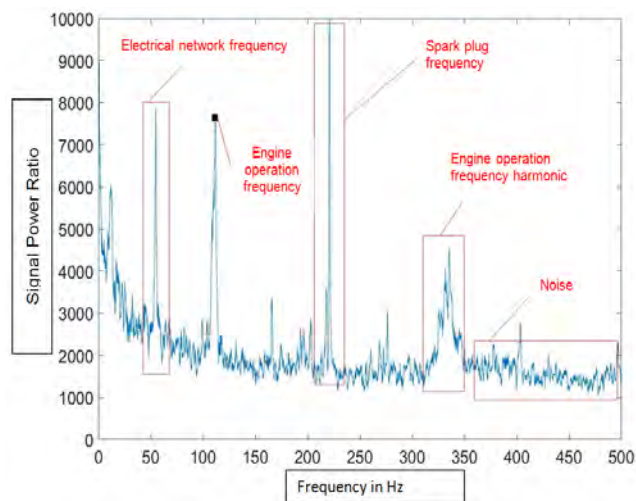


Fig. 6. Spectral analysis of signal from actual temperature thermocouple

Analyzing the spectrum image in detail (Fig. 6) a number of observations about the tested signal can be noted, inter alia it can be deduced that:

- the spectral line for a value of about 55 Hz is caused by the influence of electrical network interference,
- the spectral line for a value of approx. 230 Hz is caused by the operation of the spark plug during engine tests,
- for frequencies above 350 Hz, the spectrum is relatively flat,
- the band around 112 Hz is the frequency of the engine – this coincides with the frequencies determined by other methods.

Engine operating frequency was determined in two independent ways:

- based on spectral analysis of signal of combustion chamber actual pressure,
- based on spectral analysis of sound emitted by the engine.

The results of the evaluation of the engine operating frequency for selected tests are shown in Fig. 7.

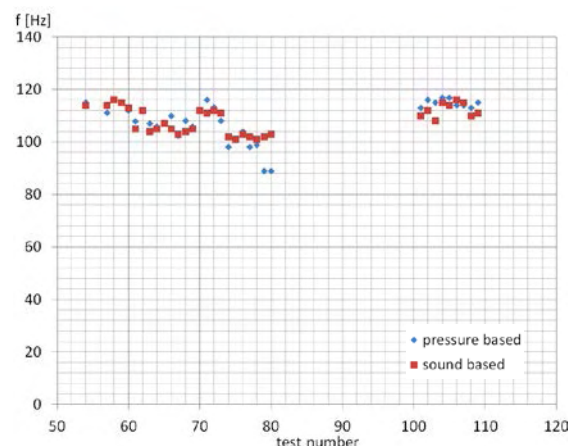


Fig. 7. The value of the engine operating frequency in function of the test number

In Figure 7 it can be seen that the highest concentration of results is in the range of 100–120 Hz. The average engine operating frequency based on pressure waveforms was found to be 108.7 Hz with a standard deviation of about 7.4 Hz, while for sound analysis it was 108.6 Hz with a standard deviation of about 5.0 Hz. The differences between the methods are insignificant.

It can be assumed that the main harmonic of the signal generated by the thermocouple was determined by the frequency of engine operation. This was confirmed by spectral analysis of the pressure signal in the combustion chamber and the sound emitted by the engine. For analyzed test the engine operational frequency was equal to 112 Hz. So, it can be deduced that the thermocouple was responding for temperature step function during engine single period. This could lead to conclusion that by using chosen thermocouple it was possible to measure exhaust gases dynamic temperature. A more detailed description of this process will be outlined in chapter 3.3.

3.3. Determination of the dynamic temperature in the exhaust section

The temperature measurement in the exhaust section of the pulsejet engine was not balanced. Due to the fact that the sensor was not in the thermal equilibrium with flowing medium it was necessary to take the thermometric lag of the sensor into account. During each test the thermocouple had its own temperature which was different from the medium temperature [12].

According to [12] thermocouple time constant was the time for the sensor to reach 0.632 part of the medium temperature excess over the sensor temperature. It was determined by its manufacturer that a time constant for the type K thermocouple in question is approx. 8 ms.

The thermocouple response to the violent temperature change provided by the manufacturer is shown in Fig. 8.

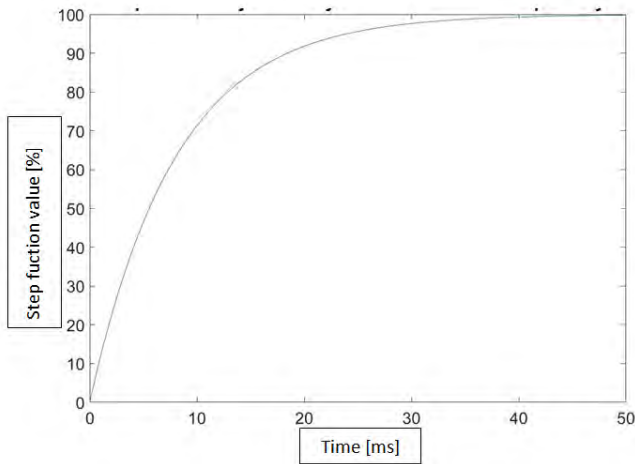


Fig. 8. Sensor response to temperature step function

It can be deduced from the chart shown in Fig. 8 that about 50 ms were needed to equalize the sensor temperature with the medium temperature. In addition, thermocouple time constant was equal to 8 ms, i.e. it was only slightly smaller than a single engine operating period, which is equal to 9 ms. It should be noted that temperature reading obtained from a thermocouple will be different from real temperature of the medium being tested. According to [13] inflow of fresh air to the combustion chamber lasts approximately 40% of the single cycle time. Due to the fact that the exhaust pipe in this engine was significantly longer than inlet pipes, the inflow of fresh air in the outlet section was even shorter so in consequence the outflow was longer than 60% of cycle time. Such behavior was a consequence of hot gases mass inertia which was outflowing from the exhaust pipe even after the negative pressure was reached in the combustion chamber [13]. After averaging the pressure and temperature waveforms, it was assumed that for the analyzed test, the gases flow out through the outlet cross-section about 75% of the entire cycle time. However, the inflow of fresh air took about 25% of the time of the single cycle. This hypothesis is also consistent with exhaust gases speed record presented in publication [9]. With such outflow to inflow ratios, it was impossible to approximate the temperature course with a sine wave. Since the temperature change in the engine was periodic, it should be remembered that the temperature of the sensor had smaller amplitude and was shifted in phase compared to real temperature course. From [12] it follows that for sine input function sensor amplitude is equal to:

$$T_a = \frac{T_{ga}}{\sqrt{1+\omega^2\tau^2}} \quad (2)$$

Phase shift is equal to:

$$\varphi = \arctg(\omega\tau) \quad (3)$$

where T_a – is the pulsation temperature amplitude, T_{ga} – mean temperature of media ω – frequency of pulsation, τ – sensor time constant, φ – phase shift between real temperature course and sensor temperature.

An exemplary temperature measurement in the outlet section was carried out for the following conditions:

- an ambient temperature of 20°C,

- fuel mass flow rate 4.5 g/s.

After using a bandpass filter with an 80-160 Hz transmission bandwidth, the dynamic temperature course from the sensor was obtained (Fig. 9). The temperature course of the sensor presented in Figure 9 is not equal to the actual engine outlet temperature. Since the analyzed waveform is not a sine wave, the relationship between the medium temperature and the sensor temperature proposed in publication [12] does not give the expected result. This will be detailed further in the text.

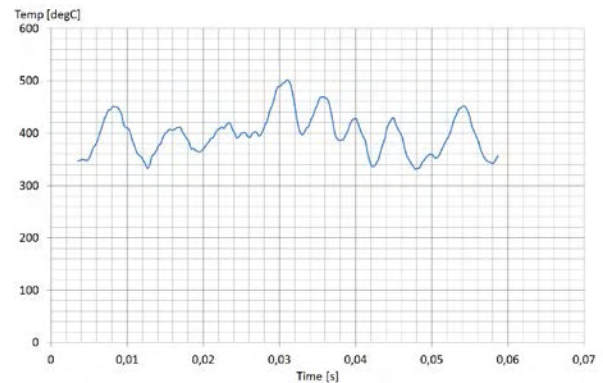


Fig. 9. The actual temperature sensor signal course

Since the estimation of the temperature course in the outlet section of the pulse jet engine by analytical method did not give satisfactory results, simulations of thermocouple behavior in given operating conditions were carried out. For the purpose of the simulation it was assumed that:

- engine operational frequency is equal to 112 Hz,
- the outflow from outlet station takes 75% of total time of single cycle time,
- the inflow through outlet station takes 25% of total time of single cycle time,
- the temperature of incoming air is equal to an ambient temperature of 20°C,
- the exhaust gases temperature – iterated variable.

During the subsequent iterations for given operational conditions the exhaust gases temperature was changed to reach the closest match between simulated and registered signal. To make simulation as close to reality as possible the behavior of mean temperature sensor was iterated in parallel. The resultant simulated course for dynamic temperature sensor is presented in Fig. 10.

In Figure 10 first simulated point corresponds to temperature which sensor reached after the outflow in first engine period. The second point corresponds to the end of inflow. From the simulated course it can be deduced that after about 35 ms the sensor was thermally stabilized.

Due to unstable work of the engine directly after the start up, only sections when the thermocouple was thermally stabilized were chosen for comparison. The comparison of simulated and real sensor behavior is presented in Fig. 11.

The presented comparison shows that the amplitudes of the real wave are slightly smaller than the simulated ones. This may be due to the fact that the air that was drawn in by the engine had a slightly higher temperature during its operation as a result of heating the environment with hot ex-

haust fumes. Secondly, the real waveform has a very irregular shape and is strongly distorted.

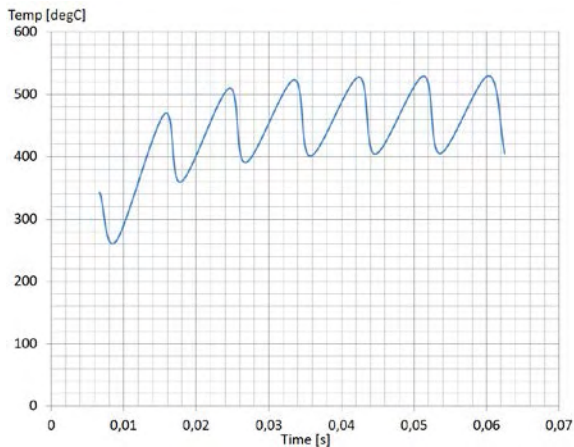


Fig. 10. Simulated signal course from instantaneous temperature sensor

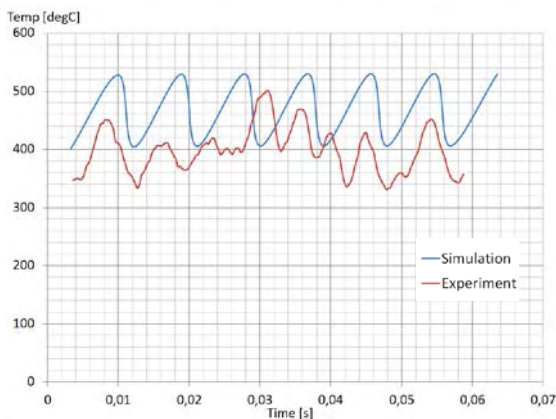


Fig. 11. Comparison of simulated and real instantaneous temperature sensor behavior

From Fig. 11 it could be also deduced that times of rise and decay are similar, what might be treated as further confirmation of assumed outflow to inflow relation, as well as confirms that the time constant taken to the simulation is appropriate.

Despite of number measures taken to improve the quality of signal from the sensor, the signal distortions were still present. This was mainly caused by the fact that the thermocouple measures temperature at one point and local flow fluctuations produces the random noise. What is more, in the outlet station of the engine a flame could be observed which resulted in further distortions of sensor readings due to ionization of air in the vicinity of the sensor. It is not possible to completely remove distortions from the analyzed waveform. Especially, the random noise mentioned above. However, the presented accuracy should be sufficient to estimate the maximum exhaust gas temperature. In the discussed case, it was around 625°C which gives an amplitude of $A = 605^\circ\text{C}$. When assuming a sinusoidal course of temperature changes, according to publication [12], the sensor amplitude calculated on the base of equation (2) should be around 450°C. This value is far from reality and confirms the statement that formula (2) is inadequate for the case considered. The course of the iterated

real, simulated and thermocouple measured signal curves are shown in Fig. 12.

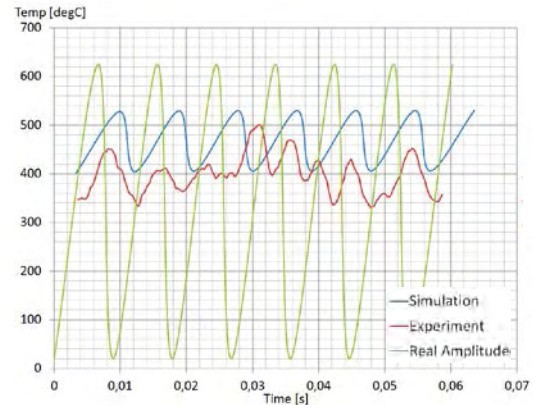


Fig. 12. Comparison of simulated and real sensor behavior with estimated real temperature course

In Figure 12 between real temperature course and thermocouple signals a phase shift calculated accordingly to equation 3 was applied. According to calculations, the temperature of the sensor reaches its maximum after 3.3 ms from reaching the maximum temperature in the outlet station, which is about 1/3 of the engine's single cycle time. As can be easily noticed in Fig. 12, the temperature of the sensor increases when the inflow of fresh air through the outlet station begins and decreases when the outflow of hot gases continues. This arrangement of the waveforms may suggest that the formula used to calculate the phase shift is inadequate or there are some errors in the initial assumptions of the simulation.

Firstly, the real temperature changes can be more violent than assumed. This could be due to the fact that hot gases leave the exhaust pipe in isothermal portions that flow through the outlet section for some time. In simulation it was assumed that it is one point with infinitely short duration. It can be similar in the inflow cycle. A portion of air with a constant temperature higher than assumed in the simulation can be sucked in. This may be due to heating the ambient air in the vicinity of outlet station by hot fumes what was described earlier in the text.

In the next drawing (Fig. 13) the simulation results with real waveform of mean temperature sensor are compared.

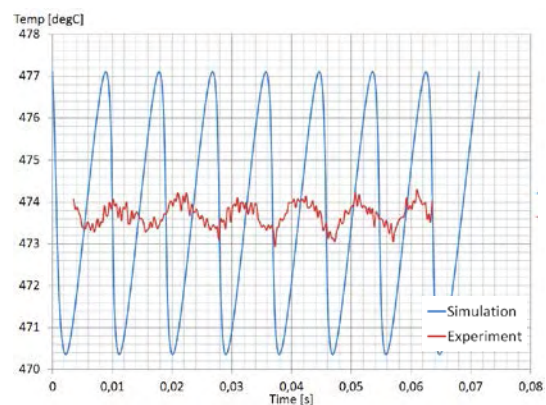


Fig. 13. Comparison of simulated and real average temperature sensor behavior

The simulated thermocouple waveform shown in Fig. 13 has a significantly greater amplitude than the real course. This can further confirm the fact that the temperature of the air sucked through the outlet is higher than the ambient temperature. However, both waveforms are consistent in terms of pattern and frequency. Both waveforms also oscillate around the same 474°C value. The simulated and recorded waveform for thermocouple with a 8 ms time constant also oscillates around this value. This may indicate that, despite the simplifications adopted, it was possible to correctly estimate the true temperature changes in the outlet section of the pulsejet engine.

4. Summary

Temperature measurement in the outlet station of a pulsejet engine is a complicated task. This undertaking is hampered by such properties of the tested object as the explosive nature of the combustion process causing large fluctuations in flow velocity, vibrations of the structure and acoustic effects, as well as the lack of generally available sensors that would allow direct measurement of temperature oscillations in the outlet section of the tested engine.

A significant difference in the duration of the outflow phase and the inflow of air through the outlet station results in the inability to use known and proven relationships to

determine the real temperature of the medium being tested. This is due to the fact that the course of temperature changes cannot be approximated by a sine wave. In addition, it is not possible to describe the actual temperature as a continuous function of time. It also translates into the inability to analytically determine the RMS or average value of the analyzed waveform.

The aim of the presented works was to determine EGT in the outlet section of a pulsejet. Its maximum value and frequency of change is particularly useful for further analysis. The method to achieve this goal should be simple and quick so that EGT can be estimated after each specific test, without causing significant breaks in work. Therefore, it was decided to develop an iterative EGT method. The method is rough, and the results should be treated as preliminary.

Iterating of the maximum temperature values in the outlet section proved to be the effective approach to the problem. Thanks to this, it was possible to determine the approximate value of exhaust gases temperature. Due to applied simplifications however, this result is also subject to uncertainty. Despite this, at the current level of work, the obtained accuracy seems to be sufficient.

Bibliography

- [1] ARJAVALINGAM, G., HAYNES, R.D., HYER, G.N. et al. High-temperature thin-film Pt-Ir thermocouple with fast time response. *Review of Scientific Instruments*. 1987, **58**(5), 875-877. <https://doi.org/10.1063/1.1139649>
- [2] BORDATCHEV, E., CHANDRA, S., HEICHAL, Y. A fast-response thin film thermocouple to measure rapid surface temperature changes. *Experimental Thermal and Fluid Science*. 2005, **30**(2), 153-159. <https://doi.org/10.1016/j.expthermflusci.2005.05.004>
- [3] CHEN, L., FRALICK, G., GREER, L. et al. Design and operation of a fast, thin-film thermocouple probe on a turbine engine. 50th AIAA/ASME/SAE/ASEE Joint Propulsion Conference, NASA Center for AeroSpace Information (CASI). *Conference Proceedings*. 2014. <https://doi.org/10.2514/6.2014-3923>
- [4] DE JONG, W., KUDRA, T., MENG, X. A state-of-the-art review of pulse combustion: Principles, modeling, applications and R&D issues. *Renewable and Sustainable Energy Reviews*. 2016, **55**, 73-114. <https://doi.org/10.1016/j.rser.2015.10.110>
- [5] FLECK, B., GAYNOR, J., HUNG, P. et al. Fast response exhaust gas temperature measurement in IC engines. *SAE Transactions. Journal of Passenger Cars: Electronic and Electrical Systems*. 2006, **115**(7), 598-609.
- [6] FLECK, R., KEE, R.J., MCENTEE, P.T. et al. Measurement of exhaust gas temperatures in a high performance two-stroke engine. *SAE Transactions. Journal of Engines*. 1998, **107**(3), 2413-2423.
- [7] HROMASOVA, M., LINDA, M. Analysis of rapid temperature changes. *Agronomy Research*. 2016, **14**(3), 768-778.
- [8] LING, Y., MIN, L., WEN, C. Experimental analysis of combustion performance in pulse jet engine. *Energy Procedia*. 2016, **100**, 248-252.
- [9] POBEZHIMOW, V.N. Flight efficiency of a pulsejet. *Russian Aeronautics*. 2010, **53**(1), 77-80. <https://doi.org/10.3103/S1068799810010137>
- [10] Pulsating Combustion. International Symposium. Monterey 1991. Print. *Combustion Science and Technology*. 1993, **1**(6).
- [11] THOMA, K. Dynamic temperature measurements on a thermally activated self-healing ionomer. *Journal of Intelligent Material Systems and Structures*. 2014, **25**(1), 25-30. <https://doi.org/10.1177/1045389X12444487>
- [12] WIŚNIEWSKI, S. Pomiary temperatury w badaniach silników i urządzeń cieplnych. *Wydawnictwo Naukowo-Tech-niczne Warszawa* 1983.
- [13] WÓJCICKI, S. Silniki pulsacyjne, strumieniowe, raketowe. *Wydawnictwo Ministerstwa Obrony Narodowej. Warszawa* 1962.
- [14] https://www.czaki.pl/content-dir/uploads/czaki-czujniki_termoparowe.pdf; accessed 02.2020.

Adrian Trzeciak, MEng., – Faculty of Power and Aeronautical Engineering, Warsaw University of Technology.
e-mail: adrian.trzeciak.dokt@pw.edu.pl



Prof. Marian Gieras, DSc., DEng., – Faculty of Power and Aeronautical Engineering, Warsaw University of Technology.
e-mail: marian.gieras@pw.edu.pl



Evaluation of the significance of the effect of the active cross-sectional area of the inlet air channel on the specific enthalpy of the exhaust gas of a diesel engine using statistics F of the Fisher-Snedecor distribution

This paper presents the application of Fisher-Snedecor distribution F statistics to assess the significance of the influence of changes in the active cross-sectional area of the inlet air channel (A_{dol}) flow in a diesel engine on the observed diagnostic parameter determined on the basis of measurements of the quick changing exhaust gas temperature in the outlet channel, which is the specific enthalpy of the exhaust gas stream within one engine operating cycle (h_{spat}). A plan of experimental tests carried out on the laboratory stand of a single-cylinder Farymann Diesel type D10 laboratory engine was presented and the method of determination of F statistics values for the obtained measurement results was characterized. Representative results of calculations were presented and the strength of A_{dol} input parameter influence on the determined diagnostic parameter h_{spat} simplified physical model of the working process of a compression ignition engine as the object of diagnosis was evaluated. It is planned to further develop the experimental research program to determine the significance of the influence of changes in the values of selected parameters of the engine structure on other diagnostic measures determined from the exhaust gas temperature signal, i.e. the mean peak-to-peak value as well as the rate (intensity) of increase and decrease in its value for individual engine cycles.

Key words: diesel engine, exhaust gas temperature, Fisher-Snedecor decomposition F statistic, diagnosis

1. Introduction

Diagnostics of the working spaces of a diesel engine, together with inlet air and exhaust gas ducts, is an important operational issue [3, 17]. The key stage of diagnosis is the process of parametric inference, allowing to determine the relationships between the state of the structural structure of a diesel engine and the observed parameters of its operation (control parameters) [2, 7]. One of the output parameters of the engine enabling such an operation is the fast-changing temperature of exhaust gases recorded in the outlet channel [8, 10]. However, in order to apply a diagnosis methodology based on this parameter, it is necessary to develop an appropriate measurement technology, taking into account the test conditions and measurement uncertainty. In the case of dynamic exhaust gas temperature measurements, the most appropriate seems to be the use of thermocouples with the lowest inertia [4]. Its time course, obtained during tests on a real object, which is a diesel engine, is burdened with numerous interferences resulting from environmental influences and the measurement network. Therefore, it should first be subjected to an appropriate mathematical treatment allowing to reproduce the course closest to the real one [11]. However, it will be of no use to the diagnostician without a properly developed test program and properly selected tools for statistical and substantive analysis of the obtained measurement data, including diagnostic inference [5, 9].

During the diagnostic test of the engine, in the steady state of operation, diagnostic parameters D are obtained from among its output parameters Y , which react more strongly to changes in the value of the structural parameters S than to changes in the value of the input parameters X , forcing the work process. The basic condition for selecting the appropriate diagnostic parameters is a much higher

sensitivity of the output parameter in relation to the W_S^Y structure parameter than its sensitivity to the W_X^Y input parameter [3]:

$$\begin{aligned} W_S^Y &= \frac{\partial Y}{\partial S} = \frac{\frac{\Delta Y}{Y_0}}{\frac{\Delta S}{S_0}} = \frac{\frac{Y_{pom}-Y_0}{Y_0}}{\frac{S_{pom}-S_0}{S_0}} \gg W_X^Y = \\ &= \frac{\partial Y}{\partial X} = \frac{\frac{\Delta Y}{Y_0}}{\frac{\Delta X}{X_0}} = \frac{\frac{Y_{pom}-Y_0}{Y_0}}{\frac{X_{pom}-X_0}{X_0}} \end{aligned} \quad (1)$$

Comparison of the sensitivity of many control parameters, given in different units of measurement, makes it necessary to adopt relative values of input, output and structure parameters for this purpose.

There are many methods of assessing the significance of the impact of the parameters that force the analyzed physical process on its course. These include the concept known from classical mathematical analysis, which is the distance between functions (metrics), information entropy derived from information theory (formulated for the first time in 1945 by Shannon), as well as non-parametric and parametric statistical tests [3, 5, 6, 15].

In the case of assessing the significance of the impact of one engine input parameter or one structural parameter on one output parameter, i.e. quick changing exhaust gas temperature, the most appropriate seems to be the application of a randomized static test program complete and the adoption of Fisher-Snedecor distribution F statistics for analysis [5, 16]. In order to determine the significance of the effect of engine load on the defined, observed in the diagnostic process, output parameters, it was necessary to carry out the research according to a simplified physical model of the working process of a diesel engine presented in Fig. 1.

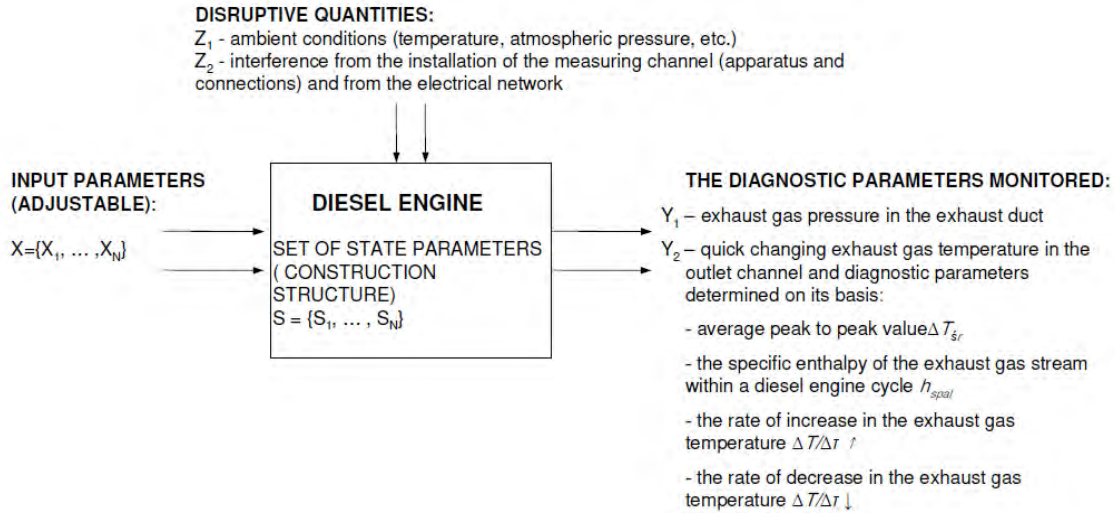


Fig. 1. Simplified physical model of the diesel engine operating process for diagnostic purposes

2. Use of Fisher-Snedecor decomposition statistics F to assess the significance of the impact

Due to the nature of the research conducted, a complete randomized static program was used [5], which allows to assess the significance of the impact of one input factor of the physical model of the process under study on one output factor. The zero hypothesis, formulated in advance and verified in statistical studies, assumes no influence of the input factor on the resultant factor. An input factor is considered significant when the computational value of the adopted statistics is equal to or greater than the critical value given in the tables for the adopted value of the significance level and number of degrees of freedom. It was considered that the Fisher-Snedecor decomposition F statistic of the Fisher-Snedecor decomposition is best suited for diagnostic testing of a diesel engine because the conditions for the use of unilateral parametric tests are met. It was assumed in advance that the results of measurements of all control parameters can be modelled as random variables with normal distribution, a specific expected value and variance, being a measure of the scatter around the mean value. It was also assumed that the variances of random variables are equal or close to the value, and the applied parametric tests concerning the variance are characterized by one-sided critical area. The possibility of making a first type error (equal to α) associated with an arbitrarily accepted level of materiality, i.e. the probability of rejecting the zero hypothesis when it is true, was also considered. However, the possibility of making a second type of error, i.e. assuming the zero hypothesis when it is false, of $\beta = 1 - \alpha$ [5].

Table 1 presents an exemplary matrix of an experimental test programme, in this case a randomised static plan, allowing the assessment of the significance of the influence of the input factor considered in the diagnostic tests of a diesel engine – the active cross-sectional area of the A_{dol} inlet air channel on the diagnostic parameter (output factor), which is the unit enthalpy of the exhaust gas stream within one operating cycle – h_{spal} .

Table 1. Matrix of the experimental research programme – complete randomized static plan

| Level of input factor | Number of experience | | |
|-----------------------|----------------------|-----|--------------|
| | 1 | ... | 6 |
| $A_{dol 1}$ | h_{spal11} | ... | h_{spal61} |
| $A_{dol 2}$ | ⋮ | ⋮ | ⋮ |
| $A_{dol 3}$ | h_{spal13} | ... | h_{spal63} |

The test (calculation) value of the Fisher-Snedecor¹ distribution F statistics is determined from the following relationship:

$$F = \frac{\sum_{i=1}^p n_i (\bar{h}_i - \bar{h})^2 \cdot (n-p)}{[\sum_{i=1}^p \sum_{j=1}^q (\bar{h}_{ij} - \bar{h})^2 - \sum_{i=1}^p n_i (\bar{h}_i - \bar{h})^2] \cdot (p-1)} \quad (2)$$

where: n_i – number of measurements of specific enthalpy at a given level, n – total number of measurements, \bar{h}_i – average specific enthalpy from the measurements in the i -line, \bar{h} – average specific enthalpy from all measurements, h_{ij} – the value of the j specific enthalpy at the i -level, p – number of levels of variation of the input medium (active cross-sectional area of the inlet air).

The calculated test value of the F_{obl} statistics is then compared with its critical value F_{kr} determined from the relevant statistical table, for the assumed level of materiality α and for the designated numbers of degrees of freedom calculated for the numerator and denominator of the statistic value $F: f_1$ and f_2 . If the determined F_{obl} value is greater than or equal to the F_{kr} critical value, the effect of the test factor should be considered significant. Otherwise, within the tested range of volatility and at the assumed level of materiality, the tested input factor is considered not to be significantly influenced by the output factor.

3. Influence of diesel engine structure parameters on the specific enthalpy of exhaust gases

In order to obtain the value of F statistics, and thus the answer to the key question concerning the significance of the influence of the tested input factors of the simplified

¹ In the following, it is also referred to as "F statistics" for short.

physical model of the diesel engine working process on the defined diagnostic measures, it was necessary to follow the developed scheme of research implementation – Fig. 2.

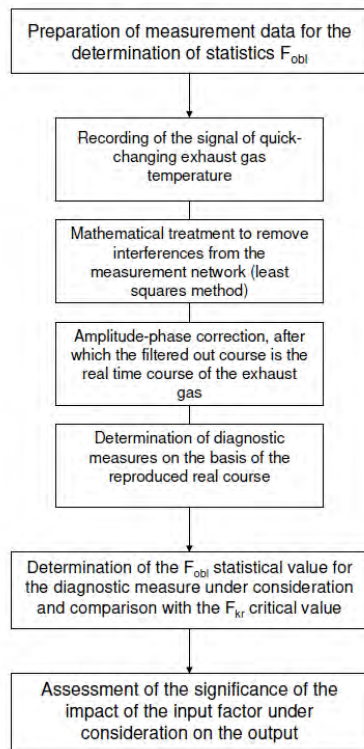


Fig. 2. Stages of preparation of measurement data for determination of Fisher-Snedecor statistic F decomposition for diagnostic purposes

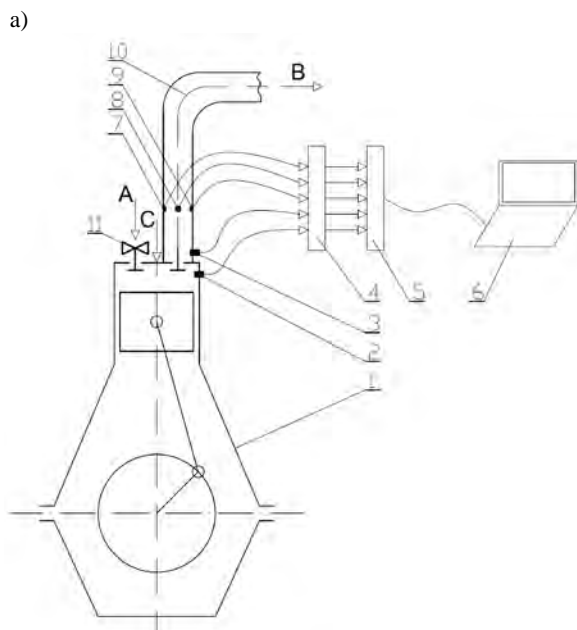
The main objective of the empirical research is to determine the diagnostic information of the observed control parameter, which is a quick changing temperature of the

exhaust gas of a diesel engine loaded with a DC generator. Therefore, its sensitivity to changes in the parameters of its construction structure should be determined. In the discussed next stage of research [13], the significance of the influence of the active cross-sectional area of the A_{dol} inlet air channel on one of the diagnostic measures obtained from the reproduced, real course of the quick changing exhaust gas temperature – the specific enthalpy of the exhaust gas stream within the range of one engine operation cycle was evaluated. The experiment was carried out according to the plan presented in tabular form – Table 2.

Table 2. Engine test plan to determine the significance of the effect of its active cross-sectional area of the A_{dol} intake air channel on the specific enthalpy of the exhaust gas stream within one h_{spal} working cycle

| Parameter Point | Points of regulatory characteristics according to the implemented plan | | | | | |
|--------------------|--|---------------|-------|-------|------------------------|-----------------------|
| | A_{dol} [m ²] | P_{obc} [W] | I [A] | U [V] | n [min ⁻¹] | Number of repetitions |
| A_{dol1} | 804×10^{-6} | 432 | 5.1 | 72 | 1444 | 6 |
| A_{dol2} | 603×10^{-6} | 432 | 5.1 | 72 | 1444 | 6 |
| A_{dol3} | 401×10^{-6} | 432 | 5.1 | 72 | 1444 | 6 |
| A_{dol1} | 804×10^{-6} | 768 | 6.8 | 96 | 1444 | 6 |
| A_{dol2} | 603×10^{-6} | 768 | 6.8 | 96 | 1444 | 6 |
| A_{dol3} | 401×10^{-6} | 768 | 6.8 | 96 | 1444 | 6 |
| A_{dol1} | 804×10^{-6} | 1200 | 8.5 | 120 | 1444 | 6 |
| A_{dol2} | 603×10^{-6} | 1200 | 8.5 | 120 | 1444 | 6 |
| A_{dol3} | 401×10^{-6} | 1200 | 8.5 | 120 | 1444 | 6 |

Both the motor load and the current and voltage at the generator terminals changed by 25% compared to the nominal value for the regulatory characteristics according to the implemented test program. For construction and regulatory



b)



Fig. 3. a) Diagram of the laboratory stand with marked places of sensor installation: 1 – Farymann Diesel engine type D10, 2 – top deadlock and speed sensor, 3 – outlet valve opening sensor, 4 – A/C converter, 5 – recorder, 6 – analysis program, 7 – water-cooled thermocouple, 8 – pressure sensor, 9 – bimetal thermometer, 10 – flue gas outlet channel, 11 – ball valve regulating the air supply, A – inlet air, B – exhaust gases, C – supply fuel; b) view of the engine inlet air ball valve

Table 3. Values of the specific enthalpy of the exhaust gas stream $h_{spal\acute{s}r}$ within one diesel engine cycle for the variable values of the active cross-sectional area of the A_{dol} intake air channel, where: a) the result for the test at point $P_1 = 432$ W of the control characteristic, b) the result for the test at point $P_2 = 768$ W of the same characteristic, c) the result for the test at point $P_3 = 1200$ W of the above characteristic

a)

| Point | Average value over one exhaust gas enthalpy cycle h_{sr} [kJ/kg] for variable values of the active cross-sectional area of the intake air duct P1 (432 W; 5.1 A; 72 V) | | | | | | | |
|--------------|--|----------------------|---------|---------|---------|---------|---------|---------|
| | A_{dol} [m ²] | Number of experience | | | | | | |
| | | 1 | 2 | 3 | 4 | 5 | 6 | y_i |
| $A_{dol 11}$ | 804×10^{-6} | 12.1299 | 12.1986 | 12.2763 | 12.2176 | 12.2669 | 12.1493 | 12.2064 |
| $A_{dol 12}$ | 603×10^{-6} | 11.4980 | 11.3782 | 11.3742 | 11.3126 | 11.3567 | 11.5817 | 11.4169 |
| $A_{dol 13}$ | 401×10^{-6} | 11.1331 | 11.4122 | 11.3092 | 11.3045 | 11.4661 | 11.3280 | 11.3255 |

b)

| Point | Average value over one exhaust gas enthalpy cycle h_{sr} [kJ/kg] for variable values of the active cross-sectional area of the intake air duct P2 (768 W; 6.8 A; 96 V) | | | | | | | |
|--------------|--|----------------------|---------|---------|---------|---------|---------|---------|
| | A_{dol} [m ²] | Number of experience | | | | | | |
| | | 1 | 2 | 3 | 4 | 5 | 6 | y_i |
| $A_{dol 21}$ | 804×10^{-6} | 13.8992 | 13.6571 | 13.4404 | 13.3947 | 13.2752 | 13.1309 | 13.4663 |
| $A_{dol 22}$ | 603×10^{-6} | 12.2129 | 12.1734 | 11.9982 | 11.8355 | 11.9983 | 11.9656 | 12.0306 |
| $A_{dol 23}$ | 401×10^{-6} | 12.1310 | 12.2085 | 12.1043 | 12.1049 | 12.0821 | 12.0763 | 12.1179 |

c)

| Point | Average value over one exhaust gas enthalpy cycle h_{sr} [kJ/kg] for variable values of the active cross-sectional area of the intake air duct P3 (1200 W; 8.5 A; 120 V) | | | | | | | |
|--------------|--|----------------------|---------|---------|---------|---------|---------|---------|
| | A_{dol} [m ²] | Number of experience | | | | | | |
| | | 1 | 2 | 3 | 4 | 5 | 6 | y_i |
| $A_{dol 31}$ | 804×10^{-6} | 15.4712 | 15.4883 | 15.3075 | 15.3299 | 15.0444 | 15.0994 | 15.2901 |
| $A_{dol 32}$ | 603×10^{-6} | 13.0105 | 12.8378 | 12.9773 | 13.0444 | 12.9890 | 12.7919 | 12.9418 |
| $A_{dol 33}$ | 401×10^{-6} | 13.6214 | 13.6125 | 13.5034 | 13.2633 | 13.3270 | 13.2022 | 13.4216 |

4. Comments and final conclusions

From the results of the calculation, it can be seen that the active cross-sectional area of the inlet air channel has a significant effect on the specific enthalpy of the exhaust stream within one diesel engine cycle. However, in order to consider the adopted method of assessing the significance of the influence of the input factors of the engine operation and its design structure on the output with the use of Fisher-Snedecor decomposition F statistics as fully useful for diagnostic tests, the experimental research programme should be extended. It is necessary, inter alia, to carry out further research to determine the effect (force) of changes in other input parameters (factors) on the defined diagnostic

measures of the diesel engine exhaust gas temperature signal, which are the average peak-to-peak value, as well as the rate (intensity) of increase and decrease in its value for single cycles of operation for which no relevant statistical studies have yet been carried out.

In the next stage of diagnostic tests, it is also planned to draw up an energy balance in the engine with the use of Sankey jet diagrams, under the conditions of introduced changes in the values of selected structure parameters. This is to determine their energy effects, as an important fire-impact of the developed methodology for diagnosing compression-ignition engines, based on measurements and analysis of exhaust gas temperature.

Bibliography

- [1] BALCERSKI, A. Siłownie okrętowe: podstawy termodynamiki, silniki i napędy główne, urządzenia pomocnicze, instalacje. *Wydawnictwo Politechniki Gdańskiej*. Gdańsk 1990.
- [2] JAREMKIEWICZ, M. Odwrotne zagadnienia wymiany ciepła, występujące w pomiarach niustalonej temperatury płynów. Rozprawa doktorska. *Wydawnictwo Politechniki Krakowskiej*. Kraków 2011.
- [3] KORCZEWSKI, Z. Diagnostyka eksploatacyjna okrętowych silników spalinowych – tłokowych i turbinowych. Wybrane zagadnienia. *Wydawnictwo Politechniki Gdańskiej*. Gdańsk 2017.
- [4] KORCZEWSKI, Z., PUZDROWSKA, P. Analytical method of determining dynamic properties of thermocouples used in measurements of quick – changing temperatures of exhaust gases in marine diesel engines. *Combustion Engines*. 2015, **162**(3), 300-306.
- [5] KORZYŃSKI, M. Metodyka eksperymentu. Planowanie, realizacja i statystyczne opracowanie wyników eksperymentów technologicznych. *Wydawnictwo WNT*. Warszawa 2017.

- [6] KUDREWICZ, J. Analiza funkcjonalna dla automatyków i elektroników. Państwowe Wydawnictwo Naukowe. Warszawa 1976.
- [7] ŁUTOWICZ, M. Identyfikacja procesu sprężania okrętowego tłokowego silnika spalinowego dla potrzeb diagnostyki jego przestrzeni roboczych. Rozprawa doktorska. Akademia Marynarki Wojennej. Gdynia 2006.
- [8] OLCZYK, A. Koncepcja pomiaru szybkozmiennej temperatury gazu z uwzględnieniem dynamicznej składowej temperatury. *Pomiary Automatyka Kontrola*. 2007, **53** Bis/9, 576-579.
- [9] PABIS, S. Metodologia i metody nauk empirycznych. Państwowe Wydawnictwo Naukowe. Warszawa 1985.
- [10] PUZDROWSKA, P. Statystyka F rozkładu Fishera-Snedecora jako narzędzie do oceny istotności wpływu mocy silnika o ZS na wybrane miary diagnostyczne. *Journal of Polish CIMAC*. 2019, **14**(1/18), 177-186.
- [11] PUZDROWSKA, P. Metoda wyznaczania stałej czasowej termopary na podstawie pomiaru szybkozmiennej temperatury spalin wylotowych silnika o ZS. *Zeszyty Naukowe Akademii Morskiej w Gdyni*. 2018, **108**, 115-133.
- [12] PUZDROWSKA, P. Signal filtering method of the fast-varying diesel exhaust gas temperature. *Combustion Engines*. 2018, **175**(4), 48-52. <https://doi.org/10.19206/CE-2018-407>
- [13] PUZDROWSKA, P. Identification on damages in the inlet air duct of a diesel engine based on exhaust gas temperature measurements. *Combustion Engines*. 2019, **177**(2), 108-112. <https://doi.org/10.19206/CE-2019-219>
- [14] RUDNICKI, J., PUZDROWSKA, P., MARSZAŁKOWSKI, K. Osłona termopary chłodzona wodą jako narzędzie zapobiegające zakłóceniom zewnętrznym podczas pomiarów temperatur szybkozmiennych spalin w kanale wylotowym silnika okrętowego. *Journal of Polish CIMAC*. 2017, **12**(1), 97-104.
- [15] SHANNON, C.E. A mathematical theory of cryptography. A classified memorandum for Bell Telephone Labs. USA 1945.
- [16] WOJTATOWICZ, T.W. Metody analizy danych doświadczalnych. Wybrane zagadnienia. *Wydawnictwo Politechniki Łódzkiej*. Łódź 1998.
- [17] ZACHAREWICZ, M. Metoda diagnozowania przestrzeni roboczych silnika okrętowego na podstawie parametrów gazodynamicznych w kanale zasilającym turbosprężarkę. Rozprawa doktorska. *AMW*. Gdynia 2009.

Patrycja Puzdrowska, MEng. – Faculty of Ocean Engineering and Ship Technology, Gdansk University of Technology.
e-mail: patpuzdr@pg.edu.pl



The impact of thermodynamics parameters of turbofan engine with ITB on its performance

Presented paper is focused on the influence of additional combustor chamber named inter turbine burner on turbofan engine unit parameters. Investigation has been made how changing selected engine parameters affect its performance. A comparison has been made between the baseline turbofan engine and the engine with ITB. Engine thermodynamics model was prepared in MATLAB software. Main combustion chamber was fueled by kerosene, commonly used in aviation transport, while inter turbine burner by alternative fuel. As an alternative fuel were chosen liquid hydrogen and methane. Numerical researches were carried out for take-off conditions. Engine specific thrust and specific fuel consumption were obtained as a function of bypass ratio, turbine inlet temperature, fan pressure ratio, HPC and LPC pressure ratio. The results of the study indicate that hybrid engine with additional combustion chamber fueled by hydrogen fuel is more efficient than other studied cases.

Key words: inter turbine burner, turbofan engine, liquid hydrogen, alternative fuels

1. Introduction

Due to the problems with global warming and air traffic increasing, future aircraft engines should be characterized by low pollutant emissions and high reliability. At the same time, low combustion emission should be accompanied by high efficiency of the combustion process. Emission from aircraft engines cannot be ignored, because aircrafts emit their pollutants in upper layers of atmosphere what may have stronger impact on environmental destruction than on the ground. Nowadays aviation industry is responsible for approximately 2% of global emissions of CO₂ generate by the human [19]. Therefore due to the dynamical development of air transport, environmental protection is the key issue, especially that it is forecast that air travel will double over the next two decades [19].

Advisory Council for Aviation Research and Innovation in Europe (ACARE) present the highly ambitious goals within a framework of FlightPath 2050. Assumption has been made that in 2050 year allowable technologies permit for reduction of CO₂ emission per passenger kilometer by 75% and for reduction of NO_x emission by 90%. The ACRAE assume also no emissions during aircraft taxiing, air vehicles recyclability and the Europe leadership in atmospheric researches [18].

Existing aircraft technologies are not sufficient to significantly reduce CO₂ emission and other harmful products of combustion process. The solution of this problem will be development new alternative propulsion systems and energy sources [19].

Due to depletion of fossil fuels it is anticipated that application of non-conventional fuels will be significant. In the first place application will find synthetic fuels (GTL-gas to liquid, CTL-coal to liquid) and biofuels [14]. Because nowadays fossil fuels are extensively use by all means of transport which translates into a significant increase in the carbon dioxide content in the atmosphere. Carbon dioxide is a product of chemical reaction of hydrocarbon fuel combustion and may be eliminated by application non-carbon fuel. In this case non-carbon fuel like liquid hydrogen or fuels with a low carbon content, like methane, may be taken

into consideration. Some potential pathways of aviation fuel evolution are presented on Fig. 1.

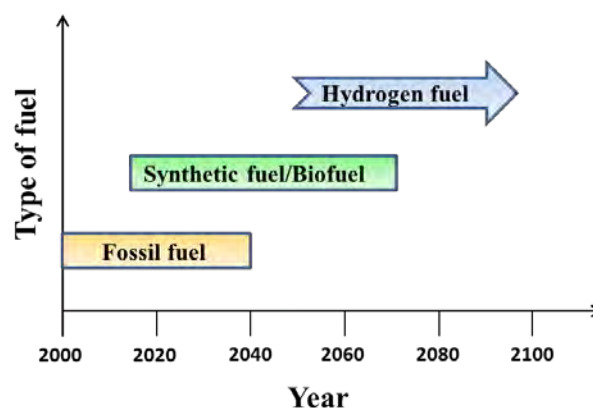


Fig. 1. Aviation fuels of the future [14]

The solution of the presented problem related to emission of harmful combustion product, will be new engine concept adapted to burn alternative fuel, characterized by higher engine efficiency.

To reduce turbine engine fuel consumption new engine concept with ITB is presented by [6–8, 11, 14–17]. Application of such conception allow for high pressure turbine inlet temperature reduction and accompanied NO_x reduction. The ITB conception permit for application flameless combustion technique, which reduce the NO_x considerable [6, 10, 16]. Flameless oxidation is a process which based on dilution of oxygen contained in the reactant stream and raising its temperature above the auto ignition temperature. Fuel oxidation is currently mainly used in industrial application [5, 6].

The ITB conception is also known as the reheat cycle. In such cycle gases expanded in HPT are reheated before the next expansion process that occur in LPT. In ITB fuel is burned at higher pressure than in conventional afterburner applied in turbine engines. That guarantee better engine thermal efficiency [13].

Hydrogen has got wider flammability limit than kerosene so the combustion process can take place at lean conditions to reduce NO_x emission [17]. NO_x emission increases with fuel to air ratio and with the temperature of combustion process [12]. Nitrogen oxides are formed during the oxidation of nitrogen contained in the air exposed to high temperatures [12]. The main parameters that are responsible for nitrogen oxide formation are the flame temperature, the nitrogen and oxygen content and the residence time of the gases in the combustion zone. Reduction of these parameters would allow for NO_x reduction, emitted by the aircraft turbine engines [2, 12].

Hydrogen is clean energy carrier [1] that require large fuel tanks due to the four time lower energy density per unit volume than kerosene. This hydrogen property will affect considerably the airframe configuration. This problem can be resolve by development of new aircraft type, namely the Blended Wing Body [11, 14]. BWB is resemble to flying wing [20]. This hybrid shape seems to be the most suitable for large hydrogen cylindrical tanks [14].

Another promising alternative fuel next to hydrogen is Liquid Natural Gas. LNG in 90% consist of methane. The remaining 10% are small fractions of liquid ethane, propane, nitrogen and other impurities. LNG is a cryogenic fluid like hydrogen. Application of LNG will allow for a 20% reduction in CO₂ emission. Further reduction is possible by adding liquid biomethane to the LNG, to create Bio-LNG [3]. Studies on cryogenic alternative fuels bring to the conclusion that fuel tanks should be placed within the fuselage [3].

2. Inter turbine burner concept

In conventional turbofan engine fuel is burn in main combustion chamber and then hot gases are expand through the turbine. In turbofan engine configuration with inter turbine burner combustion is continued in additional combustion chamber, situated between high pressure turbine (HPT) and low pressure turbine (LPT). The main goal of this conception is to increase engine efficiency and specific thrust [8, 16]. The ITB as an additional source of heat influence on increase of power output for a given engine size. In accordance with [16] the specific fuel consumption (SFC) is lower than for engine with afterburner due to the fact that operating pressure of an ITB is higher and it help to improve the thermal efficiency of the Brayton cycle [16].

The turbofan engine configuration with marked engine stations is presented on Fig. 2.

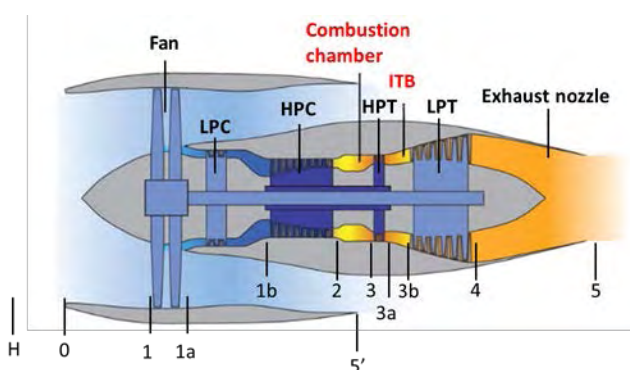


Fig. 2. Turbofan engine configuration with ITB [14]

Description of sections numbers presented on Fig. 2: H – ambient conditions, 0 – inlet conditions, 1 – conditions at the fan inlet, 1a – conditions at the LPC inlet, 1b – conditions at the HPC inlet, 2 – conditions at the combustion chamber inlet, 3 – conditions at the HPT inlet, 3a – condition at ITB inlet, 3b – conditions at the LPT inlet, 4 – conditions at the LPT outlet, 5 – conditions at the exhaust nozzle outlet, 5’ – conditions at the cold nozzle outlet.

3. Turbofan engine numerical model

The thermodynamics model of turbofan engine with dual combustor chamber was implemented in Matlab software and is described in detail in references [9]. A twin spool configuration of engine is considered, where the high pressure compressor (HPC) is driven by the high pressure turbine (HPT), whereas the fan and low pressure compressor (LPC) are driven by low pressure turbine (LPT). Engine performance analysis was carried out for off-design conditions. Working fluid was describe as semi-perfect gas [9]. Engine operating conditions are presented in Table 1.

Table 1. Operating conditions

| Description | Notation | Unit | Take-off |
|-------------------------------|-------------|------|----------|
| Mach number | Ma | – | 0 |
| Altitude | H | m | 0 |
| Air mass flow | \dot{m} | kg/s | 670 |
| Fan pressure ratio | FPR | – | 1.65 |
| Bypass ratio | BR | – | 4.4 |
| LPC pressure ratio | π_{LPC} | – | 1.6 |
| HPC pressure ratio | π_{HPC} | – | 12.8 |
| HPT turbine inlet temperature | TIT_{HPT} | K | 1500 |
| LPT turbine inlet temperature | TIT_{LPT} | K | 1300 |

Engine numerical model consist of blocks that describe the work of individual engine components like: inlet, fan, low pressure compressor, high pressure compressor, combustion chamber, high pressure turbine, inter turbine burner, low pressure turbine, exhaust nozzle and bypass. The scheme of numerical model is presented on Fig. 2. Prepared thermodynamics model do not taking into consideration turbine cooling process.

The design of turbofan engine is a compromise between turboprop and turbojet engines. This construction is characterized by the occurrence of two streams of air [4]. In the analyses case, the air in primary core (hot stream) goes through the fan, low pressure compressor, high pressure compressor, combustor chamber, high pressure turbine, low pressure turbine, inter turbine burner, low pressure compressor and exhaust nozzle. The second part of air (cold stream) goes through fan and then to the outer duct ended by the “cold” nozzle.

Bypass ratio is defined as:

$$BR = \frac{\dot{m}_c}{\dot{m}_h} \quad (1)$$

where: \dot{m}_c – mass flow rate through the bypass, \dot{m}_h – mass flow rate through the primary engine core.

High-bypass pressure ratio turbofan engines found application in large commercial aircraft, as much fuel efficient than other types of turbine engines [4]. The variation of BR influence directly variation in engine components diameters and rotational speed [12].

There are two fundamental indicators that define the performance of turbine engines – specific thrust and specific fuel consumption. Specific thrust is the engine thrust per mass flow rate:

$$ST = \frac{T}{\dot{m}_h} \quad (2)$$

Specific fuel consumption is defined as the fuel mass flow rate per unit thrust and can be expressed by following equation:

$$SFC = \frac{m_{fuel,1} + m_{fuel,2}}{T} \quad (3)$$

where: $m_{fuel,1}$ – fuel burn in main combustion chamber, $m_{fuel,2}$ – fuel burn in ITB.

In analysis case, the fuel flow rate is the sum of the fuel flow related to the main combustion chamber and the fuel flow related to the ITB.

Engine thrust force for turbofan engine with ITB:

$$T = \dot{m}_h BR V'_5 + \dot{m}_h (1 + f + f_{tb}) V_5 - \dot{m}_h (1 + BR) V \quad (4)$$

where: \dot{m}_h – mass flow rate (main gas path), BR – bypass ratio, V'_5 – velocity of bypass air, V_5 – velocity of hot gases, f – fuel to air ratio, f_{tb} – fuel to air ratio for turbine burner, V – velocity of the flight.

The presented block structure of the engine numerical model (Fig. 2), illustrate the order of performed calculations.

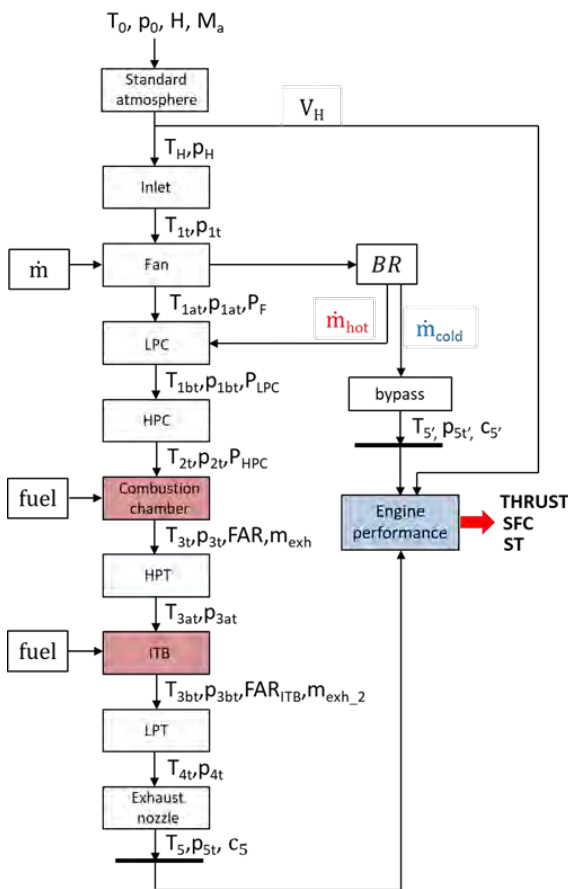


Fig. 2. The schematic of numerical model of turbofan engine with ITB in Matlab software

The model was developed based on the basic thermodynamics relations [4, 9, 12]. Prepared model allow analyze the performance of hybrid turbofan engine.

Turbofan engine performance are influence by the following thermodynamics parameters:

- bypass pressure ratio,
- fan pressure ratio,
- overall pressure ratio,
- turbine inlet temperature.

Low specific fuel consumption is achieve by continuously increasing the overall pressure ratio (OPR), and bypass ratio (BR) [16]. Turbine inlet temperature is the most important design parameter that influence thermodynamic cycle of turbine engine [4]. For a conventional turbine engine, the HPT inlet temperature is a design variable. In case of engine configuration with ITB, both the HPT and LPT inlet temperatures are design variables [16].

4.Scope of the work

The main scope of presented work is analysis how variation of selected engine parameters influence engine performance. Numerical analysis was carried out for take-off conditions. As the variable parameters were choose: bypass ratio, turbine inlet temperature, fan pressure ratio, HPC and LPC pressure ratio. Performance comparison was made between hybrid engine with ITB and baseline turbofan engine.

Two options of engine feeding were taken into consideration. In first case assumptions has been made that main combustion chamber is fueled by kerosene while the ITB is fueled by liquid hydrogen. In second case the main combustion chamber is invariable fueled by kerosene while ITB by liquid methane.

It can be seen in Fig. 6 to Fig. 14 that researches was carried out for three values of bypass ratio: 4.4, 6 and 8.

Thermodynamics calculations were carried out in order to determine the flow parameters at characteristic engine sections (Fig. 2) and to calculate specific thrust and specific fuel consumption.

5.Result discussion

The variations of engine performance with selected thermodynamics parameters changes are presented on Fig. 3 to Fig. 14.

The relation between bypass ratio (BR) and engine specific thrust (ST) is presented on Fig. 3.

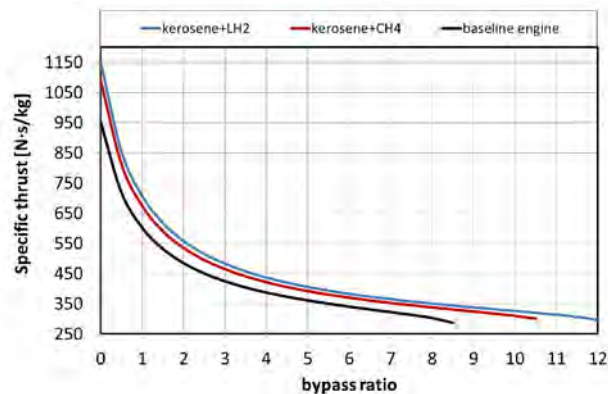


Fig. 3. Bypass ratio vs. specific thrust

The graph shows the decreasing dependence of the specific thrust with the increase of engine BR (Fig. 3). BR is relation between cold stream of air and the air in the main engine core, described by equation (1). If the BR increase, more air goes through the outer duct, what affect significantly the increase in engine outer diameter. This issue cause the drag increase as well as reduction of ground clearance [14].

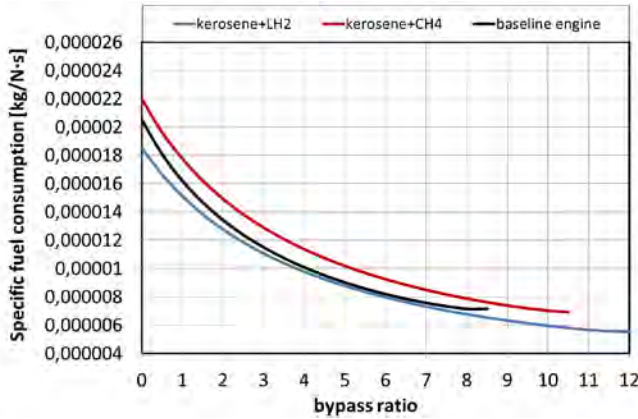


Fig. 4. Bypass ratio vs. specific fuel consumption

It can be seen on Fig.4, that increasing the BR improves the specific fuel consumption at the expense of specific thrust decrease. The lowest value of SFC is obtained for engine with inter turbine burner fueled by liquid hydrogen (Fig. 4). At the same time, for this case the highest specific thrust was received (Fig. 3). In addition for a given working conditions, the highest values of BR are possible to applied for engine configuration with inter turbine burner fueled by hydrogen. Analyzing the chart on Fig. 3 and Fig. 4 it can be seen that for an accepted operating conditions wider range of bypass ratio can be implemented for turbofan engine with additional combustor chamber. For hydrogen fueled ITB this range is wider than for methane.

Figure 5 present the variation of engine specific thrust with the changes of high pressure turbine inlet temperature (TIT_{HPT}).

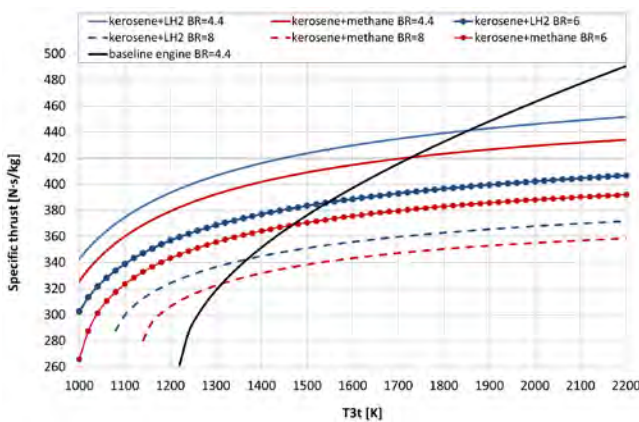


Fig. 5. TIT_{HPT} vs. specific thrust

Growth of the TIT_{HPT} cause the increasing of engine specific thrust (Fig. 5). It is noticeable that for baseline turbofan engine, thrust increase with the TIT_{HPT} is quicker

than for modified construction. In case of an engine with ITB, for lower inlet turbine temperatures higher values of ST are obtained in comparison to the baseline engine. This will significantly reduce emission of NO_x with simultaneous ensuring better engine performance. In addition temperature reduction will increase engine component life. The value of turbine inlet temperature is a design variable and is limited by material properties.

Increase in BR value result in lower specific thrust value attained by the power plant as well as lower SFC (Fig. 6).

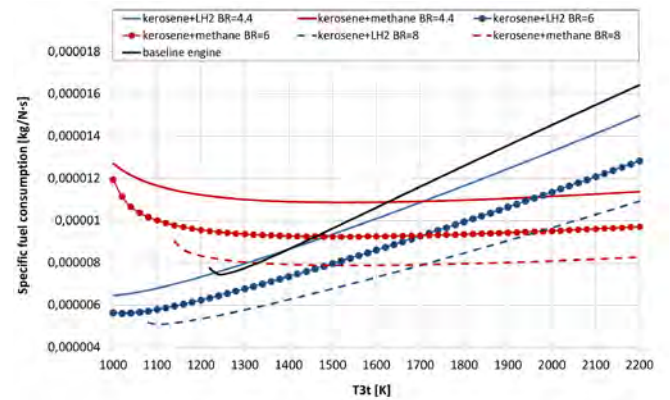


Fig. 6. TIT_{HPT} vs. specific fuel consumption

Application of alternative fuel in additional combustion chamber exert evident effect on variation of specific fuel consumption with the TIT_{HPT} changes (Fig. 6). For liquid hydrogen SFC show upward trend while for methane the graph is decreasing to a minimum at temperature about 1520 K, and then slowly increases.

For turbine inlet temperatures higher than 1700 K, the power plant with additional combustor chamber fueled by methane remains more economical than engine with ITB fueled by hydrogen and baseline engine (Fig. 6).

Figure 7 represents the relation between the specific thrust and low pressure turbine inlet temperature. The shape of the graph demonstrates the increase of engine specific thrust with low pressure turbine inlet temperature increase. Application of higher values of BR results in a reduction of specific thrust.

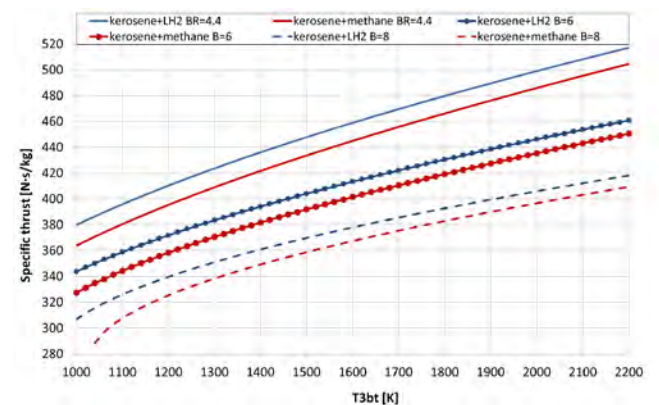


Fig. 7. TIT_{LPT} vs. specific thrust

The decrease of ST with the growth of BR is accompanied by a reduction of specific fuel consumption (Fig. 8).

The graph on Fig. 8 depict that the growth of SFC for modified engine supplied by methane is much rapid than for hydrogen.

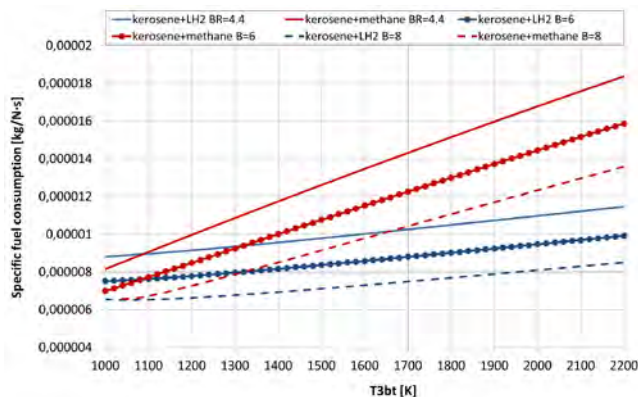


Fig. 8. TIT_{LPT} vs. specific fuel consumption

The relation between the fan pressure ratio and engine performance is presented on Fig. 9 to Fig. 10.

For the engine with an additional combustion chamber, the specific thrust as a function of fan pressure ratio is increasing relationship (Fig. 9), while the specific fuel consumption is decreasing (Fig. 10). Application of hydrogen or methane in additional combustor chamber exert visible influence on engine specific thrust in comparison to the baseline engine.

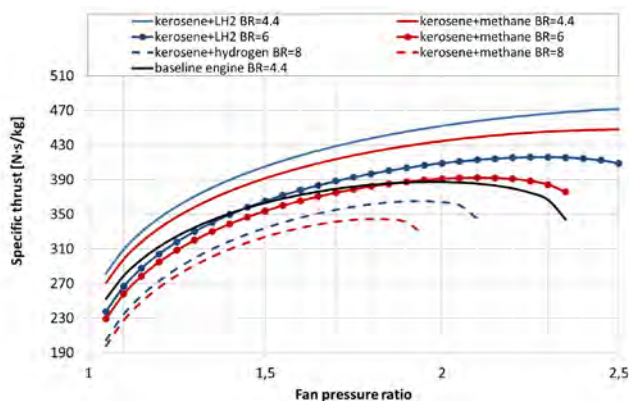


Fig. 9. Fan pressure ratio vs. specific thrust

With the growth of bypass ratio, shorter range of fan pressure ratio (FPR) can be implemented as well as lower values of specific thrust (Fig. 9) and SFC (Fig. 10) are obtained. It can be seen on Fig. 9 that the optimum of FPR decrease with increase in BR.

The course of the specific fuel consumption as a function of fan pressure ratio for the baseline engine is similar to the engine with ITB fueled by hydrogen (Fig. 10).

The engine performance parameters in function of HPC pressure ratio are presented on Fig. 11 and Fig. 12.

The graph on Fig. 11 shows that ST increase with HPC pressure ratio to achieve the maximum, and then slowly go down. For hydrogen fuel, the optimal pressure ratio is about 21 while for methane fuel about 22. For baseline engine optimal pressure ratio is about 18. SFC has a decreasing tendency (Fig. 12). For hydrogen fueled ITB the highest

values of ST are obtained with simultaneous the lowest SFC. Comparing the SFC for conventional turbofan engine and hybrid engine fueled by methane, it is noticeable that for HPC pressure ratios up to about 26, the lowest values of SFC are obtained for modified engine configuration. Opposite situation is observed for HPC pressure ratios higher than 26. The SFC curve for conventional engine is much steep while for engine with ITB fueled by methane much flatten (Fig. 12).

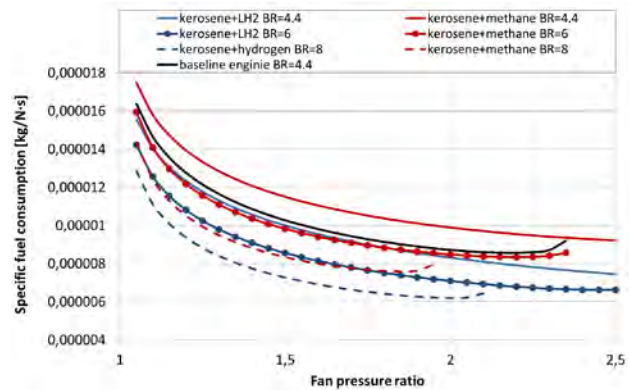


Fig. 10. Fan pressure vs. specific fuel consumption

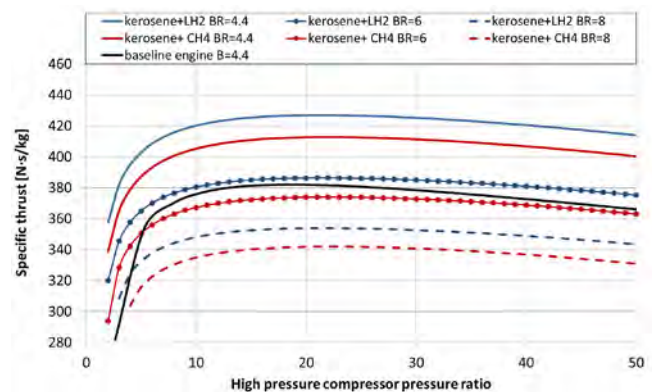


Fig. 11. HPC pressure ratio vs. specific thrust

Increasing the compressor pressure ratio (as well as overall engine pressure ratio) result in longer and heavier engine construction.

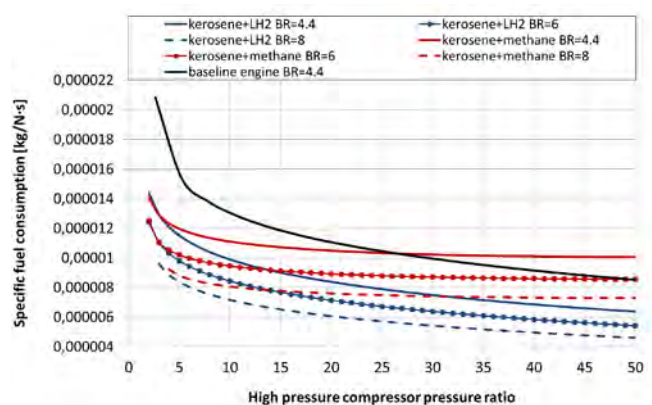


Fig. 12. HPC pressure ratio vs. specific fuel consumption

The variation of engine ST and SFC with LPC pressure ratio increase is presented on Fig. 13 and Fig. 14 respectively. Higher specific thrust values are achieved by the hybrid engine. Better performance are obtained for hybrid configuration adapted for burning hydrogen fuel (Fig. 13 and Fig. 14). It is noticeable that ST determined for baseline configuration, decrease more rapid with the growth of the LPC pressure ratio than for configuration with ITB.

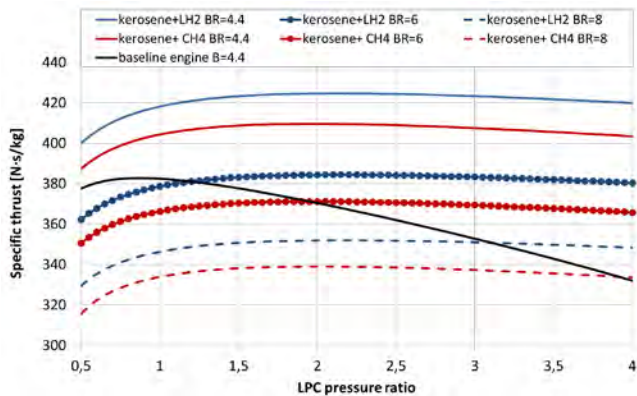


Fig. 13. LPC pressure ratio vs. specific thrust

The graph presented on Fig. 14 shows that the more efficient SFC curves were obtained for engine with hydrogen fueled ITB.

The SFC curve that present the baseline turbofan engine has got similar course like for hybrid engine with combustor chamber adapted for hydrogen fuel (Fig. 14).

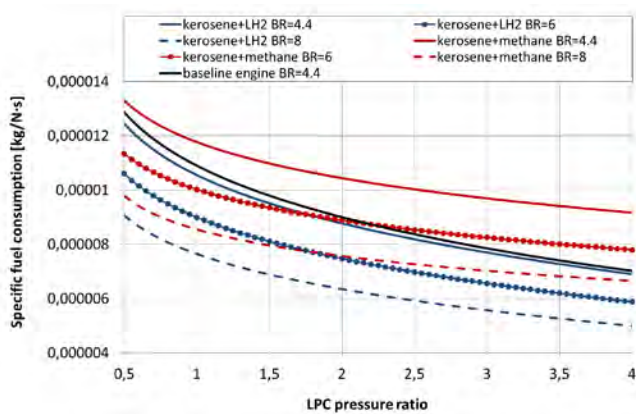


Fig. 14. LPC pressure ratio vs. specific fuel consumption

6. Summary

The significant influence on specific thrust and specific fuel consumption value has got not only a choice of alternative fuel burned in additional combustor chamber but also selection of appropriate turbine engine operating parameters. Presented work is focused on conception of turbofan engine with ITB fueled by alternative fuel – hydrogen or methane, while the main combustion chamber is supply by kerosene. Studies devoted by the scientist on ITB application in turbine engines are mostly focused on the case in which the main combustion chamber is fueled by liquid hydrogen, while second combustion chamber by biofuel or kerosene. The advantage of the adopted and presented in this paper conception is less complexity of the engine and airframe assembly. Such solution will be cheaper and easiest to implementation than application hydrogen as a fuel dedicated to the main combustion chamber. In addition application of ITB fueled by hydrogen will provide valuable data to the further researches on hydrogen fueled aircraft.

Based on analysis of the presented results, better from a performance point of view presents the engine with additional combustion chamber fueled by hydrogen. Conducted analysis indicate the possibility to reduce turbine inlet temperature significantly for engine configuration with ITB, what will permit for reduction of NO_x emission. The temperature depression result also in lengthen engine overhaul life. Generally the reduction in TIT cause the reduction in engine thrust but also in specific fuel consumption. In case of hydrogen fueled ITB the reduction in SFC is considerable than in case of methane fuel. Lower fuel consumption makes engine more economical, which is very important engine attribute that determines the choice of a given power plant and affect the range of the aircraft.

Presented advantages of using hydrogen as a fuel make the proposed hybrid engine concept very promising for future aviation.

Presented results come from the numerical simulations of engine thermodynamic cycle. Model has been elaborated based on the basic thermodynamics equations. The written code is able to predict the turbofan engine performance. Elaborated numerical model of hybrid turbofan engine require validation with data obtained during the experimental researches, conducted on the engine prototype. Model should be adjusted to the experimental data and then used for more detailed analysis. This type of advanced experimental researches are the domain of manufacturers of the largest aircraft engines and definitely go beyond the scope of the available laboratory.

Nomenclature

BR bypass ratio
 BWB blended wing body
 CTL coal to liquid
 FAR fuel to air ratio
 GTL gas to liquid
 HPC high pressure compressor
 HPT high pressure turbine
 ITB inter turbine burner

LNG liquid natural gas
 LPC low pressure compressor
 LPT low pressure turbine
 OPR overall pressure ratio
 SFC specific fuel consumption
 ST specific thrust
 T engine thrust
 TIT turbine inlet temperature

Bibliography

- [1] AL-BAGHDADI, M. An overview of hydrogen as an alternative fuel. *Encyclopedia* 2020. <https://doi.org/10.32545/encyclopedia202006.0003.v1>
- [2] BOYCE, M.P., Gas turbine engineering handbook. *Butterworth-Heinemann*. Fourth edition, 2012.
- [3] BURSTON, M., CONROY, T., SPITERI, M. et al. Conceptual design of sustainable liquid methane fuelled passenger aircraft. *20th ISPE International Conference on Concurrent Engineering*. 2013. <https://doi.org/10.3233/978-1-61499-302-5-391>
- [4] EL-SAYED, A.F. Aircraft propulsion and gas turbine engines. *CRC Press*. 2017.
- [5] GUTHE, F., HELLAT, J., FLOHR, P. The reheat concept: the proven pathway to ultra-low emissions and high efficiency and flexibility. *ASME Turbo Expo 2007: Power for Land, Sea and Air*. 2007, Montreal.
- [6] LEVY, Y., ERENBURG, V., SHERBAUM, V. et al. Development of combustor for a hybrid turbofan engine. *International Journal of Turbo and Jet Engines*. 2019. <https://doi.org/10.1515/tjj-2019-0042>
- [7] LIEW, K.H., URIP, E., YANG, S.L. et al. Performance cycle analysis of turbofan engine with interstage turbine burner. *Journal of Propulsion and Power*. 2006, **22**(2). <https://doi.org/10.2514/1.13394>
- [8] LIU, F., SIRIGNANO, W.A. Turbojet and turbofan engine performance increase through turbine burners. *Journal of Propulsion and Power*. 2001, **17**(3). <https://doi.org/10.2514/2.5797>
- [9] MARSZALEK, N. Performance analysis of turbofan engine with additional combustion chamber fueled by alternative fuel. *Combustion Engines*. 2019, **179**(4), 249-253. <https://doi.org/10.19206/CE-2019-441>
- [10] PERPIGNAN, A.A.V., RAO, A.G. Effects of chemical reaction mechanism and NO_x formation pathways on an inter-turbine burner. *The Aeronautical Journal*. 2019, **123**(1270), 1898-1918. <https://doi.org/10.1017/aer.2019.12>
- [11] RAO, A.G., YIN, F., van BUIJTENEN, J.P. A hybrid engine concept for multi-fuel blended wing body. *Aircraft Engineering and Aerospace Technology*. 2014, **86**(6), 483-493. <https://doi.org/10.1108/AEAT-04-2014-0054>
- [12] SARAVANAMUTTO, H., ROGERS, G., COHEN, H. et al. Gas turbine theory. *Pearson Prentice Hall*. England 2009.
- [13] SIRIGNANO, W.A., LIU, F. Performance increases for gas-turbine engines through combustion inside the turbine. *Journal of Propulsion and Power*. 1999, **15**(1), 111-118. <https://doi.org/10.2514/2.5398>
- [14] TANG, K., RAO, A.G., van BUIJTENEN, J.P. Conceptual study of a hybrid turbofan engine with inter turbine burner. *Proceedings of the ASME Turbo Expo 2010*. ASME. 2010, 239-248. ASME. <https://doi.org/10.1115/GT2010-22719>
- [15] VOGELER, K. The potential of sequential combustion for high bypass jet engines. *Proceedings of the International Gas Turbine and Aeroengine Congress and Exhibition*. 1998. <https://doi.org/10.1115/98-GT-311>
- [16] YIN, F., RAO, A.G. Off-design performance of an inter-stage turbine burner turbofan engine. *Journal of Engineering for Gas Turbines and Power*. 2017. <https://doi.org/10.1115/1.4035821>
- [17] YIN, F., RAO, A.G., van BUIJTENEN, J.P. Performance characteristic of a multi-fuel hybrid engine. *Proceedings of the ASME Turbo Expo 2013: Turbine Technical Conference and Exposition*. Volume 2: Aircraft Engine; Coal, Biomass and Alternative Fuels; Cycle Innovations. San Antonio, Texas 2013. ASME. <https://doi.org/10.1115/GT2013-946012012>
- [18] <https://www.acare4europe.org>
- [19] <https://www.airbus.com/company/sustainability/environment/decarbonisation.html>
- [20] <https://www.nasa.gov/centers/langley/news/factsheets/FS-2003-11-81-LaRC.html>

Natalia Marszałek, MEng. – Faculty of Fluid Mechanics and Aerodynamics, Rzeszow University of Technology.
e-mail: n.marszalek@prz.edu.pl



Energy balance comparison of small unmanned vehicle equipped with electric and hybrid propulsion system

Article presents comparison of the energetic balance of vehicle powertrain – pure electric vehicle and vehicle equipped with electric hybrid power transmission. Society is more and more often persuaded to buy electric cars as an environmentally friendly solution because they have opinion of ecological vehicles. Electrification in military applications is also widely considered, especially in case of small to medium UGV's such as wide range of robotic systems introduced to the military operations. The article presents the problems of comparing the efficiency and others parameters such as the range of a two presented powertrains. The research was carried out on an small unmanned land platform equipped with a hybrid propulsion system supplied as standard with Diesel power generator and electrically only powered. Energy used for charging of the battery, from tank-to-wheel, was calculated. This also enables to calculate total efficiency of electric and hybrid power transmission. By calculating different capacity of battery and power of generator, it is possible to determine the vehicle range.

Key words: hybrid propulsion, UGV, electric propulsion, energy balance

1. Introduction

Unmanned vehicles can patrol area, measure contamination level of the environment, deliver supplies, operate as a movable fire stand or help to evacuate wounded from danger area (Fig.1a, 1b) [12]. Military or civil use of those vehicles is more often introduced [5]. Especially, their use in military conflict region can have impact on safety of soldiers attending in this conflict.



Fig. 1. Example of use UGV vehicles: a) operating in contaminated area [14], b) firefighting unmanned system [15]

To comply its tasks, it is necessary to ensure quiet relocation and long range or long operating time in conflict area

without support. Those requirements can be met by vehicles equipped with electric or hybrid drive – power transmission system with electric engines enable to quiet operate in endangered area [7, 8]. For such operations, series hybrid transmission and its variants are become more and more often present is UGVs and other vehicles. High efficiency of electric engines cause slight thermal trace, improve undetectability by enemy forces. Electric vehicles are quite simple in use and in construction. Mostly they propulsion system consist of battery, electric engine with controller. This simplicity is important in many operations but because of small capacity of the battery, still insufficient volumetric and mass factors and its ability of caught fire. Battery operated vehicles disadvantages turn many researchers to give attention to hybrid propulsion, especially series with small power generator. Vehicles, equipped with power generator, enable to load battery and increase range and operation time without need of fast come back to the base [11]. Because fuel deliveries can be interrupted by different reasons, for instance in warfare conditions, or others aspects such as economical or ecological, this solution can be useful in military vehicles. Such construction can use different fuels besides Diesel. For example, vehicles could use other fuels such as F-34 which is introduced as a unified battlefield fuel [2] or different mixtures of fuels that will work with CI engines. Because mentioned fuels have different parameters, they will impact to the engine parameters. Requirements for unmanned vehicles, especially their power transmission, is not easy to achieve. Costs of production and total mass of vehicle are contradictory to use cheap but heavy electrochemical batteries. Long range require use of high energy density of power sources but combustion engines are noisy and emitting a lot of thermal radiation (easy to detect). Other aspects are for example: compatibility with existing infrastructure (combustion engines), fast recharging (combustion engines) [1, 6] etc. Most foredesigns exclude of use one or other solution, other technology. It is necessary to take under consideration a tank-to-wheel (and battery-to-wheel) energy balance in efficiency and vehicle's mobility point of view.

2. Vehicle's investigated power transmission

Power transmissions of the investigated vehicles came from small unmanned ground vehicle (Fig. 2a) of total mass 500 kg, LiFePO₄ battery pack and six independent driving modules which were assembled with electric engine, inverter and transmission gears, wheel and shock absorber. Each module was connected to the 48 VDC battery pack (Table 1).



Fig. 2. a) investigated UGV with power transmission during tests, b) Diesel engine for vehicle's power generator [16]

Power transmission system was installed inside the hull of the vehicle. Vehicle itself is more widely described in [3, 9, 10]. For tests two variants of vehicle's powertrain were examined, electric and with small Diesel power generator (Fig. 2b). In result, second variant of power propulsion system was designed as a serial hybrid called range extender or REX. It was assumed, that for electric propulsion, battery will have higher capacity, equal to the mass of power generator (Fig. 3). Operating range of unmanned ground vehicle and its power transmission systems were then examined.

Table 1. Vehicle's power transmissions main components parameters

| Component | Electric propulsion | Hybrid propulsion |
|-----------------|---------------------|-------------------|
| Electric engine | 6 × 2.8 kW, PMS | 6 × 2.8 kW, PMS |
| Battery | 210 Ah@48 VDC | 70 Ah@48 VDC |
| Power generator | – | 5.5 kVA |
| Fuel tank | – | 5 dm ³ |

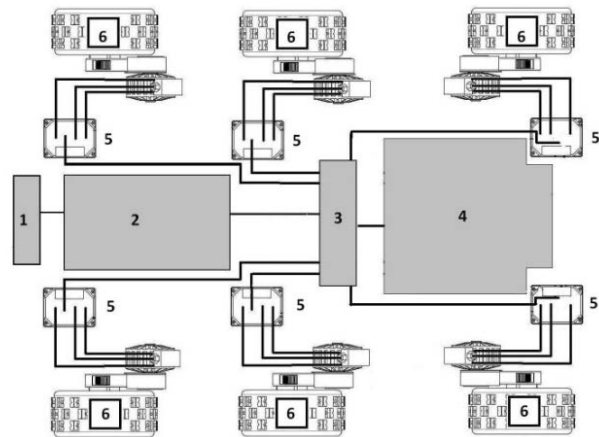


Fig. 3. Schematic connections of hybrid power propulsion: 1) steering system, 2) power generator, 3) junction box, 4) battery, 5) inverters, 6) driving modules with electric engines, wheels and gears

3. Laboratory testing of electric and hybrid power transmission

The main goal of laboratory tests of electric and hybrid power transmission system of UGV was to determine energy balance of this systems after integration and installation on a vehicle hull. Test was held on stands belonging to combustion engines laboratory of Military University of Technology. Range of the tests included:

- measurements of lithium LiFePO₄ battery charging and discharging efficiency,
- measurements of power generator efficiency,
- measurements of electric engines efficiency of vehicle,
- measurements of power transmission efficiency.

Based on efficiency of particular elements of power transmission systems and fuel calorific value, fuel consumption, energetic balance of unmanned vehicle was calculated and determined.

3.1. Test stands

During tests, five stands were used:

- LiFePO₄ battery charging test stand (Fig. 4). A stand for measuring charging characteristics of battery while charging process.



Fig. 4 Charging test stand: 1 – power generator, 2 – current-voltage parameters acquisition system, 3 – constant-current power station, 4 – battery

- LiFePO₄ battery discharging stand (Fig. 5). Test stand for measuring discharging parameters of battery enable to set discharging characteristics under different loads.

For battery load, water resistor was build. This type of resistor enable fast and simple operation of resistor, by submerge metal plates of resistor in wear. Discharging current could be increased by increasing number of metal plates or water additives. Battery was equipped with voltage sensors.

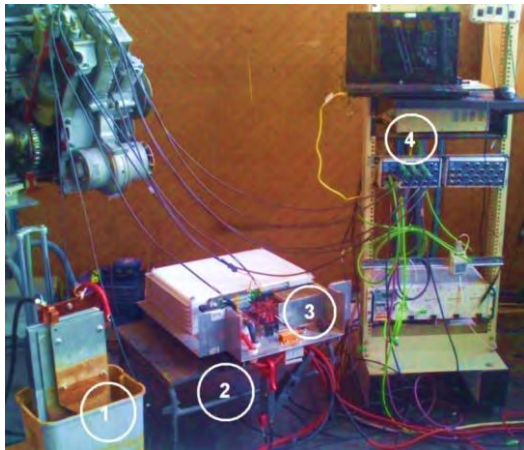


Fig. 5. Battery discharging test stand: 1) water resistor, 2) current clamps, 3) battery with voltage sensors, 4) acquisition computer

– electric engines test stand (Fig. 6). On this stand, changes of the engine torque were measured if function of engine speed. Investigated engine was mounted on a dyno stand and connected through the clutch with dyno. Engine mounted on the stand worked as a dynamometer. On his housing, force meter was mounted and force was measured. Examined engine was connected to the inverter and inverter was connected to the power supply. Current and voltage sensors were connected to the acquisition card and computer. Speed of the engine was measured by speed encoder connected to the acquisition card.



Fig. 6. Electric engines test stand: 1) acquisition equipment 2) electric engine, 3) force sensor, 4) acquisition hardware, 5) current inverter, 6) electric engine of the dyno stand

– power generator characteristic determination test stand. This stand was equipped in similar instrumentation as during battery charging, but with extra load for generator. Load characteristic of the power generator was determined, after connecting load to the generator.

– power transmission internal resistances test stand (Fig. 7). Measurements of internal resistance of the power transmission was made after lifting vehicle by warehouse truck to loose contact between wheels and ground. Speed was increased in stages to the maximum and then decreased to the wheels stop. Rotation velocity of the wheels was set by voltmeters indication, placed next to the controller (Fig. 8).



Fig. 7. Internal resistance measurements



Fig. 8. Connected voltmeters for speed verification

4. Energetic balance comparison of the power transmissions

To determine energetic balance, calorific value of the Diesel oil was determined as 43 MJ/kg. Total energy of a single charging process of the battery was equal to 50.282 MJ/kg, and came from fuel of 1.15 kg. Energy from fuel powered generator and charged battery with power 10.555 MJ/kg, after sweep to electric energy, this mean the efficiency is equal to 21% with specific fuel consumption of 300 g/kWh (Fig. 9), what is satisfied value in small Diesel engines.

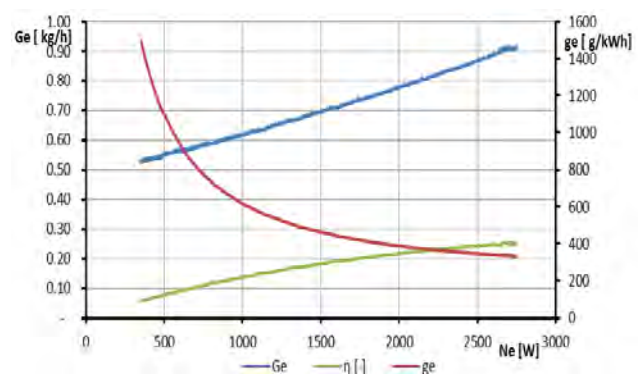


Fig. 9. Load characteristic of power generator

Charging the battery need 9.65 MJ of energy (Fig. 10). During discharging process, the energy level reaches 9.0 MJ of energy. Calculations leads to the assumption that such amount of energy should provide power for travelling distance of 16 km with speed of 5 km/h. Fuel tank capacity enable to charge the battery more than three times to its full capacity. This enables to reach distance over 65 km with fully charged battery at the beginning.

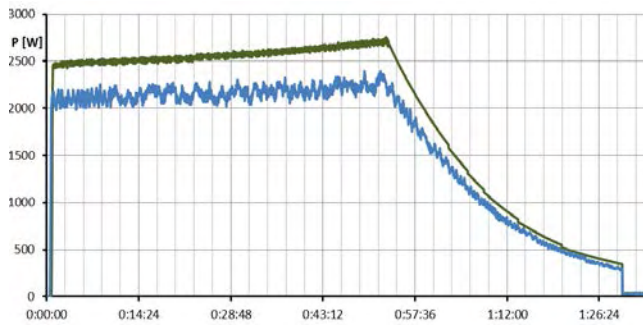


Fig. 10. Charging power of the battery (blue line) and electric power of the generator (green line)

Theoretical efficiency of each vehicle’s module (from engine to wheel) should reach ca. 90%. Because of the quality of components (the vehicle is technology demonstrator) efficiency of driving modules reaches 75% averages.

Efficiency of energy conversion from chemical energy of fuel to the energy converted for wheels powering is quite small. It is caused mostly by low efficiency of combustion engine that power the generator. It is small, naturally aspirated one cylinder compressed ignition engine. His internal resistance is big if compare to power produced. Efficiency of power transmission powered from battery is bigger and reach 70%. Total efficiency of hybrid power transmission, when combustion engine was turned on, reaches 13.6% (from tank to the wheel). It is important to know, that power generator can work temporary, when its need and do not cover all energetic needs of vehicle. That means total efficiency must be seen partly as a efficiency of the hybrid with power generator and partly as a electric transmission.

Power consumed by the vehicle in different road conditions (speed, quality and type of the surface), and parameters of the power transmission, enable to determine range of the vehicle and speed of the vehicle with power generator.

Based on results of charging and discharging of the hybrid power transmission battery, measurements of internal resistances, energetic parameters of the power transmission and energetic balance were determined. Based on that calculation, it was possible to determine range of the vehicle. During calculations, internal resistances were took into account. Results were presented in Table 2.

Nomenclature

- BEV battery electric vehicle
- CI compressed ignition
- CNG compressed natural gas
- G_e fuel consumption [kg/h]
- g_e specific fuel consumption [g/kWh]
- HEV hybrid electric vehicle

Table 2. Efficiency of power transmission subassemblies

| Component | Energy | Average efficiency |
|-----------------------------|----------|--------------------|
| Fuel | 50.28 MJ | – |
| Battery (hybrid) | 9 MJ | 94% |
| Battery (electric) | 26.8 MJ | 95% |
| Power generator | 10.56 MJ | 21% |
| Electric average efficiency | | 70% |
| Hybrid average efficiency | | 13.6% |

Vehicle powered only from the power generator, enable to charge the battery in time of 93 minutes. During driving this time is elongated, because some part of the energy is consumed by the wheels of the moving vehicle. This time can be elongated or if road resistance will be higher than power generated, battery will never be fully charged. In case of totally discharged or damaged battery, maximum vehicle speed is about 20 km/h, when moving on a concrete or asphalt, without charging.

Efficiency of pure electric transmission is higher than hybrid, but if battery mass will be equal to the mass of battery and power generator, traveling distance of such vehicle will be smaller ca 25%. It is important to know that increasing the mass (and volume) of the battery will cause mass of vehicle’s components increase (up to 40% of battery mass) [13].

5. Conclusions

1. Laboratory tests of power transmission subassemblies enable verification of their characteristics and parameters. Battery parameters measurements enable to estimate vehicle’s range in different driving modes.
2. Energetic parameters were set of two investigated power transmissions. Efficiency of the energy consumption in pure electric drive was ca. 70%. A set of batteries with mass equal to the mass of the power generator enable to drive distance of ca. of 45 km with speed of 5 km/h. In hybrid power transmission, efficiency with working power generator drops down up to 13.6%. Fuel tank capacity enable to charge the battery more than three times to its full capacity. This enables to travel distance over 65 km on a flat surface.
3. During one charging cycle (93 minutes) generator used 1150 g of fuel, which means, that extra 3.5 kg of fuel can double the traveling distance in respect to the extra 180 kg of battery (plus ca. 40% mass of battery for strengthened vehicle structure).
4. Energetic balance efficiency of pure electric power transmission is much higher (ca. 70%) than efficiency of serial hybrid transmission with turned on power generator (ca. 13%), but travelling distance of hybrid transmission vehicle was ca. 25% higher.

Bibliography

- [1] FLUDER, K., PIELECHA, I., CIEŚLIK, W. The impact of drive mode of a hybrid drive system on the energy flow indicators in the RDE test. *Combustion Engines*. 2018, **175**(4), 18-25. <https://doi.org/10.19206/CE-2018-403>
- [2] KARCZEWSKI, M., SZCZĘCH, L. Influence of the F-34 unified battlefield fuel with bio components on usable parameters of the IC engine. *Eksploatacja i Niezawodność – Maintenance and Reliability*. 2016, **8**(3), 358-366. <https://doi.org/10.17531/ein.2016.3.6>
- [3] KARCZEWSKI, M., SZCZĘCH, L., POLAK, F. Energetic balance of unmanned ground vehicle hybrid power transmission. *Journal of KONES Powertrain and Transport*. 2018, **25**(2). <https://doi.org/10.2478/kones-2019-0094>
- [4] KARCZEWSKI, M., SZCZĘCH, L., POLAK, F. Energetic balance of unmanned ground vehicle. *Journal of KONES Powertrain and Transport*. 2019, **25**(2). <https://doi.org/10.5604/01.3001.0012.2797>
- [5] LOPEZ, R., DARPA Develops tactical robots for dirty and dangerous missions. unmanned systems. 2001, 12-13.
- [6] PIELECHA, I., CIEŚLIK, W., FLUDER, K. Analysis of energy management strategies for hybrid electric vehicles in urban driving conditions. *Combustion Engines*. 2018, **173**(2), 14-18. <https://doi.org/10.19206/CE-2018-203>
- [7] POLAK, F., WALENTYNOWICZ, J. Problemy doboru zespołów układu napędowego do małego taktycznego pojazdu bezzałogowego. *Journal of KONES Powertrain and Transport*. 2007, **14**(4), 343-350.
- [8] POLAK, F., SZCZĘCH, L. Driving module of the unmanned vehicle. *Journal of KONES Powertrain and Transport*. 2011, **18**(1).
- [9] POLAK, F., SZCZĘCH, L., WALENTYNOWICZ, J. Napęd lekkiej platformy bezzałogowej do działań w terenie zurbanizowanym. *Technologie podwójnego zastosowania, Wybrane Technologie Wojskowej Akademii Technicznej* (red.). Najgebauera, A. WAT, Warszawa 2012.
- [10] POLAK, F., SZCZĘCH, L. Propulsion module for unmanned vehicle. *Journal of KONES Powertrain and Transport*. 2011, **18**(1).
- [11] REDELBACH, M., ÖZDEMİR, E.D. Optimizing battery sizes of plug-in hybrid and extended range electric vehicles for different user types. *Energy Policy*. 2014, **73**, 158-168. <https://doi.org/10.1016/j.enpol.2014.05.052>
- [12] RYBAK, P., WYSOCKI, J., HRYCIÓW, Z. et al. Experimental research on identifying data for modelling special purpose vehicles. *Journal of KONES Powertrain and Transport*. 2017, **24**(3). <https://doi.org/10.5604/01.3001.0010.3086>
- [13] SANDY, T.C.E. Sustainable transportation options for the 21st century and beyond. Appendix A: Range limitations of battery electric vehicles. *Springer International Publishing*. Switzerland 2015. <https://doi.org/10.1007/978-3-319-16832-6>
- [14] www.altair.com.pl access: 2015.05.17
- [15] <https://www.fireapparatusmagazine.com/2014/06/24/pg06/#gref> access: 2020.04.14
- [16] <https://www.yanmar.com/us/> access: 2020.05.21

Filip Polak, DEng. – Faculty of Mechanical Engineering, Military University of Technology.
e-mail: filip.polak@wat.edu.pl



Soot contamination of engine oil – the case of a small turbocharged spark-ignition engine

The paper presents the results of thermogravimetric tests of engine oil used in a small turbocharged spark-ignition engine. The main observation from the research was a significant soot contamination of engine oil, that appears even at its low mileage. This indicates that also in the case of port fuel injection spark-ignition engine, high particulate matter emissions may occur. A rapid soot contamination of the oil in this engine indicates that the oil change interval should be shortened.

Key words: engine oil, thermogravimetric analysis, soot, particulate matter, spark-ignition engine

1. Introduction

Internal combustion engines will be primary drive source for many years, probably decades. Thus, it is clearly important to perform research and development to provide a better understanding of the fundamental processes affecting engine efficiency and the production of undesirable emissions [9].

The combustion of real fuels in a real engine is always imperfect. This results in the presence of incomplete combustion products in the exhaust gas. One of these components is particulate matter (PM), consisting of inter alia soot. Particulates belong to the most harmful components of exhaust gases [11].

Particulate matter emissions are primarily considered from the perspective of diesel engines. The process of reducing particulate emissions in engine exhaust has been going on for many years. For many years as well, PM emissions from passenger cars with spark-ignition engines were not limited at all. Currently, the PM limit applies only to direct injection gasoline engines (GDI) and is the same as for diesel engines (Table 1).

Table 1. European emission standards on PM emissions for passenger cars (category M), g/km [2]

| | Effective from (first registration) | Diesel | Spark-ignition |
|--------------|-------------------------------------|--------|----------------------|
| Euro 1 | January 1993 | 0.14 | – |
| Euro 2 | January 1997 | 0.08 | – |
| Euro 3 | January 2001 | 0.05 | – |
| Euro 4 | January 2006 | 0.025 | – |
| Euro 5a | January 2011 | 0.005 | 0.005 ^{*)} |
| Euro 5b | January 2013 | 0.0045 | 0.0045 ^{*)} |
| Euro 6b | January 2015 | 0.0045 | 0.0045 ^{*)} |
| Euro 6c | January 2018 | 0.0045 | 0.0045 ^{*)} |
| Euro 6d-Temp | January 2019 | 0.0045 | 0.0045 ^{*)} |
| Euro 6d | January 2021 | 0.0045 | 0.0045 ^{*)} |

^{*)} Applies only to vehicles with direct injection engines

Port fuel injection (PFI) gasoline engines are considered to emit little particulate matter. Presented by Liang et al. [7] tests of two Euro 4 cars (the same model) with GDI and PFI engines showed that over the NEDC cycle the PM emission for a car with an MPI engine was 3 mg/km, and for this with a GDI engine as much as 14 mg/km.

Most of the particulate matter (soot) formed in the engine's combustion chamber is removed with the exhaust gases, but some of it is also absorbed in the engine oil. It is easy to notice that as engine oil is used, it changes its color to darker, which is caused inter alia by increase in soot content. There is no doubt that the amount of soot in oil depends both on the intensity of soot formation in the engine's combustion chamber, as well as on the mileage of the oil. Thus, the soot content of engine oil at a given mileage is to some extent an indicator of the tendency of a given engine to smoke. The soot content increases with increasing oil mileage and can reach level of several percent. At this concentration, soot significantly changes (worsens) the lubricating properties of engine oil.

Increasing the soot content in the oil increases engine wear. Results described in [4] show that soot interacts with oil additives reducing the oil's anti-wear properties possibly by abrasive wear mechanism. Ball-on-flat-disk type tests also revealed the increased wear due to the presence of soot. Scanning electron microscope studies of wear scar diameters suggest that soot is abrasive.

Similar research results are presented in [5]. Cumulative wear was more for samples with soot contamination. A negative impact of soot on wear was already observed at 2% soot in engine oil. Oil samples with low dispersant and high zinc dithiophosphate (ZDP) content performed better than samples having high dispersant and low ZDP concentrations at high soot levels. The reason behind this could be the fact that high dispersant levels together with soot contamination results in lubricant thickening resulting in increased wear.

By worsening the lubrication conditions, soot contained in the oil also increases fuel consumption. Although it is not a very significant impact, it cannot be ignored at present when seeking maximum fuel savings and striving to minimize CO₂ emissions. According to [8] low friction lubricants provide fuel savings of around 0.5%.

The aim of the tests described in this article was to check the soot content in the engine oil of a small turbocharged spark ignition engine used in a mini city car. The soot content in this oil will allow concluding on the tendency of this engine to emit particulate matter. It will also indicate if the original oil change interval of 15,000 km is appropriate taking into account oil contamination.

2. Test apparatus and procedures

The tests were carried out on oil used in a small turbocharged spark-ignition engine driving mini city car Smart. Some technical data and key features of the Smart's engine are shown in Table 2. The tested oil was grade: 5W-30 ACEA A3/B4 API SL. It was oil designed for engines operating in start-stop mode. Fresh oil and used oils collected after 5000 km and 8000 km after oil change were used in the tests. Table 3 shows some key parameters of the fresh oil.

Table 2. Technical data/key features of SMART's engine

| | |
|------------------------|--|
| Engine code | M160 E07 LA |
| Engine type | Spark ignition, in-line three |
| Displacement | 0.698 dm ³ |
| Bore/stroke | 66.5 mm/67 mm |
| Compression ratio | 9.5 |
| Maximum power | 46 kW@5250 rpm |
| Maximum torque | 95 Nm@2000–4000 rpm |
| Valvetrain | Single overhead camshaft, 2 valves per cylinder |
| Injection system | Multipoint sequential injection, max injection pressure 4.8 bar |
| Ignition | Dual ignition – 2 spark plugs per cylinder |
| Forced induction | Turbocharging with intercooling |
| Charge air control | Map-guided |
| Exhaust aftertreatment | Three-way catalytic converter |
| Emissions standard | Euro 4 |
| Engine oil capacity | 3 dm ³ |

Table 3. Characteristics of the fresh engine oil [1]

| Name | Method | Units | Value |
|----------------------------|---------------------------|--------------------|-------|
| Density @ 15°C | ASTM D4052 | g/ml | 0.855 |
| Kinematic viscosity @100°C | ASTM D445 | mm ² /s | 12.0 |
| Viscosity, CCS –30°C (5W) | ASTM D5293 | mPa·s | 6400 |
| Kinematic viscosity @40°C | ASTM D445 | mm ² /s | 73 |
| Viscosity index | ASTM D2270 | – | 161 |
| Pour point | ASTM D97 | °C | –43 |
| Flash point, PMCC | ASTM D93 | °C | 201 |
| Ash, sulphated | ASTM D874 | % (m/m) | 1.3 |
| Grade | 5W-30, ACEA A3/B4, API SL | | |

Thermogravimetric characteristics of oils were determined using a PerkinElmer thermogravimetric analyzer TGA 8000. Thermogravimetric analyzer (abbreviation: TGA) measures the change in mass of the sample as it is heated, cooled, or held at a constant temperature in a controlled atmosphere. Table 4 shows the characteristics of TGA 8000 and Fig. 1 shows the picture of TGA 8000. Figure 2 presents a sample of the used engine oil just before the start of the test, placed on the autosampler of the TGA 8000 analyzer (visible black oil color).

Thermogravimetric characteristics of the tested oils were determined according to the temperature program based on the temperature program described in the ASTM D5967 standard. ASTM D5967 is a test method which covers engine test procedures for evaluating diesel engine performance characteristics including viscosity and soot concentrations. Annex A4 is a recommendation on how to measure soot in engine oils. Details of the thermogravimetric analyzer working conditions during the tests are presented in Table 5. Pyris software version 13.3.1 was used to analyze the obtained results.

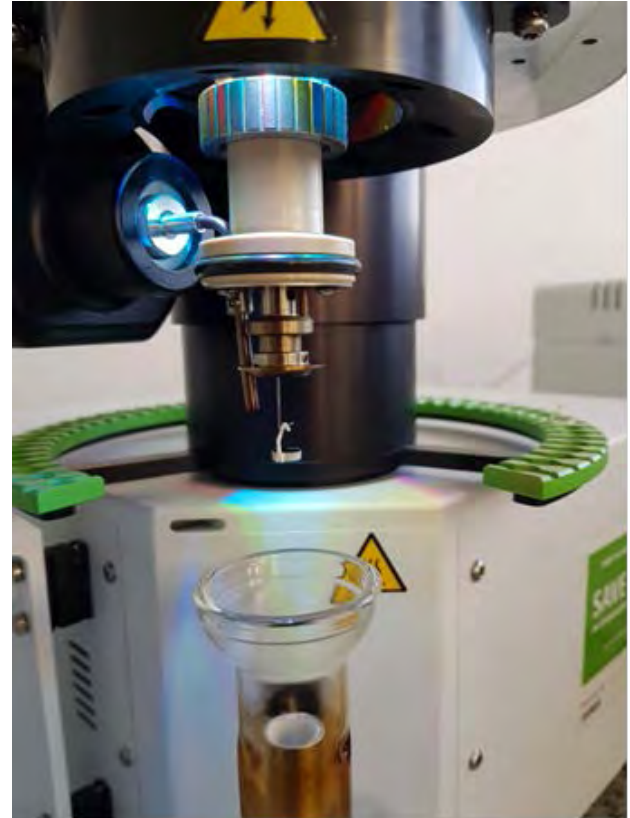


Fig. 1. PerkinElmer thermogravimetric analyzer TGA 8000

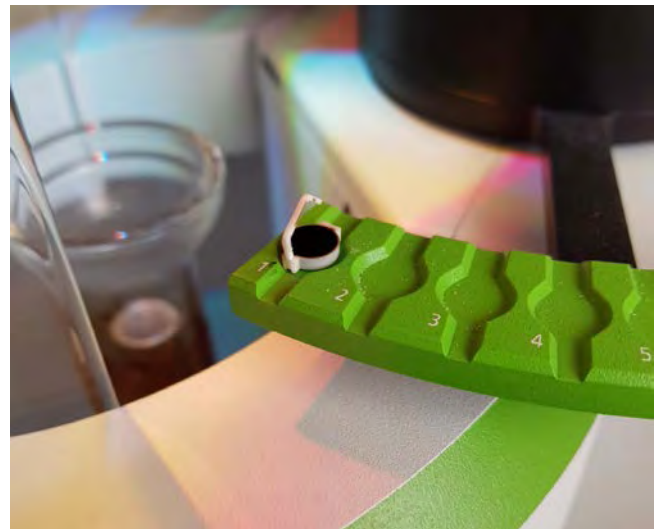


Fig. 2. Sample of used engine oil placed on the autosampler of TGA 8000 analyzer

Table 4. Specifications of TGA 8000 thermogravimetric analyzer used in the research

| | | |
|-------------|--------------------|--|
| Design | | A vertical design with a high sensitivity balance and quick response furnace. The balance is located above the furnace and is thermally isolated from it. A precision hang-down wire is suspended from the balance down into the furnace. At the end of the hang-down wire is the sample pan. The sample pan's position is reproducible. |
| Balance | Sensitivity | 0.1 µg |
| | Capacity | 1300 mg |
| | Accuracy | better than 0.02% |
| | Precision | 0.01% |
| Temperature | Furnace | Low mass (< 10 g); Platinum heating element with ceramic protective coating; resistant to inert and oxidative gas over the full temperature range. |
| | Range | -20°C to 1200°C |
| | Scan rates | 0.1°C/min to 500°C/min |
| | Precision | ±1°C |
| Cooling | Method | Forced air cooled with an external fan |
| | Cycle time | 1100°C to 50°C < 13 min |
| Sample Pans | | Platinum or ceramic (60 µL) |
| Atmosphere | Sample environment | Static or dynamic, including nitrogen, argon, helium, carbon dioxide, air, oxygen, or other inert or reactive gases. Analyses done at normal or reduced pressures. |
| | Gas control | Balance purge (mass-flow controlled); Sample purge (switch between 2 gases; mass-flow controlled); Reactive purge. |
| | Gas mixing | Up to 3 gases |
| | Vacuum | 10 ⁻⁵ Torr |
| Autosampler | | 48-position |

Table 5. TGA experimental conditions

| Instrument conditions | ASTM D5967 Annex A4 [10] | Conditions applied in this research |
|-----------------------|--|---|
| Temperature program | 1. Hold for 1 min at 50°C 2. Heat from 50°C to 550°C at 100°C/min 3. Hold for 1 min at 550°C 4. Heat from 550°C to 650°C at 100°C/min 5. Heat from 650°C to 750°C at 100°C/min 6. Hold for 5 min at 750°C | 1. Hold for 4 min at 50°C 2. Heat from 50°C to 550°C at 50°C/min 3. Hold for 2 min at 550°C 4. Heat from 550°C to 650°C at 10 °C/min 5. Heat from 650°C to 750°C at 10°C/min 6. Hold for 15 min at 750°C |
| Pan type | Platinum | Ceramic |
| Balance purge | 40 ml/min | 60 ml/min |
| Sample purge | N ₂ , 30 ml/min for step 1 to 4 O ₂ , 30 ml/min for step 5 and 6 | N ₂ , 40 ml/min for step 1 to 4 air, 40 ml/min for step 5 and 6 |
| Sample quantity | Around 10 mg | Around 20 mg |

3. Test results and discussion

The thermogram for fresh oil is shown in Fig. 3. Fig. 4, in turn, shows comparative thermograms of fresh oil and used oils – after 5 and 8 thousand kilometers. As can be seen from this comparison, the thermogram curves are similar in all cases, however, the distillation of fresh oil takes place in the narrowest temperature range (the curve is steeper). This confirms the correctness of the measurements carried out. For used oils, it can be seen that the visible weight loss during the thermogravimetric test starts at a lower temperature. This indicates that as oil mileage increases, its fuel contamination increases. At the same time, it is noted that the used oils contain more substances with high boiling points. These substances are the result of oil decomposition at high temperatures in the engine. Fresh oil contains practically no components with a boiling point higher than 450°C.

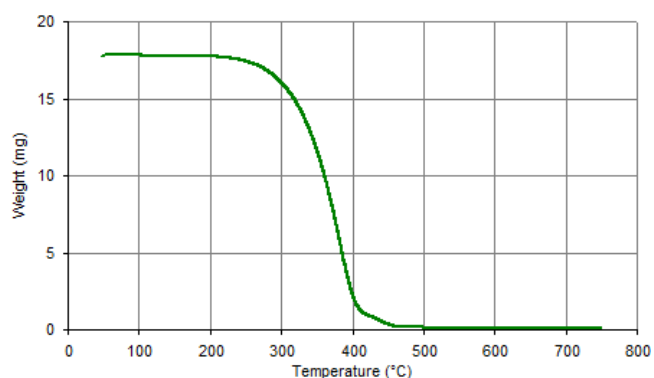


Fig. 3. Thermogram of fresh engine oil obtained during the temperature program presented in the Table 5

The main aim of thermogravimetric tests was to determine the soot content of fresh and used engine oils. Looking at the engine oil thermogram – the first weight loss that occurs as the sample is heated is the evaporative loss of the lubricating oil and any other volatile materials present. All that remains will be soot and other solid residues present in the sample. Switching the purge gas from nitrogen to oxygen or air will remove any soot present in the sample. The calculation of soot content was performed for the weight loss that commences after switching over the purge gas from nitrogen to oxygen or air at 650°C up to the temperature where constant residue was obtained around 750°C [3].

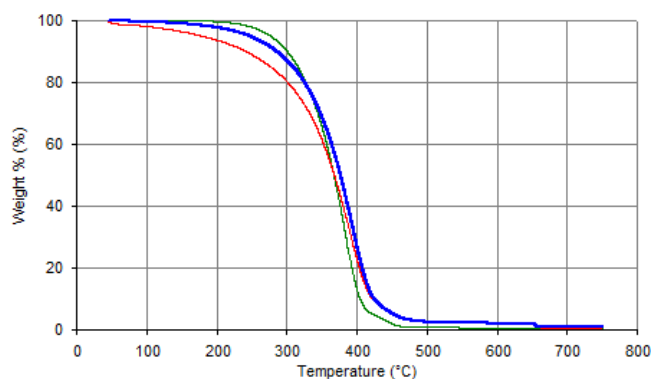


Fig. 4. Comparison of thermograms of fresh (green curve) and used oils (blue curve – mileage of 5000 km and red – 8000 km)

Figures 5–7 show enlarged parts of the thermograms for fresh and used oils, as well as the decrease in sample mass under conditions of oxidizing atmosphere. This weight loss corresponds to the soot content in engine oil. As can be seen in Fig. 4, fresh oil does not contain any soot at all. Engine oil after 5000 km already contained about 1% (m/m) soot, and after 8000 km about 1.5% (m/m).

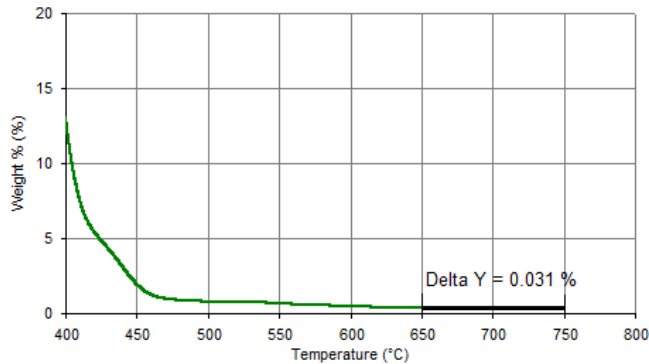


Fig. 5. Thermogram showing percentage soot content in the fresh engine oil sample

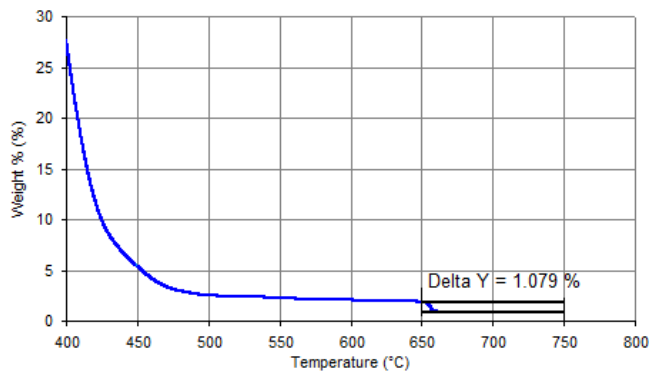


Fig. 6. Thermogram showing percentage soot content in the used engine oil sample (oil mileage: 5000 km)

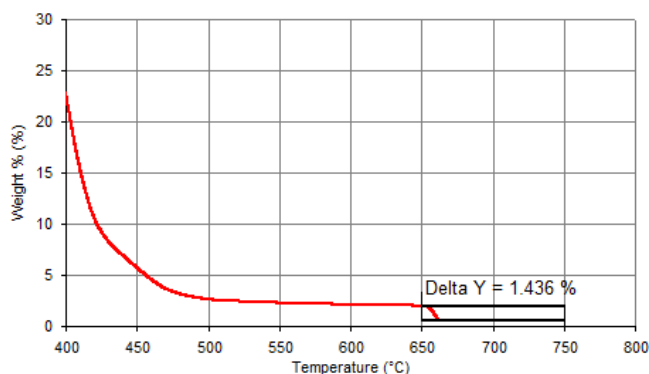


Fig. 7. Thermogram showing percentage soot content in the used engine oil sample (oil mileage: 8000 km)

It should be pointed out that the soot content found is, for a spark-ignition engine, powered in a PFI system, surprisingly large. The more so that the oil has not yet reached the qualifying mileage for its change (15,000 km). These values even exceed the soot content of used diesel engine oils. For example, in the tests of oils from four passenger cars with diesel engines presented by Skoczylas [12] it was found that in the case of good technical condition of the engine (low oil consumption), the content of soot in used oil does not exceed 1% (m/m). Similar results were obtained by author for an oil with a mileage of 16,000 km from a turbocharged diesel engine with a capacity of 3.0 dm³ [6].

It seems that the main reason for this situation (high soot contamination) was a turbocharger working in the forced induction system of the engine and very dynamic (unfavorable) conditions of engine operation – only urban traffic conditions. It is very important that as it turns out also a spark-ignition engine in good technical condition can be a source of high particulate matter emissions.

Assuming a linear increase in soot content, at 15,000 km mileage (oil change period) it will be around 3% (m/m). This value is definitely unfavorable when it comes to the oil's lubricating role.

4. Conclusions

The results described in this article relate to the determination of thermogravimetric characteristics and soot content in engine oil from a small turbocharged spark-ignition engine. It should be noted that the tests described in the article are tests of the oil from one car only. However, the authors do not know any reason that could diminish the credibility of the obtained test results. There was no indication that the engine was in poor condition. The engine did not consume oil. The tests conducted first of all lead to interesting conclusions regarding the content of soot in oil.

Firstly, the spark-ignition engine powered in the PFI system can generate large amounts of soot, and thus emit a large mass of particle matter. It seems that in the present case this is due to the design of the engine and its operating conditions. The results should be verified by measuring PM emissions from this engine, which is a part of the planned further tests. It may therefore turn out that the small city car can be more harmful to the environment than much larger vehicles.

Secondly, another important observation is that the recommended oil change interval – 15,000 km – for this engine (vehicle) is too long. Rapidly increasing soot oil contamination causes deterioration of oil lubricating properties and contributes to increased abrasive wear of the engine. Given the soot content of oil, this period should be reduced by up to half.

Nomenclature

ACEA European Automobile Manufacturers' Association
 API American Petroleum Institute
 ASTM American Society for Testing and Materials
 GDI gasoline direct injection
 NEDC New European Driving Cycle

PFI port fuel injection
 PM particulate matter
 TGA thermogravimetric analyzer
 ZDP zinc dithiophosphate

Bibliography

- [1] Castrol MAGNATEC Stop-Start 5W-30 A3/B4. [https://msdspds.castrol.com/bpplis/FusionPDS.nsf/Files/F9CDF2948AC20BD38025838D00576749/\\$File/BPXE-A7YAVM.pdf](https://msdspds.castrol.com/bpplis/FusionPDS.nsf/Files/F9CDF2948AC20BD38025838D00576749/$File/BPXE-A7YAVM.pdf)
- [2] DELPHI Technologies. 2019-2020 Worldwide emissions standards – passenger cars and light duty vehicles. <https://www.delphi.com/sites/default/files/2019-05/2019-2020%20Passenger%20Car%20&%20Light-Duty%20Vehicles.pdf>
- [3] DESHMUKH, P. Soot content determination of in-service lubricants of diesel engine as per ASTM D5967 Annex A4. Perkin Elmer Application Note – Thermal Analysis. [https://www.perkinelmer.com/lab-solutions/resources/docs/APP_Soot_Content_Determination_Diesel_Engine\(012934_A_01\).pdf](https://www.perkinelmer.com/lab-solutions/resources/docs/APP_Soot_Content_Determination_Diesel_Engine(012934_A_01).pdf)
- [4] GAUTAM, M., CHITTOOR, K., DURBHA, M. et al. Effect of diesel soot contaminated oil on engine wear — investigation of novel oil formulations. *Tribology International*. 1999, **32**(12), 687-699. [https://doi.org/10.1016/S0301-679X\(99\)00081-X](https://doi.org/10.1016/S0301-679X(99)00081-X)
- [5] GEORGE, S., BALLA, S., GAUTAM, M. Effect of diesel soot contaminated oil on engine wear. *Wear*. 2007, **262**(9-10), 1113-1122. <https://doi.org/10.1016/j.wear.2006.11.002>
- [6] KOZAK, M. A comparison of thermogravimetric characteristics of fresh and used engine oils. *Combustion Engines*. 2019, **178**(3), 289-292. <https://doi.org/10.19206/CE-2019-350>
- [7] LIANG, B., GE, Y., TAN, J. et al. Comparison of PM emissions from a gasoline direct injected (GDI) vehicle and a port fuel injected (PFI) vehicle measured by electrical low pressure impactor (ELPI) with two fuels: Gasoline and M15 methanol gasoline. *Journal of Aerosol Science*. 2013, **57**, 22-31. <https://doi.org/10.1016/j.jaerosci.2012.11.008>
- [8] NATIONAL RESEARCH COUNCIL. Assessment of fuel economy technologies for light-duty vehicles. The National Academies Press, Washington 2011. <https://doi.org/10.17226/12924>
- [9] REITZ, R. Grand challenges in engine and automotive engineering. *Frontiers in Mechanical Engineering*. 2015, **1**, 1-3. <https://doi.org/10.3389/fmech.2015.00001>
- [10] SATPUTE, Y. Estimation of soot content in engine oil using Thermo Gravimetric Analysis (TGA) as per ASTM D5967 Method. Perkin Elmer Application Note – Thermal Petro. http://www.perkinelmer.com/CMSResources/Images/20130104_6-Estimation%20of%20soot%20content%20in%20engine%20oil.pdf
- [11] SCHEEPERS, P.T.J., BOS, R.P. Combustion of diesel fuel from a toxicological perspective. *International Archives of Occupational and Environmental Health*. 1992, **64**, 149-161. <https://doi.org/10.1007/BF00380904>
- [12] SKOCZYLAŚ, W. Thermogravimetric analysis in automotive industry research (in Polish). BSc Thesis, 2019, Faculty of Transport Engineering, Poznan University of Technology.

Miłosław Kozak, DSc., DEng. – Faculty of Civil and Transport Engineering, Poznan University of Technology.

e-mail: miłoslaw.kozak@put.poznan.pl



Piotr Siejka, MEng.

e-mail: piotr_siejka@wp.pl



ECU calibration for gaseous dual fuel supply system in compression ignition engines

The dual fuel (DF) combustion mode is proven solution that allows to improve or get at the same level engine performance and reduce toxic compounds in exhaust gases which is confirmed by researchers and end-users. DF combustion mode uses two fuels gaseous fuel as a primary energy source and a pilot quantity of diesel fuel as ignition source. However, in order, to fully take advantage of the potential of the dual fuel mode, DF system must be proper calibrated. Despite the existence of commercial control systems for dual fuel engines on the market, the literature on the important parameters for the engine's operation introduced during calibration is scarce. This article briefly describes a concept of working algorithm and calibration strategy of a dual fuel electronic control unit (ECU) The purpose of calibration is to achieve the greatest possible use of an alternative gaseous fuel without causing accelerated engine wear.

Key words: compression ignition engine, ECU calibration, dual fuel mode, alternative fuels, emission reduction

1. Introduction

Despite the fact that the crude oil reserves will drain away in the near future (oil will sufficiently meet the worldwide demand for another 39 years [3, 7]), fuel demand is increasing in many sectors, especially in transportation sector (Fig. 1). Depletion of the non-renewable fossil resources leads to energy and political crisis.

Moreover, transport sector is a major contributor to the harmful gas emissions in the world, with a share of about 23.5–28% [1, 5, 19]. That brings us to environmental concerns caused by the rapid increase of harmful exhaust emissions due to the burning of fossil fuels. Depletion of crude oil and environmental considerations are driving the research towards the alternative combustion modes, exhaust after-treatment systems and nonconventional fuel sources.

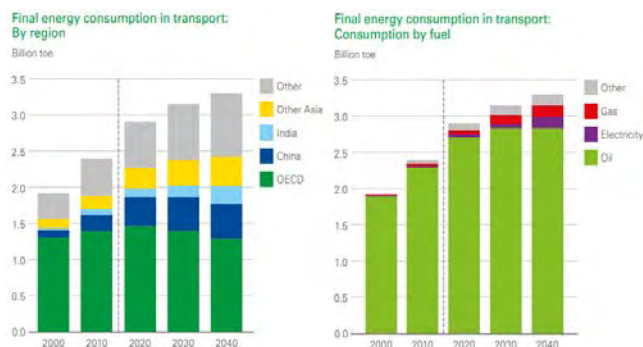


Fig. 1. Energy consumption in transport [3] (* other includes biofuels, coal and hydrogen)

Diesel engines have been widely used in heavy-duty vehicles, construction equipment, buses, and diesel generators due to its unmatched efficiency, durability and flexibility compared to a spark ignition engines. However, diesel engines are one of the main sources of the nitrogen oxides (NO_x) and particulate emissions (PM). In order to lower NO_x and PM emissions an after treatment systems have been widely used in diesel engines. However, catalyst materials are highly expensive and current technology cannot afford stringent emission regulations.

Thus, turning us to alternative energy sources such as: biogas, liquefied petroleum gas (LPG), compressed natural gas (CNG), liquefied natural gas (LNG) etc. The use of alternative gaseous fuels is a promising approach that allows to lower the dependence on conventional fuels and to reduce the harmful compounds in exhaust gases, which has been confirmed by numerous investigations [3, 4, 7, 10–13, 17, 18] and many others. However, the additional gaseous fuel burned with diesel fuel does not always have a positive effect on the content of toxic exhaust components. This applies, for example, to hydrogen, which was described in the doctoral dissertation [6].

Another not at all less important factor that determining the alternative fuels perspectives is a fuel price competition (Table 1). Each fuel has different calorific value so it is important to compare fuels with their energy content as kilowatt hour. In this way, the differences between fuels in terms of energy content would be directly visible without the “detour” of a reference fuel [9].

Table 1. Comparison of fuel prices [9]

| Type of fuel | Energy content | | Price | Price* |
|---------------------|----------------|---------|-------|-----------|
| | [MJ/l] | [kWh/l] | [€1] | [€10 kWh] |
| Petrol | 32 | 8.88 | 1.536 | 1.730 |
| Diesel | 36 | 10 | 1.398 | 1.398 |
| Natural gas | 44.4 | 12.3 | 1.103 | 0.897 |
| Biogaz (biomethane) | 44.4 | 12.3 | 1.103 | 0.897 |
| LPG | 24 | 6.6 | 0.693 | 1.050 |

* 10 kWh is equivalent to the energy content in one liter of diesel fuel

All this factors that mentioned above promote an important increment in the use of gaseous fuels as alternative fuels in the transportation sector in the recent years (Fig. 1).

However, engine operation on such alternative fuels may be sub-optimal with regard to both combustion process, fuel economy and emissions performance, as the engine has been designed and calibrated for operation on conventional fuel. Thus, the use of alternative fuels requires the calibration of the engine operating conditions including injection strategy and control parameters of the engine dual fuel electronic control unit, in relation to the physicochemical properties of alternative fuels.

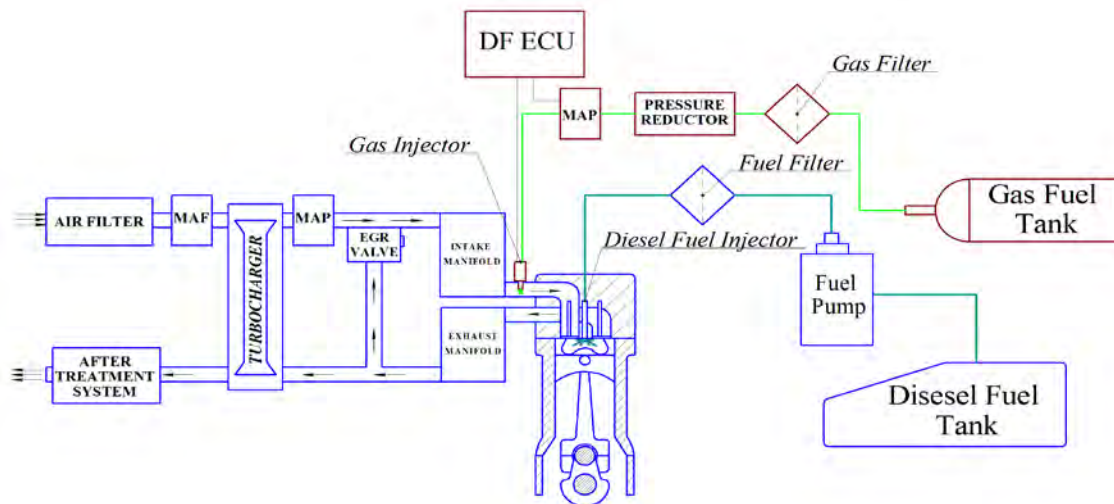


Fig. 2. Simple* overall scheme of Dual fuel mode in AJM 1.9 TDI (*Does not contain all electrical connections)

The dual fuel engine has some pitfalls such as the poor utilization of the LPG fuel at low and intermediate loads which results in poor engine performance, high HC, CO emissions and misfiring at higher gas inducted levels. Poor part load performance results from incomplete combustion of LPG. Due to this poor thermal efficiency high level of unburnt hydrocarbons in the exhaust is found. The performance of a dual fuel engine at idling and low loads can be improved by optimizing some engine operating and design parameters, such as engine speed, load, pilot fuel quantity, injection timing, intake manifold condition and intake gaseous fuel compositions [2].

In order to perform DF ECU calibration used special software solutions dedicated by ECU manufacturers [14, 16] and many others. This software, vary visually and may use various principle to reduce the amount of fed diesel. On the one hand, software that uses „diesel oil reduction map” and emulate common rail pressure signal [16], another software uses „emulator map” to emulate APP, MAP and MAF signals individually or simultaneously [14]. As, a reference software for DF ECU calibration in this work second type software was selected, due to more calibration freedom.

The present work is a part of an extensive experimental investigation devoted to the calibration DF ECU control parameters in order to finding the best compromise between reduction of fed diesel, engine performance and emission.

The purpose of this paper is to briefly describe a concept of working algorithm and “traditional” calibration strategy of a “gas diesel” ECU and to share useful information with researchers, engineers and anyone who interested in calibration of DF ECU control parameters in order to use alternative fuels in more efficient way.

2. Diesel engine modifications

There are a variety of technologies to meter gaseous fuels for internal combustion engines. These technologies vary in cost and complexity. For example, due to a high octane number of LPG and CNG they can be used in spark ignition engines in lover cost without major modifications. In contrast, low cetane number and high self-ignition tem-

perature (Table 2) (bad self-ignition abilities during the compression) of gaseous fuels (LPG, LNG, CNG) makes them difficult to be used in large proportions in compression ignition engines.

Table 2. Fuel properties

| Parameter/Fuel type | Diesel Fuel | Butane | Propane | Methane |
|--------------------------------|-------------|--------|---------|---------|
| Self-ignition temperature [°C] | 254 | 365 | 470 | 470 |
| Cetane number | 40-55 | 10 | 5 | 0 |
| Octane number | - | 102 | 102 | 120 |

However, there are two main application modes of gaseous fuels in compression-ignition engines:

1. Single fuel mode. This solution technically is very complex and requires intervention in the engine block and installation of additional spark plug as ignition source. Moreover, conventional electronic control unit for proper engine work must be calibrated.

2. Dual fuel mode (Fig. 2). In this operation mode gaseous fuels in a liquid or gaseous form inducted into the intake air of the inlet manifold to form homogeneous mixtures and then ignited by the directly injected pilot quantity of diesel fuel in the cylinder at the end of the compression stroke. This mode is inexpensive and requires only minor modifications by adding typical components (“auto gas” conversion kit), e.g. fuel tank with auxiliaries, gas filter, fuel lines, LPG/CNG injectors, reducers, additional sensors, signal emulators and dual fuel electronic control unit.

Due to simplicity and lower engine failure possibility, the second solution is widely used.

3. Dual fuel ECU working concept

There are many conversion kits for diesel engines available commercially. But, working algorithm is the same.

The DF ECU in order to operate in dual fuel mode requires signals from the crank position sensor (RPM), accelerator pedal position sensor (APP), manifold absolute pressure (MAP) sensor and mass air flow (MAF) sensor and additional sensors from dual fuel conversion kit (Fig. 3). During the dual fuel operation, the gas injector will be

controlled by the DF ECU while the diesel injector shall be controlled by the conventional ECU. In this mode, a portion of the fed diesel needs to be reduced and then replaced with gaseous fuel. In order to do so, DF ECU reads the lookup tables called “maps” (Fig. 4, 5) and produces continuous emulated/modified signal of the sensors (APP, MAF, MAP) and fed it into diesel ECU and then DF ECU set the injection duration for gas injectors. Depending on the received signal, the conventional ECU changes diesel fuel quantity. The set of parameters for the lookup tables obtained from experimental studies via calibration algorithm (discussed later in the article).

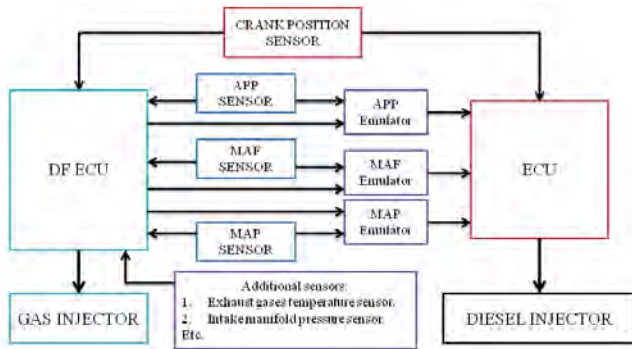


Fig. 3. Dual fuel mode control setup

Fig. 4 shows “emulation map”. Based on the set values contained in the map the amount of fed diesel could be changed (reduced or increased). The upper bar in the map represents the signal's voltage. This map allows to set individual emulation strength (in percentage) for active analog emulator (E1, E2, E3) and/or digital emulator (De1, De2) according to emulated signal's value [14].

| Var | 0,00 | 0,40 | 0,80 | 1,20 | 1,60 | 1,80 | 2,20 | 2,60 | 3,00 | 3,40 | 3,80 | 4,20 | mod.char.points | |
|-----|------|------|------|------|------|------|------|------|------|------|------|------|-----------------|----|
| E1 | 0 | 5 | 5 | 10 | 20 | 20 | 25 | 25 | 10 | 5 | 0 | 0 | +5 | -5 |
| E2 | 0 | 5 | 5 | 10 | 20 | 20 | 25 | 25 | 10 | 5 | 0 | 0 | +1 | -1 |
| E3 | 0 | 5 | 5 | 10 | 20 | 20 | 25 | 25 | 10 | 5 | 0 | 0 | | |
| De1 | 0 | 5 | 5 | 10 | 20 | 20 | 25 | 25 | 10 | 5 | 0 | 0 | | |
| De2 | 0 | 0 | 0 | 0 | 0 | 0 | 0 | 0 | 0 | 0 | 0 | 0 | active | |

Fig. 4. Emulator lookup table [14]

Figure 5 demonstrated different type of map. The set values in the “gas map” has an integer range between 0 and 254, where such values produce the gas dosage from 0% to 100% respectively. Gas map contains set values that correspond revolutions per minute (X axis) and pressure in the intake manifold (Y axis). Depending on the engine actual rpm and pressure inside intake manifold DF ECU choose correspond value in the map and increase the amount of gaseous fuel. However, set values in the “gas map”, does not represent exact fuel quantity and does not give absolute injection duration of the gas fuel. Those values are used as a reference, taking into consideration the number of gas injector installed and their static flow rate in order to gas fuel injection quantity calculation.

The percentage of the premixed gas can be quantified as substitution ratio on an energy basis according to the following equation [7]:

$$SR = \frac{\dot{m}_G \times LHV_G}{\dot{m}_D \times LHV_D + \dot{m}_G \times LHV_G} \times 100\% \quad (1)$$

The screenshot shows a software interface for a gas fuel lookup table. It features a grid with RPM on the X-axis (ranging from 1000 to 2500) and pressure on the Y-axis (ranging from 1.1 to 2.1 bar). The grid contains numerical values representing gas dosage percentages. Below the grid, there are control options for 'mod char points', 'map type', 'map smooth', and 'map reset'.

Fig. 5. Gas fuel lookup table [14]

Reducing the fed diesel quantity and increasing gas substitutions ratio means changing the air–fuel ratio (λ). In order to ensure similar engine performance for both single fuel (diesel only) mode and dual fuel mode the air–fuel ratio must be at the same level.

Another, not at all less important problem that can arise when two fuels are fed simultaneously, is a risk of the engine thermal and/or mechanical overloading. In order to protect the engine against failure, DF ECU measured the exhaust gas temperature and rpm. The maximum values of the exhaust gas temperature and rpm are entered as a boundary gas cut-off conditions in the software during the calibration procedure (Fig. 6).

In addition, knock effects can occur in the engine during the combustion. To identify this effect DF ECU requires additional signal from knock sensor. One way to limited this phenomenon could be reducing of the gas substitution ratio. From the other hand this phenomenon can be limited by increasing injection time delay of pilot diesel.

The screenshot displays the DF ECU basic configuration screen. It is divided into several sections:

- rpm signal:** Set to 5V.
- rpm type:** D90.
- EGT sensor:** on.
- EGT max:** 2,2V 629°C.
- turbo:** turbo engine.
- TG sensor:** 4k7(SM033).
- TR sensor:** 4k7(SM033).
- gas sensor:** Freescale 4.0 BAR(SM).
- MAP:** Freescale 4.0 Bar(SM).
- min.pres.[Bar]:** 1,1.
- on temp.[°C]:** 35.
- on rpm:** 1200.
- on Delay:** 2,0.
- minimum rpm:** 1000.
- maximum rpm:** 4450.
- Regulator:** vacuum/boost disconnected.
- work time diesel:** 120386 [s] 98,28 [%].
- work time gas:** 2106 [s] 1,72 [%].
- Power:** 90 - 150 HP.
- TPS connection:** TPS on Analog channel 1.
- LPG:** DOUBLE INJECTION TIME!
- Inj time x2:** 1x.
- level:** 0,35.
- ref.time[s]:** 25.
- invert sensor:** unchecked.
- valve powered:** unchecked.
- save data if 24->12V converter:** unchecked.
- don't save work time, fuel rate:** unchecked.

Fig. 6. DF ECU basic configuration screen [14]: 1 – main parameters, 2 – additional parameters, 3 – level sensor settings, 4 – save function

4. Dual fuel ECU calibration

ECU calibration is the process of determining the optimal balance between several parameters correlated with each other and the engine operating conditions. This process helps to identify the optimal balance of engine performance, emissions, and fuel economy. The common goal of

this process is to achieve maximum substitution rate of fed diesel, while still meeting all the requirements (Table 3).

As mentioned by authors [17] providing LPG “auto gas” and increasing its injection time (at constant emulation level) results in a non-linear increase in temperature, non-linear decrease in the air–fuel equivalence ratio, the initial growth of the vehicle’s power, and after a certain point its decline and uneven operation of the engine. The lack of simple relations in case of a simultaneous changes of the control parameters (gas injection duration, APP, MAF and MAP emulation). As a result, DF ECU calibration process is becoming more difficult to optimize, and it cannot be put in a simple framework of mathematical relations or linear patterns.

The calibration procedure itself does not seem complicated (evident in Fig. 7). However, it is a laborious trial and error process in finding the optimal balance between parameters in the full range of the engine working cycle. The “traditional”, testing-intensive method in comparison with

modern numerical model-based calibration methods (zero dimensional models, CFD models) is sub-optimal with regard to time consumption and requires many engine data driving cycles. However, “traditional” calibration method can be quite effective, when it is impossible to gather all required data to prepare proper zero dimensional or CFD model.

Table 3. Requirements for dual fuel system [8, 11]

| No. | Requirement |
|-----|--|
| 1 | Obtaining the same air–fuel equivalence ratio (λ) for an engine running in single- or dual- fuel mode. |
| 2 | No noticeable increase in exhaust gases temperature. |
| 3 | No noticeable increase/decrease in engine output power after switching into dual fuel mode. |
| 4 | Steady work of engine in dual fuel mode (no jerking). |
| 5 | Lowering amount of toxic emissions in the exhaust gases, especially NO _x and PM. |

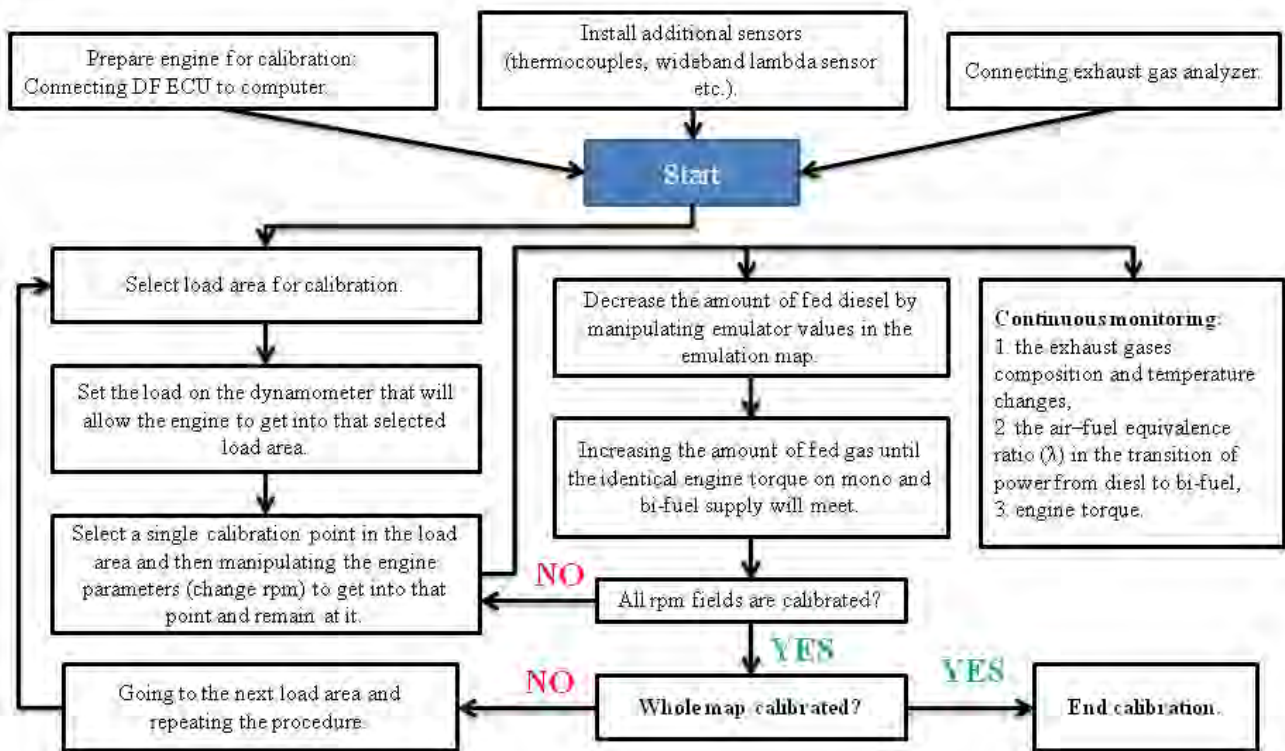


Fig. 7. DF ECU calibration algorithm

5. Conclusions

The “Dual fuel combustion concept” is a relatively simple strategy that allows to lowering the dependence on petroleum based liquid fuels and reduce the harmful compounds in exhaust gases. The modification work for the conversion of any diesel engine into the dual fuel system is inexpensive and requires minimum installation of additional components.

In terms of calibration, the proper DF ECU calibration is a laborious process that requires knowledge and experience. It is important to perform proper calibration because

its quality has a very large impact on the combustion process, fuel economy and emission performance that is confirmed by numerous investigations. The purpose of calibration is to achieve the greatest possible use of an alternative gaseous fuel. This goal is best achieved by using a feedback loop as a function of exhaust gas temperature or control based on the measurement of the pressure in the intake manifold. Exceeding the permissible exhaust gas temperature should be assumed as a criterion for the assessment of possible engine damage with too large substitution of diesel oil by gaseous fuel.

Nomenclature

| | | | |
|----------------|--|------------|---|
| APP | accelerator pedal position | LNG | liquefied natural gas |
| CNG | compressed natural gas | LPG | liquefied petroleum gas |
| DF | dual fuel | m_G, m_D | the mass flow rates of gas and diesel fuels |
| ECU | electronic control unit | MAF | mass air flow |
| LHV_G, LHV_D | the lower calorific values of gas and diesel fuels | MAP | manifold absolute pressure |
| | | SR | substitution ratio |

Bibliography

- [1] Agency, E.E. Greenhouse gas emissions from transport in Europe. <https://www.eea.europa.eu>. 2019.
- [2] ASHOK, B., DENIS ASHOK, S. et al. LPG diesel dual fuel engine – a critical review. *Alexandria Engineering Journal*. 2015, **54**(2), 105-126. <https://doi.org/10.1016/j.aej.2015.03.002>
- [3] BP, E. BP Energy Outlook 2019 edition. The Energy Outlook explores the forces shaping the global energy transition out to 2040 and the key uncertainties surrounding that. 2019.
- [4] BRZEŻAŃSKI, M., GOLEC, K. Nowoczesne systemy zasilania silników spalinowych paliwami gazowymi. *Zeszyty Naukowe Politechniki Częstochowskiej. Seria Mechanika, Silniki Gazowe*. 2003, **25**.
- [5] CHEN, X., WANG, Z., PAN, S. et al. Improvement of engine performance and emissions by biomass oil filter in diesel engine. *Fuel*. 2019, **235**, 603-609. <https://doi.org/10.1016/j.fuel.2018.08.038>
- [6] DASZKIEWICZ, P. Badania możliwości poprawy wskaźników ekologicznych silników o zapłonie samoczynnym zasilanych paliwami konwencjonalnymi z domieszką wodoru. *Doctoral Dissertation*, Poznań 2014.
- [7] GENG, P., CAO, E., TAN, Q. et al. Effects of alternative fuels on the combustion characteristics and emission products from diesel engines: a review. *Renewable and Sustainable Energy Reviews*. 2017, **71**, 523-534. <https://doi.org/10.1016/j.rser.2016.12.080>
- [8] JARZYŃSKI, W., KNEBA, Z. Research on the influence and the methodology of the calibration process for diesel-LPG dual fuel supply systems. *Combustion Engines*. 2015, **162**(3), 649-657.
- [9] KOLB, O., SIEGEMUND, S. Final report: study on the implementation of Article 7(3) of the “Directive on the deployment of alternative fuels infrastructure” – fuel price comparison. German Energy Agency 2017.
- [10] MERKISZ, J., PIELECHA, I. Alternatywne paliwa i układy napędowe pojazdów. *Wydawnictwo Politechniki Poznańskiej*, Poznań 2004.
- [11] NAPOLITANO, P., FRAIOLI, V., GUIDO, C. et al. Assessment of optimized calibrations in minimizing GHG emissions from a dual fuel NG/diesel automotive engine. *Fuel*. 2019, **258**, 115997. <https://doi.org/10.1016/j.fuel.2019.115997>
- [12] PARK, S.H., LEE, C.S. Applicability of dimethyl ether (DME) in a compression ignition engine as an alternative fuel. *Energy Conversion and Management*. 2014, **86**, 848-863. <https://doi.org/10.1016/j.enconman.2014.06.051>
- [13] QI, D.H., BIAN, Y.Z., MA, Z.Y. et al. Combustion and exhaust emission characteristics of a compression ignition engine using liquefied petroleum gas-diesel blended fuel. *Energy Conversion and Management*. 2007, **48**(2), 500-509. <https://doi.org/10.1016/j.enconman.2006.06.013>
- [14] SCALMAX. Scalmax Diesel Software Manual. 2018.
- [15] SEMELSBERGER, T.A., BORUP, R.L., GREENE, H.L. Dimethyl ether (DME) as an alternative fuel. *Journal of Power Sources*. 2006, **156**(2), 497-511. <https://doi.org/10.1016/j.jpowsour.2005.05.0822016>
- [16] STAG. CLB-2000/LB-2000 Installation and Configuration Manual. 6377. 2000.
- [17] STELMASIAK, Z., LARISCH, J., PIELECHA, J. et al. Particulate matter emission from dual fuel diesel engine fuelled with natural gas. *Polish Maritime Research*. 2017, **24**(2). <https://doi.org/10.1515/pomr-2017-0055>
- [18] STELMASIAK, Z., LARISCH, J., PIETRAS, D. Selected problems of adaptation car diesel engine for dual fuel supplying. *Combustion Engines*. 2015, **162**(3), 1021-1029.
- [19] US Environmental Protection Agency. Inventory of US. Greenhouse Gas Emissions and Sinks: 564. 2015. <https://doi.org/EPA-430-R-13-001>

Denys Stepanenko, MEng. – Faculty of Mechanical Engineering, Gdansk University of Technology.
e-mail: denys.stepanenko@pg.edu.pl



Zbigniew Kneba, DSc., DEng. – Faculty of Mechanical Engineering, Gdansk University of Technology.
e-mail: zkneba@pg.edu.pl



Piotr MICHALAK

Jerzy MERKISZ 

Włodzimierz STAWECKI

Maciej ANDRZEJEWSKI Paweł DASZKIEWICZ 

The selection of the engine unit – main engine generator during the modernization of the 19D/TEM2 locomotive

The paper aims to present a generating set selection methodology for a modernized diesel locomotive. An analysis of the number of rolling stock, with particular emphasis on the number of diesel locomotives owned by national carriers was performed. Based on the popularity of the locomotives operated on Polish railways, the TEM2 locomotive was chosen to be the base reference for the modernized 19D locomotive described in the paper. The scope of the locomotive's modernization was described. Modernization included: replacement of the internal combustion engine, replacement of the generator set, installation of a new braking system with a pneumatic board and air preparation and treatment system, application of a modern control and diagnostics system with anti-slip system at start-up and braking, and the installation of railway traffic safety devices.

Key words: railway, diesel locomotive, modernization, CFD simulation, exhaust emission

1. Introduction

Road transport is not the only branch of transport subject to strict restrictions, whereby it is required to meet said restrictions in tests performed to estimate the environmental impact of vehicles [4, 24]. The legal regulations in force [8] and the exhaust emission norms [7] force carriers to invest in improving the technical condition, reducing the environmental impact [5, 10] and increasing the efficiency of vehicles in operation, including diesel locomotives. Meeting these types of requirements is possible in several ways, ranging from innovative technical solutions [2, 16, 17], the purchase of new units, renovation and repair of older units or through retrofitting in the ecological aspect [18]. One of the solutions combining economic benefits with improved technical condition of the vehicle is its modernization [11, 12, 20, 22]. This type of operation can include a wide range of activities. It may consist of only single changes [14] such as replacement of the drive unit with a newer one that meets the applicable exhaust emission standards or it may include a thorough modernization of the entire vehicle.

This article describes the modernization process of the type 19D locomotive series SM48 (TEM2) (Fig. 1).



Fig. 1. The SM48 (TEM2) locomotive before modernization

The six-axle, single-cabin locomotive was constructed with the CoCo system. In the original version, it had an electric transmission and an 880 kW internal combustion engine. The unit was produced in the USSR and was intended for servicing the eastern border regions. It was used for heavy shunting and reloading works. After the Polish rail safety systems have been installed [6], it is also possible to use it in a freight train. Some of the manufactured units were adapted to move on tracks with a rail gauge of 1435 mm and 1520 mm. Shifting to a different track is possible by replacing the wheelsets.

After thorough analyzes of the technical condition and parameters of the locomotive a decision was made to modernize the described vehicle. It was decided that a complete modernization of the vehicle would be performed. This meant replacing all the main assemblies of the locomotive. The exceptions were the frames and bogies with drive systems. After major repairs were carried out, the original technical condition of the locomotive was reached and the vehicle modernization was considered complete.

Activities related to the thorough modernization of the SM48 (TEM2) diesel locomotive included:

- Performing numerical simulations and analyzes to determine the technical and operational parameters of the main devices, machines, apparatus and generating sets that could be used in the locomotive,
- Development, manufacturing and commissioning of models of the main units and systems,
- Performing control tests of the main units and systems,
- Development of a project of vehicle fitting with devices and systems,
- Installing the necessary devices and systems in the locomotive,
- Construction and preparation of acceptance requirements and preparation of acceptance procedures,
- Development and preparation of technical documentation for the modernized locomotive,
- Performing stationary vehicle tests,

- Performing dynamic vehicle tests,
- Preparation of legal procedures in order to obtain documented permissions for taking part in rail traffic,
- Launching the procedures related to type approval and operational tests.

2. Polish rail market overview

According to statistical data [1], rail transport is a dynamically developing branch of transport in Poland. Since 2010, there has been an increase in performed operational work by 17% (Fig. 2). In the case of freight transport, according to [27], the annual forecast volume dynamics of the total demand for freight transport in rail transport is to increase depending on the scenario, from 13.4% to even 25% (Fig. 3) by 2030. Even considering the most pessimistic forecast, this will translate into a significant increase in rail transport.

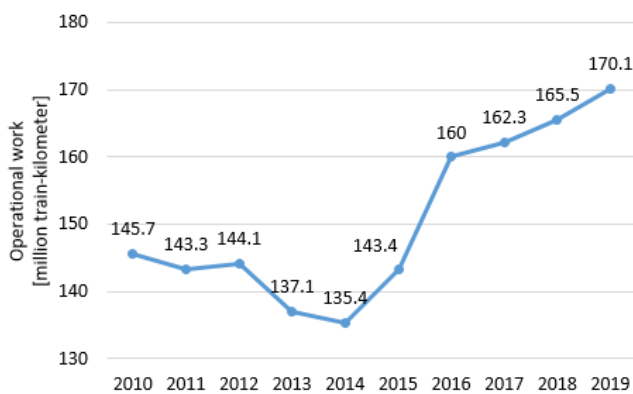


Fig. 2. Operational work in passenger rail transport in Poland in 2010–2019 (standard-gauge transport) [1]

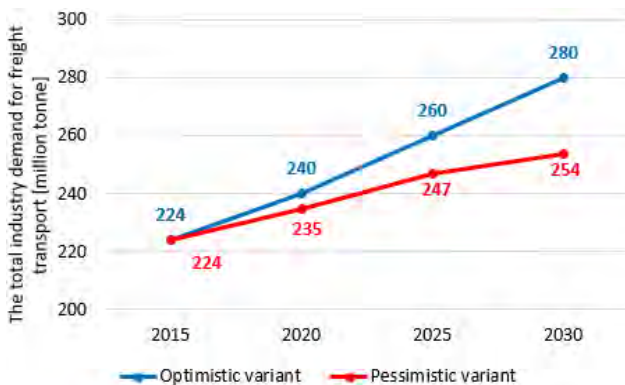


Fig. 3. The projected volume of the total industry demand for freight transport by rail in Poland (carried out by Polish and foreign carriers) [27]

The growing demand for rail transport in Poland is realized on the railway lines, whose total length is 19,235 km [25]. With this value, there are 6.2 km of railway lines per every 100 km² of the country's land area. Presented as ratio of rail line length per 10 thousand people, this value is 5 km. The density of the railway network in Poland is not high when compared, for example, to the situation in the neighboring country – the Czech Republic – where the same indicators are almost twice as high [13]. The electrified lines in Poland with a total length of 11,894 km constitute 62% of the total network size. However, electrification

(Fig. 4) and the density of railway lines in the country are not uniform. Especially in the areas of eastern Poland, the share of railway lines with electric traction has a low percentage. For example, in the Podlaskie Voivodeship the electric traction is only 219 km out of 759 km (29%), in the Lubelskie Voivodeship 416/1048 km (40%), and in the Podkarpackie Voivodeship 370/978 km (38%) [25]. This means that only rail vehicles equipped with a drive system that can operate independent of electric traction can travel on most of the railway routes in these areas. In practice, this means locomotives and multiple units equipped with diesel engines.

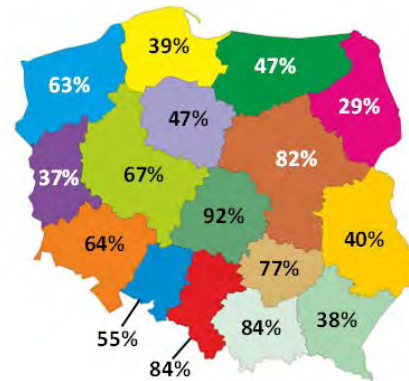


Fig. 4. Share of electrified railway lines in individual voivodeships in Poland

The planned increase in the number of rail transport operations, both passenger and freight, requires carriers to have an appropriate sized rolling stock, including units that can operate fully independent of electric traction. In addition, the demand for rail transport will also increase the amount of shunting work performed mainly by rail vehicles with a diesel engine. Currently, 109 diesel passenger locomotives and 269 diesel traction units are used in passenger transport [21]. In the case of freight rolling stock in Poland, there is a constant trend of increasing use of diesel locomotives, characterized by greater operating autonomy, compared to electric locomotives [26] (Fig. 5).

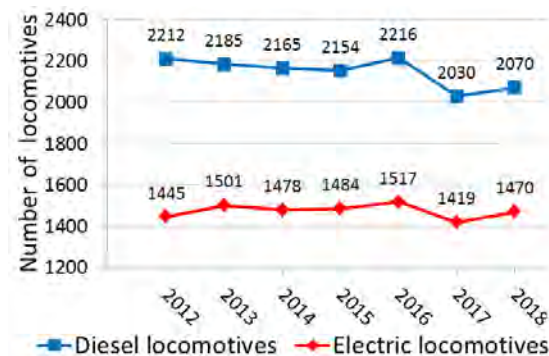


Fig. 5. Freight locomotives in Poland in the years 2012–2018

In Poland, the most frequently used rolling stock was manufactured between 1970 and 1980. This means that a large part of the locomotives were still manufactured in the times when there were no exhaust emission norms or

when the regulations in force related to the reduction of engine exhaust emissions were very liberal. The average age of freight diesel locomotives in Poland is 36.9 years [26], and passenger diesel locomotives 41.7 years [21]. Additionally, worn-out shunting locomotives constitute a large share of diesel locomotives in the country. As a result, in 2018 over 80% of diesel locomotives were over 40 years old [15]. Due to the significant age of rail vehicles and the continuous aging process, rail carriers have been increasing the locomotive utilization index since 2016 in order to improve the efficiency of their operation and work organization (Fig. 6). These activities translated into a relative increase of the discussed indicator by 18.9% from 2016.

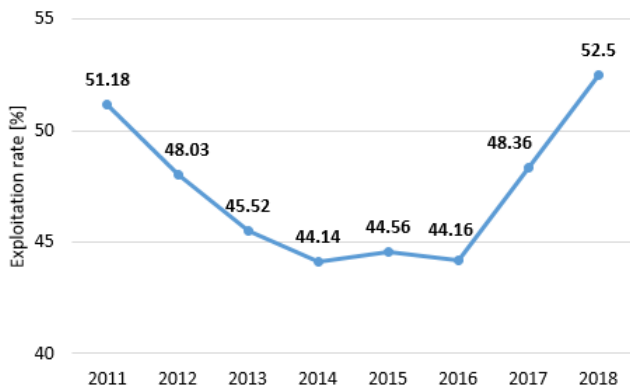


Fig. 6. The use of locomotives in Poland according to the daily quantity in years 2011–2018

A significant portion of the rolling stock in Poland is at an advanced stage of wear and tear. This situation is pointed out by the President of the Office of Rail Transport in Poland: “The figures provided show how large the scale of rolling stock investments is needed in the upcoming 10 years” [15]. For this reason, the Ministry of Infrastructure introduced the National Railway Program that is to last until 2023, which includes a number of railway investments [19]. The effects of the project include planned investments in rolling stock. By 2023, investments of approximately €360 million are expected to cover 116 electric locomotives and 168 diesel locomotives (Fig. 7). In the case of diesel locomotives, the operations are to include renovation and modernization of old vehicles, purchase of used vehicles, lease and purchase of new vehicles (Fig. 8).

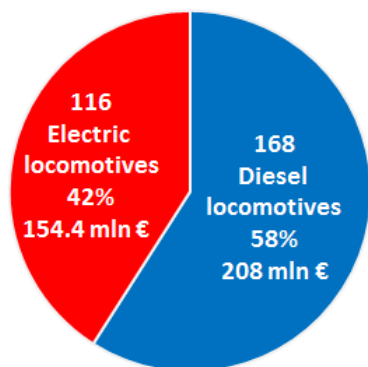


Fig. 7. Investments into diesel and electric locomotives planned for 2023 in Poland (for the group of surveyed carriers performing 80% of national transport operations)

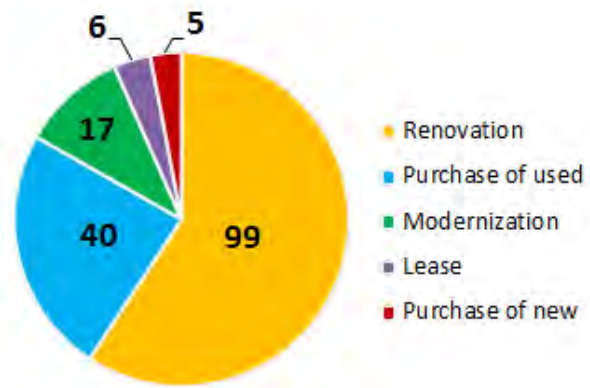


Fig. 8. Number of diesel locomotives included in the planned investments until 2023 in Poland (for the eight surveyed carriers)

3. Locomotive modernization process

3.1. Extent of works

Modernization works are a very complex processes that require vast knowledge and an experienced team of specialists and engineers from the railway sector. The TEM2 locomotive modernization project was created by the Łukasiewicz Research Network – Institute of Rail Vehicles "TABOR" in Poznań. All repair and modernization works were carried out by Pojazdy Szynowe PESA Bydgoszcz S.A.

The project included a number of activities related to the overhaul of the frames and bogies, as well as modifications that allowed for the installation of a new drive system and body. The most important of them were:

- Replacing the drive system,
- Installation of a new, autonomous driver's cab with two independent desks and seats, control cabinets, cameras facilitating operation and improving safety,
- Installation of the control and diagnostics system,
- Replacement of the pneumatic control cabinet,
- Installation of a new anti-slip system when starting and braking,
- Installation of a new air preparation and treatment system with a screw compressor driven by an electric motor,
- Installation of devices related to safety in motion and devices related to radio communication,
- Installation of electronic recorders of operating parameters and speedometers, including the ability of remote viewing of selected data,
- Modernization of the brake lever system on the bogey,
- Installation of a permanent fire control system with aerosols.

3.2. Generator set

One of the main goals of the modernization process was to replace the engine unit. The worn-out PD1M combustion engine manufactured in the USSR was replaced with a type 12V4000R84 MTU engine. This engine with a power of 1800 kW at 1800 rpm and dimensions of 2675×1700×2005 mm, dedicated to rail transport, meets the Stage IIIB emission norms [3]. The generator set was also replaced along with the internal combustion engine – the main generator

and the auxiliary JENOPTIK generator, and a built-in rectifier. The main generator, adapted to the specific working conditions in railway vehicles, had a rated power of 1800 kW. The generator's operating range was between 600 and 1800 rpm. The maximum current was 6600 A, and the maximum voltage was 750 V. The 120 kW synchronous auxiliary generator with a voltage of 3×450 V AC was directly flanged to the main generator. Figure 9 shows the generating set before and after the modernization.

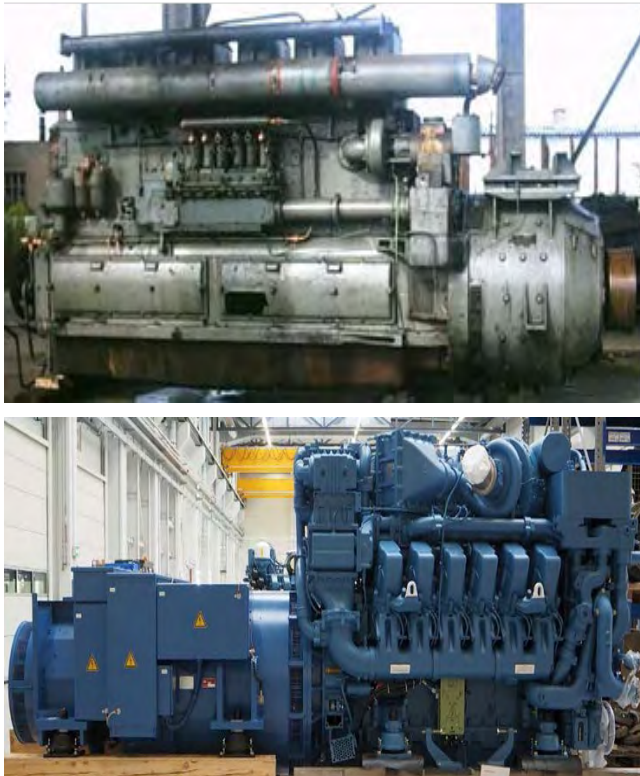


Fig. 9. View: top – generator set with engine type PD1M (before modernization) and bottom – generator set with engine type MTU 12V4000R84 (after modernization)

The process of replacing the main engine was highly complex. The installation of the internal combustion engine gave rise to many construction and design challenges that had to be completely resolved during the modernization of the locomotive. The installation of a modern engine concerned not only the main propulsion unit but also connected devices and secondary systems. Examples include the power supply system, the cooling system with the pre-heater system and the hydrostatic fan, the exhaust system with the Diesel Particle Filter (DPF), and the air intake system with its filters. The installation of the internal combustion engine also required precise data from the manufacturer on the engine attachment method to the locomotive's frame, couplings of the engine with the generator set, and mounting of the hydrostatic pump of the radiator fan drive. Data on the values of maximum negative pressures in the fuel systems and air consumption in various operating conditions were also required. The MTU 12V4000R84 internal combustion engine attached to the frame with peripheral devices is shown in Fig. 10.

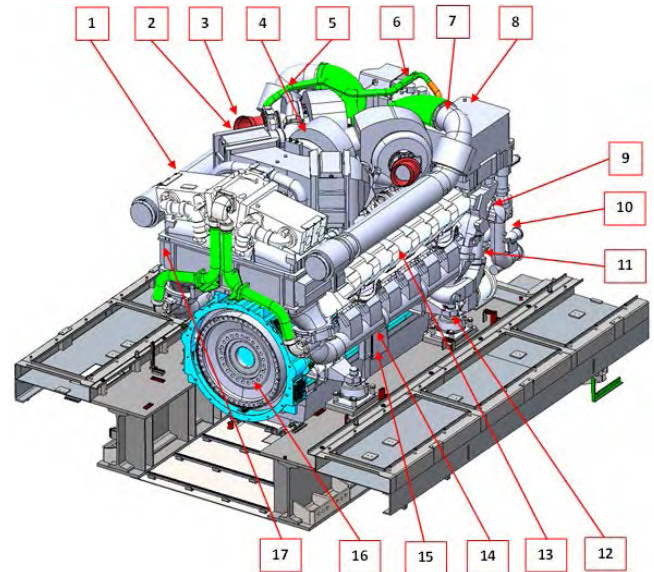


Fig. 10. MTU 12V4000R84 combustion engine, where: 1 – exhaust gas recirculation cooler (EGR cooler), 2 – charge air cooler (high temperature), 3 – air inlet, 4 – exhaust gas driven turbocharger (high pressure), 5 – exhaust gas driven turbocharger (low pressure), 6 – venting crankcase, 7 – exhaust outlet, 8 – oil heat exchanger, 9 – engine coolant inlet, 10 – charge air coolant outlet, 11 – coolant pumps (LT/HT), 12 – elastic support, 13 – cylinder head, 14 – starter control module (POM), 15 – engine oil sump, 16 – power receiver on the drive side, 17 – charge air cooler (low temperature)

3.3. Selection of the intake duct

The constructors' task was to meet the requirements specified by the manufacturer. Verification of the correct operation of individual systems was also possible thanks to simulations and computer analyzes. They ensure the correct speed of operation and eliminate the need to carry out some of the time-consuming and costly bench and dynamic tests.

An example of how analyzes and computer simulations can be used in the design phase of the modernized locomotive were CFD (*Computational Fluid Dynamics*) simulations of air intake necessary for the combustion process. The installation of the new internal combustion engine required the design of an air intake duct to have an optimal shape that connects the engine turbocharger with air filters. The duct had to have a sufficiently low level of flow resistance, which was to make it easier to cover the air demand. The turbocharger is able to take the required amount of air into the inlet channel with a new filter installed only for pressure drops not greater than 2500 Pa. In the case of a dirty filter, the pressure drops may not exceed 3500 Pa. The new air filter generates a pressure drop of 1000 Pa for the air flow of 1.1 m³/s. Therefore, the airflow through the duct with the new filter can operate correctly with a pressure drop of 1500 Pa in the inlet ducts. Due to the lack of space when installing the engine, it was necessary to use a strong bend of the inlet channel with a radius of 200 mm. The inlet conduit at the bend was a flexible hose with a length of 500 mm. According to the manufacturer's specification, the pipe had a smooth surface, therefore, for simulation purposes, it was decided to model this element as a steel pipe.

Three configurations of the inlet channel were created and labelled: A, B and C. Numerical models 1, their divi-

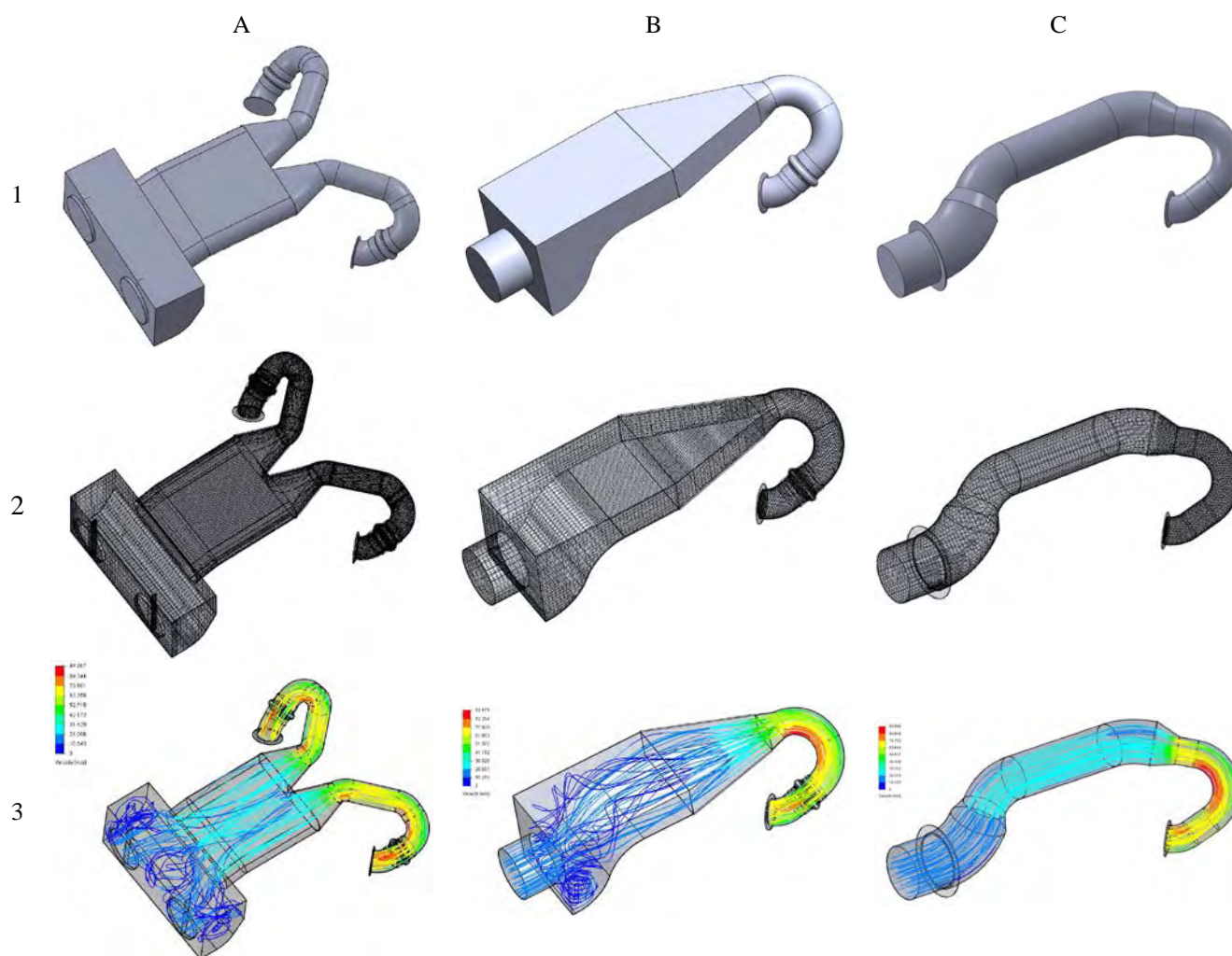


Fig. 11. CFD simulations of the intake systems in configurations A, B, and C of the 19D locomotive: 1 – numerical models, 2 – division of numerical models into finite elements, 3 – distribution of air velocity

sion into finite elements 2 and the flow velocity distribution 3 in the described systems were shown in Fig. 11. Due to the software requirements, the inlets and outlets of the tested parts were closed. An atmospheric pressure of 1013.25 hPa was applied to each air inlet to the system. At the outlet of the system, the value of the air volume flow required to be delivered to the turbocharger was set at 1.1 m³/s.

The flow resistance values occurring in the inlet channels for a given configuration were obtained through the performed simulations. The highest flow resistance was observed in the system A – 2028 Pa. System B generated a loss of 1122 Pa in the intake channel. The smallest values of flow resistance occurred in configuration C – 522 Pa. The permissible pressure drop level of the air stream going into the turbocharger, which was 1500 Pa, was met by the B and C systems. The C system turned out to be the most advantageous configuration. Thanks to the laminar flow of the air stream and the use of an elastic duct with a constant cross section the generated flow resistance values were the smallest in the system C, despite having a more complex shape than system B. In addition, system C takes up much less space, which facilitates servicing and maintenance actions thanks to the ease of access to other engine components.

4. Results of modernization

After modernization the SM48 (TEM2) locomotive was designated as 19D. The new design adopted a modular structure for the locomotive. Thus, the vehicle has been built into block sections that could be mounted independently. The design was divided into: refrigeration-compressor, generator set, driver's cab, and electro-pneumatic (Fig. 12) compartments. The internal combustion engine with the generator – the generator set compartment – were installed on the underframe. The compressor set, the traction cabinet and fans of the traction motors were also attached to the body frame. The remaining sections were made so that they could be lifted with an overhead crane during service and maintenance work. In addition, the modules were equipped with flaps, multi-wing doors and removable roofs to facilitate access and accelerate the replacement of damaged elements. Figure 13 shows the arrangement of the main devices in the locomotive. The modular construction of the locomotive allowed for the acceleration of design and production works, and also allowed for the efficient preparation of construction and technical documentation.

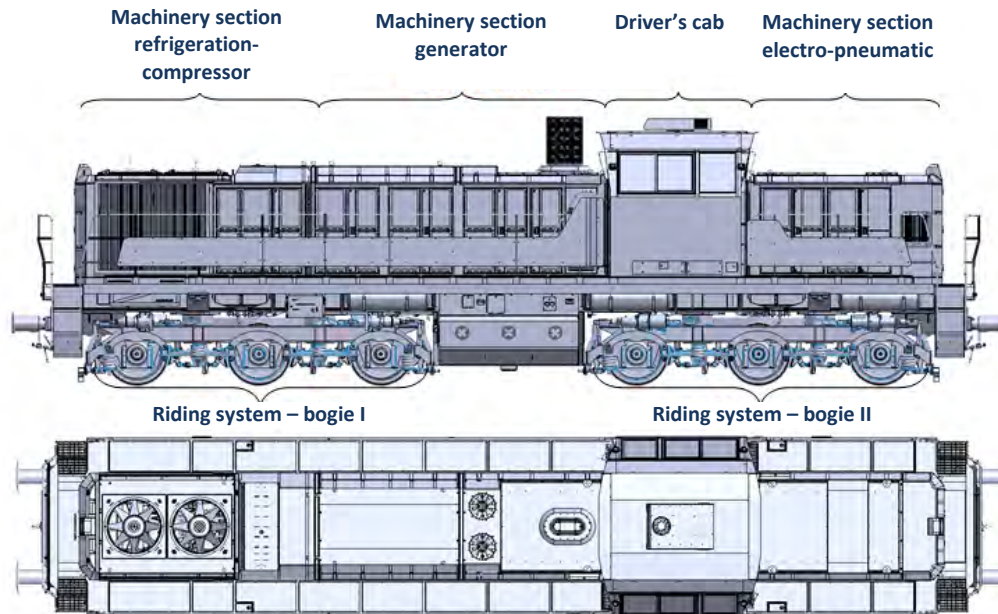
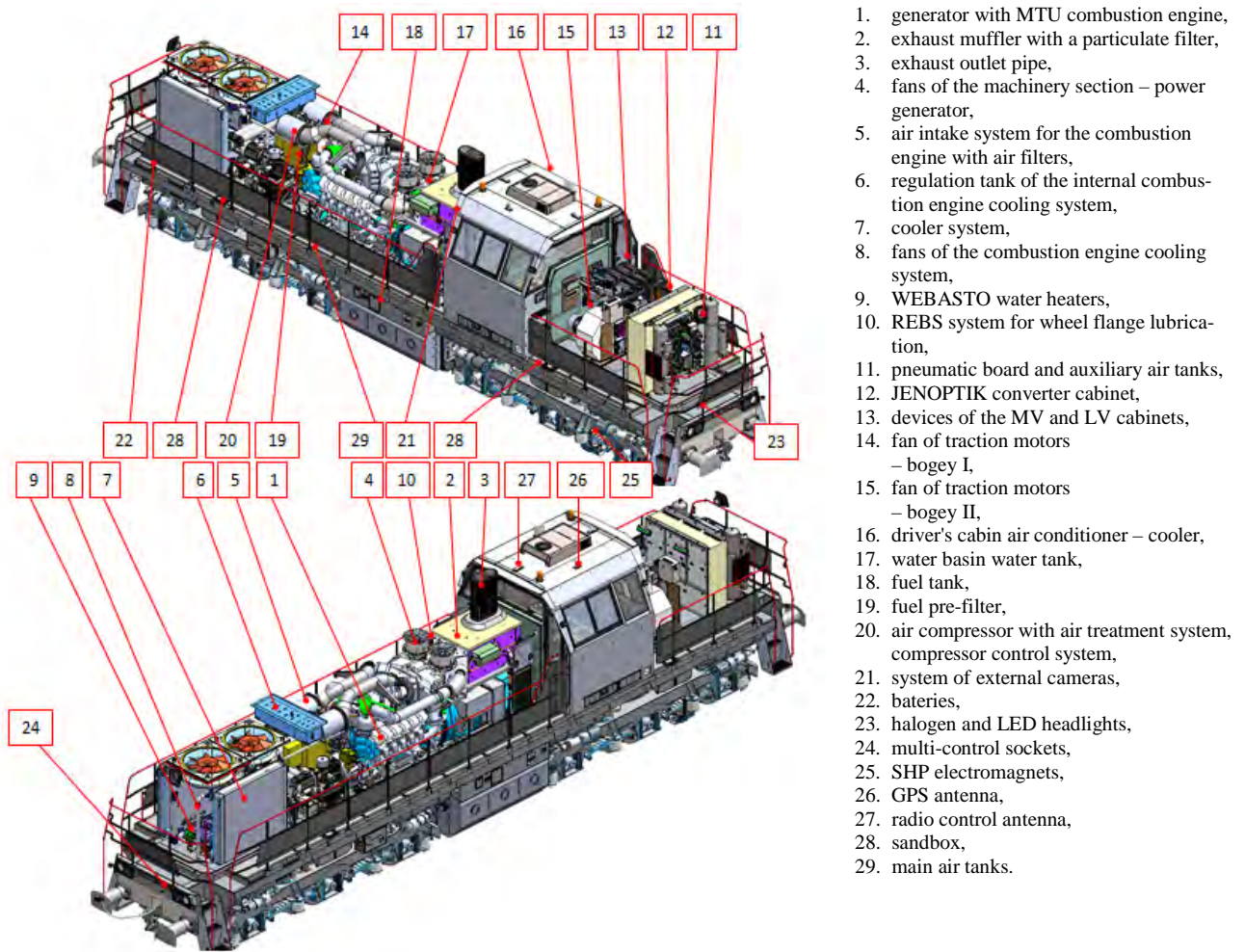


Fig. 12. Arrangement of the main compartments on the 19D locomotive (left and top view)



1. generator with MTU combustion engine,
2. exhaust muffler with a particulate filter,
3. exhaust outlet pipe,
4. fans of the machinery section – power generator,
5. air intake system for the combustion engine with air filters,
6. regulation tank of the internal combustion engine cooling system,
7. cooler system,
8. fans of the combustion engine cooling system,
9. WEBASTO water heaters,
10. REBS system for wheel flange lubrication,
11. pneumatic board and auxiliary air tanks,
12. JENOPTIK converter cabinet,
13. devices of the MV and LV cabinets,
14. fan of traction motors – bogey I,
15. fan of traction motors – bogey II,
16. driver's cabin air conditioner – cooler,
17. water basin water tank,
18. fuel tank,
19. fuel pre-filter,
20. air compressor with air treatment system, compressor control system,
21. system of external cameras,
22. batteries,
23. halogen and LED headlights,
24. multi-control sockets,
25. SHP electromagnets,
26. GPS antenna,
27. radio control antenna,
28. sandbox,
29. main air tanks.

Fig. 13. Arrangement of the main components on the 19D locomotive

The 19D locomotive, after modernization, had a maximum power of 1350 kW at the wheel circumference, a tractive force of 122 kN and a tractive starting force of 455 kN. The vehicle could travel with a continuous speed of 40 km/h. Additionally, the designers made sure that the locomotive could be operated with multiple traction as an option. A summary of the basic locomotive parameters before and after the modernization was presented in Table 1.

The modernization of the 19D locomotive in terms of the drive system was planned in an effort to meet the requirements of the Stage IIIB exhaust emission norms, according to Directive 2004/26/EC of the European Parliament, in the scope of limiting the exhaust emission of gaseous pollutants and particulates [9]. The modern MTU 12V4000R84 engine installed in the locomotive meets the above-mentioned limits. The worn-out PD1M unit, which was replaced from the vehicle, met the exhaust emission limits specified in the ORE B13 standard, which was in force until 1981. The presented test was carried out in real

operating conditions (Fig. 14). There is a large range of variability of the parameters (in terms of rotational speed and load). The conditions have a negative impact on the emission of pollutants, as presented in the paper [23]. The obtained results were compared with the standards for which tests are performed under steady engine operating conditions.

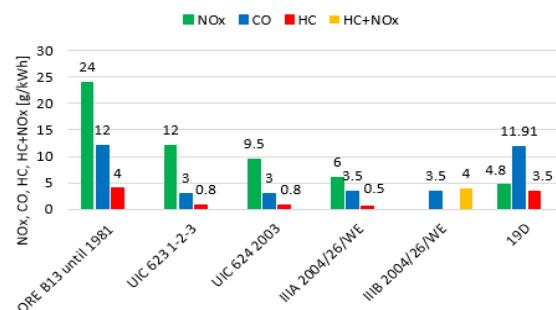


Fig. 14. Example of exhaust emission for a diesel engine of the locomotive SM48 (19D)

Table 1. Basic locomotive parameters before and after modernization

| No. | Device, parameter | | Unit | Value | |
|-----|---|------------------------|---------------------|-----------------------------|--|
| | | | | Before modernization | After modernization |
| 1. | Base locomotive manufacturer | | – | USSR MZ Briańsk | |
| 2. | Type | | – | TEM2 | 19D |
| 3. | Service weight of the locomotive | | [Mg] | 118 ^{-3%} | |
| 4. | Top speed | | [km/h] | 100 | |
| 5. | Transmission type | | – | electric | electric |
| 6. | Brake | main | – | DC–DC | AC–DC |
| | | parking | | Matrosow | MH |
| 7. | Traffic safety devices | | – | none | SHP, CA, RS |
| 8. | Combustion engine | manufacturer | – | USSR | MTU |
| | | type | – | PD1M | 12V 4000 R84 |
| | | rated power | [kW] | 883 | 1800 |
| | | engine speed | [rpm] | 750 | 1800 |
| | | exhaust emissions | – | No data | EU 26/2004 stage III B |
| | | fuel consumption | g/kWh | 229 | 202 ^{+5%} |
| | | lubricant consumption | g/kWh | No data | 0.2% of the fuel consumed |
| 9. | Main generator | manufacturer | – | USSR | JENOPTIK |
| | | type | | GP-300BU2 | SDV 95.50-12 |
| | | continuous rated power | [kW] | 780 | 1800 |
| 10. | Auxiliary generator | manufacturer | – | USSR | JENOPTIK |
| | | continuous rated power | | [kW] | MWG-25/IIU2 5.75 |
| 11. | Traction motors | type | – | ED 118 AU2 | |
| | | continuous rated power | | kW | 105 |
| 12. | Control circuit voltage | | [V] | 75 | 24 |
| 13. | Control system | | – | electric | digital |
| 14. | Air compressor | type, supply | m ³ /min | piston, from the crankshaft | screw, electric motor, 3x400 V _{AC} , 22 kW |
| | | air output | | 4.6 | 2.9 |
| 15. | Radiator fan drive | | – | Cardan shaft | hydrostatic – stepless speed control |
| 16. | traction motors fans drive | | – | belt transmission | electric motor, 3x400 V _{AC} |
| 17. | Driver's cab | | – | | new equipment that meets the current requirements in terms of ergonomics and work safety |
| 18. | Fixed fire extinguishing device in the engine compartment | | – | none | aerosol generator |

5. Conclusions

The 19D locomotive project is an example of how the 3D environment can be used in design and construction works. By creating the locomotive model, and performing analyzes and simulations the work was significantly accelerated, which contributed to reducing the overall costs of vehicle modernization. In the described locomotive, modern assemblies and systems were used, which increased the reliability and extended the maintenance intervals.

The main aim of the article was to present the activities related to the modernization of the SM48 (TEM2) locomotive, in particular the equipment used and the work carried out on the vehicle drive system. The modernized locomotive was characterized by low environmental impact. The use of the modern 12V4000R84 internal combustion engine manufactured by MTU, which meets the Stage IIIB emission norms, has significantly reduced the generated exhaust emissions. The drive unit was characterized by lower specific fuel consumption – 202 g/kWh – and consequently higher efficiency. In addition, the new engine has twice the power of the previous one. As a result of the modernization,

the 19D locomotive is the locomotive with the highest rated power of this type in Poland. The vehicle was put into use by carriers, where it currently performs the most difficult maneuvering and shunting works and is used to move heavy freight trains.

To sum up, given the current technical condition of the railway infrastructure and rolling stock, as well as its average age, the modernization of rail vehicles in Poland is a procedure necessary to improve the technical level, reliability and operating safety of the existing rolling stock. In addition, this type of activity increases the drivers work comfort as well as making the vehicle maintenance easier. For this reason, the purchase of new units, along with renovation and modernization of older rolling stock should be a permanent part of the activity of the railway carriers in Poland.

Acknowledgements

Applied Research Program 3 No PBS3/B6/33/2015 titled: „Platform of modernized combustion 6-axle locomotives meeting the requirements of European Union with using locomotives operated in the country”.

Nomenclature

| | | | |
|------------|---|-------|----------------------------------|
| CFD | Computational Fluid Dynamics | SHP | Automatic braking system |
| DPF | Diesel Particle Filter | REBS | A manufacturer in Germany |
| Stage IIIB | European Non-Road Emission Standard | EGR | Exhaust Gas Recirculation |
| MTU | A manufacturer of internal combustion engines | LT/HT | Low Temperature/High Temperature |
| ORE B13 | A regulation of emission limits | POM | Power Output Module |

Bibliography

- [1] 2019 in passenger and freight transport – Summary of Office of Rail Transport. *Office of Rail Transport*. 2020.
- [2] ANDRZEJEWSKI, M., GALLAS, D., DASZKIEWICZ, P. et al. The latest technical solutions in rail vehicles drives. *MATEC Web of Conferences*. 2017, **118**. <https://doi.org/10.1051/mateconf/201711800015>
- [3] BAUMGARTNER, C., WEIß, T., ZITZLER, G. et al. New MTU series 4000 rail engine fulfilling most ambitious emission regulation. *Heavy-Duty-, On- und Off-Highway-Motoren 2017*. 2018, 137-149. https://doi.org/10.1007/978-3-658-21029-8_8
- [4] BIELACZYK, P., MERKISZ, J., PIELECHA, J. et al. RDE-compliant PEMS testing of a gasoline Euro 6d-TEMP passenger car at two ambient temperatures with a focus on the cold start effect. *SAE Technical Paper 2020-01-0379*. 2020. <https://doi.org/10.4271/2020-01-0379>
- [5] CARVALHAES, B.B., ROSA, R.A., D'AGOSTO, M.A. et al. A method to measure the eco-efficiency of diesel locomotive. *Transportation Research Part D: Transport and Environment*. 2017, **51**, 29-42. <https://doi.org/10.1016/j.trd.2016.11.031>
- [6] CICHY, R. Authorization of vehicles for placing in service after modernization and renewal. European and national requirements. *Pojazdy Szynowe*. 2017, **1**, 31-43.
- [7] DALLMANN, T., MENON, A. Technology pathways for diesel engines used in non-road vehicles and equipment. *White Paper, The International Council on Clean Transportation*. 2016.
- [8] DASZKIEWICZ, P., RYMANIAK, Ł., KAMIŃSKA, M. Issues of emission evaluation of road-rail vehicles in the aspect of current type approval regulations. *Combustion Engines*. 2019, **178**(3), 269-273. <https://doi.org/10.19206/CE-2019-347>
- [9] Directive 2004/ 26/EC of the European Parliament and of the Council of 21 April 2004 amending Directive 97/68/EC on the approximation of the laws of the Member States relating to measures against the emission of gaseous and particulate pollutants from internal combustion engines to be installed in non-road mobile machinery
- [10] KAPETANOVIĆ, M., VAN OORT, N., NÚÑEZ, A. et al. Sustainability of railway passenger services – a review of aspects, issues, contributions and challenges of life cycle emissions. *8th International Conference on Railway Operations Modelling and Analysis (ICROMA)*. 2019.
- [11] LIUDVINAVIČIUS, L., DAILYDKA, S. The aspects of modernization of diesel-electric locomotives and platform for transportation of railway switches in Lithuanian Railways. In: *Sladkowski A. (eds) Rail Transport–Systems Approach*. 2017, **87**. https://doi.org/10.1007/978-3-319-51502-1_4
- [12] LIUDVINAVIČIUS, L., JASTREMSKAS, V. Modernization of diesel-electric locomotive 2M62 and TEP-70 locomotives with respect to electrical subsystem. *Procedia Engineering*. 2017, **187**, 272-280. <https://doi.org/10.1016/j.proeng.2017.04.375>
- [13] MAŠKOVÁ, K. Economy of railway transport from the point of view of the client. *Master's Thesis, Czech Technical University, Prague* 2019.
- [14] MIKLASZ, R., MILECKI, S. Modernization of the TEM2 locomotive bogies with the aim of reducing operational con-

- tamination of the environment. *Pojazdy Szynowe*. 2017, **1**, 44-52.
- [15] Office of Rail Transport. Internet website: <https://utk.gov.pl/>
- [16] PIELECHA, I., MERKISZ, J., ANDRZEJEWSKI, M. et al. Ultracapacitors and fuel cells in rail vehicle drive systems. *Pojazdy Szynowe*. 2019, **2**, 9-19.
- [17] PIELECHA, J., ANDRYCH-ZALEWSKA, M., SKOBIEJ, K. The impact of using an in-cylinder catalyst on the exhaust gas emission in real driving conditions tests of a diesel engine. *IOP Conference Series: Materials Science and Engineering*. 2018, **421**(4). <https://doi.org/10.1088/1757-899X/421/4/042064>
- [18] Progress Rail Services: EMD Tier 4 (PM) Aftertreatment Upgrade on a Line Haul Locomotive. Final Report 2010-2012.
- [19] Resolution No. 162/2015 of the Council of Ministers of September 15, 2015 on the establishment of the National Railway Program until 2023. 2015.
- [20] RJABTŠIKOV, V., RASSÖLKIN, A., VAIMANN, T. et al. Possibilities of changing the transport characteristics of the TEP70 locomotive. *27th International Workshop on Electric Drives (IWED2020)*. 2020. <https://doi.org/10.1109/IWED48848.2020.9069576>
- [21] Rolling stock potential, Trends and forecasts. *Office of Rail Transport*. 2019.
- [22] RYABKO, E., RYABKO, K. Effectiveness of diesel-locomotive shunter modernization and ways for its definition. *Bulletin of Bryansk State Technical University*. 2020, **5**(90), 23-31. <https://doi.org/10.30987/1999-8775-2020-5-23-31>
- [23] RYMANIAK, Ł. Comparison of the combustion engine operating parameters and the ecological indicators of an urban bus in dynamic type approval tests and in actual operating conditions. *MATEC Web of Conferences*. 2017, **118**. <https://doi.org/10.1051/mateconf/201711800009>
- [24] RYMANIAK, Ł., FUĆ, P., LIJEWSKI, P. et al. Evaluating the environmental costs in Poland of city buses meeting the Euro VI norm based on tests in real operating conditions. *Archives of Transport*. 2019, **52**(4), 109-115. <https://doi.org/10.5604/01.3001.0014.0212>
- [25] Statistics Poland. Internet website <https://stat.gov.pl/en/>
- [26] The rolling stock of freight carriers – current state and plans until 2023. *Office of Rail Transport*. 2018.
- [27] Transport Sustainable Development Strategy until 2030. *Polish Council of Ministers*. 2019.

Piotr Michalak, MEng. – Łukasiewicz Research Network – Rail Vehicles Institute “TABOR” in Poznan.
e-mail: piotr.michalak@tabor.lukasiewicz.gov.pl



Prof. Jerzy Merkisz, DSc., DEng. – Faculty of Civil and Transport Engineering, Poznan University of Technology.
e-mail: jerzy.merkisz@put.poznan.pl



Włodzimierz Stawecki, Ph.D. – Łukasiewicz Research Network – Rail Vehicles Institute “TABOR” in Poznan.
e-mail: wlodzimierz.stawecki@tabor.lukasiewicz.gov.pl



Maciej Andrzejewski, DEng. – Łukasiewicz Research Network – Rail Vehicles Institute “TABOR” in Poznan.
e-mail: maciej.andrzejewski@tabor.lukasiewicz.gov.pl



Paweł Daszkiewicz, DEng. – Łukasiewicz Research Network – Rail Vehicles Institute “TABOR” in Poznan.
e-mail: pawel.daszkiewicz@tabor.lukasiewicz.gov.pl



Sylwin TOMASZEWSKI Marian MEDWID Maciej ANDRZEJEWSKI 

Maksymilian CIERNIEWSKI

Wojciech JAKUSZKO

New rail-road tractor with a combustion engine and an alternative electric drive

The paper presents the general concept of an innovative rail-road tractor solution. The innovation of the solution is characterized by equipping the combustion engine tractor with an additional electric drive for the wheels of the rail drive system. The options of using the tractor in operation along with rolling stock were presented. The results of preliminary conceptual work on the selection of electric propulsion and energy storage devices to power electric motors has been illustrated. Directions for further conceptual and design research were also determined. The aim of the paper is to popularize the results of the performed research work carried out at the Institute in the field of rail-road vehicle development.

Key words: rail-road tractor, combustion engine, electric drive system

1. Introduction

The rapid consumption of fossil fuel and increased environmental damage caused by it have given a strong impetus to the development of fuel-efficient vehicles. Hybrid electric vehicles (HEVs) have evolved from their inchoate state and are proving to be a promising solution. Not only do HEVs provide better fuel economy and lower emissions satisfying environmental legislations, but also they dampen the effect of rising fuel prices on consumers. HEVs combine the drive powers of an internal combustion engine and an electrical machine [10].

The directions of road and rail vehicle drives development aim to implement hybrid and electric drives due to their ecological and economic advantages. The state of the art in the field of energy storage devices enables the design of fully or partially electrically powered vehicles [2, 4].

Existing energy storage in the form of battery packs, e.g. lithium-ion, do not ensure satisfactory mileage of motor vehicles or operating time of electric drives and require the vehicle to be shut down in order to recharge the battery.

Robust and affordable batteries are a primary challenge for hybrid vehicles. Various HEV battery compositions have been tried in the past with the best results from lithium-ion derivatives. Battery should be able to supply high power over short periods and must be capable of enduring millions of transient shallow cycles over vehicle life. [10].

In the case of hybrid diesel-electric vehicles, continuous operation of the vehicle is possible through appropriate synchronization of the cooperation of the internal combustion engine with the electric drive system.

The conducted literature review revealed a small and lacking stock of domestic and foreign publications on the subject of rail-road vehicles with HEV drives. This article is based mainly on the experience of the designers and producers of rail-road vehicles from the Łukasiewicz Research Network – Institute of Rail Vehicles "TABOR" included in several publications. A previous study [7] presents the parameters and design features of the base tractor, which was selected for adaptation to a rail-road vehicle. The process of creating a road-rail tractor by equipping the base tractor with devices that make it possible to adapt it for

track driving and shunting work with wagons was described in [8]. The simulation results of derailment safety tests [3] showed that with the minimum pressure of the rail rollers on the track (pressure in the actuators being 1.5 MPa), the criteria for safe travel through the standard test track curve with a radius of 150 m were met. In the publication [5], the Authors presented characteristics of rail-road vehicles designed at the Institute. The study [9] discussed the design features and the possibility of using a rail-road tractor for shunting works on railway tracks and other specific works on both railway and road infrastructure.

Having a well-developed rail-road vehicle and also wanting to respond to the developing trends in HEV vehicles, in Łukasiewicz – IPS "TABOR", an indirect diesel-electric drive system between the electric and hybrid drive was proposed. The main drive system is an internal combustion engine, during engine operation the energy storage systems are charged, and within a limited time defined by the capacity of energy storage, it is possible to drive solely using the electric motors. This drive concept is planned to be implemented in the C120 type rail-road tractor shown in Fig. 1 (based on the CLAAS Arion 610 diesel agricultural tractor), which is intended for shunting works on railway sidings in open areas.



Fig. 1. Rail-road tractor design based on the CLAAS Arion 610

A diesel-electric tractor may be used in locomotive sheds, railway depots and rolling stock repair plants. In such cases, there is a need to push the rolling stock from the open space to an enclosed inspection or repair hall, where the emission of exhaust gases becomes harmful to the staff engaged in maintenance or repair of the rolling stock.

The proposed concept of the diesel-electric drive allows the drive to be switched from combustion to electric mode before moving the rolling stock into enclosed spaces, eliminating harmful exhaust emissions.

The maximum possible tractive force of the tractor in the electric drive mode, determined by the weight of the tractor and the adhesion of the driving rollers of the rail running gear, is (theoretical/maximum force resulting from the assumed coefficient of friction and tractor weight):

$$F = Q \cdot \mu = 100 \text{ kN} \cdot 0,3 = 30 \text{ kN} \quad (1)$$

where: Q – total pressure of the rollers of the rail running gear on the track rails, μ – maximum friction coefficient of the drive rollers against track rail heads.

With such tractive force, a set of 20 passenger wagons can be brought into the hall, e.g. at the Warsaw–Grochów rail station. To achieve the tractive force of a tractor with a value of $\sim 30 \text{ kN}$, it is necessary to install electric motors of appropriate power and sufficient energy storage to power them.

Based on the conducted analyzes, it can be concluded that classic slow-running asynchronous motors, due to their dimensions, can provide $\sim 20 \text{ kW}$ of power, which is insufficient to generate a tractive force of $\sim 30 \text{ kN}$.

The conceptual work focused on increasing the energy storage capacity in order to extend the tractor operating time in electric driving mode and the use of a classic asynchronous electric motor to drive the rail axis rollers.

2. Tractor design concept

The tractor concept based on classic low-rpm asynchronous motors was shown in Fig. 2.

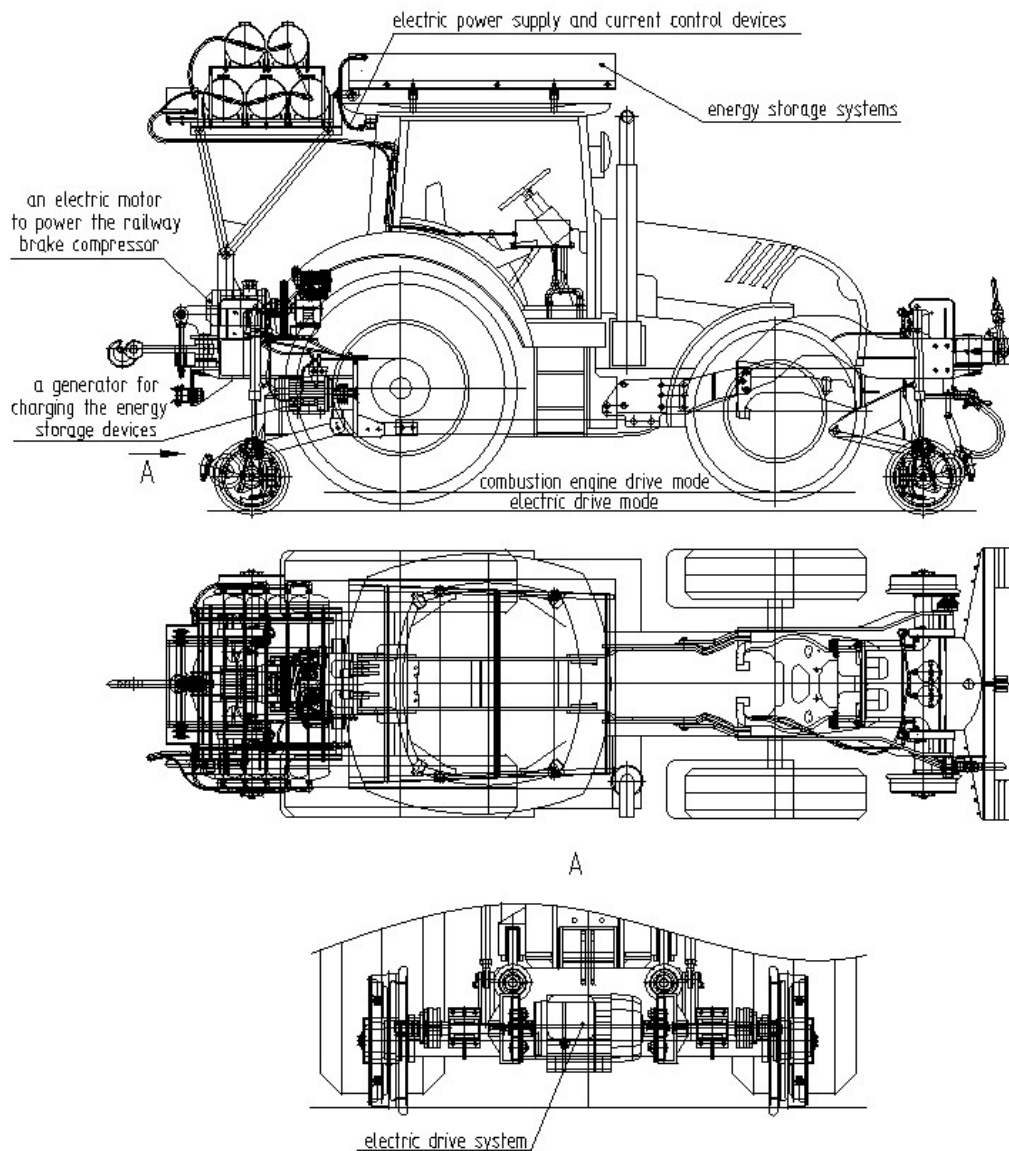


Fig. 2. Schematics of the rail-road tractor with a diesel-electric drive

The tractor construction design was presented in more detail in [6].

In order to convert the currently manufactured diesel-powered tractor into a diesel-electric tractor, it was equipped with the following additional devices:

- electric drive system for the guide rollers mounted on the rail chassis **1**
- energy storage systems **2**
- the necessary electric power supply and current control devices **3**
- a generator for charging the energy storage devices **4**
- an electric motor to power the railway brake compressor **5**.

In the diesel driving mode, the tractor rests with its tires on the rail heads, driving and braking the tires on the track rails with the natural forces of friction that occur. The coefficient of friction of the tires on the rails as well as the vehicle mass and the power of the internal combustion engine (characteristics shown in Fig. 3) allows for a tractive force of ~55 kN to be achieved on the pull-buffer systems, which enables the rolling of 10 freight wagons with a total weight of 800 tons.

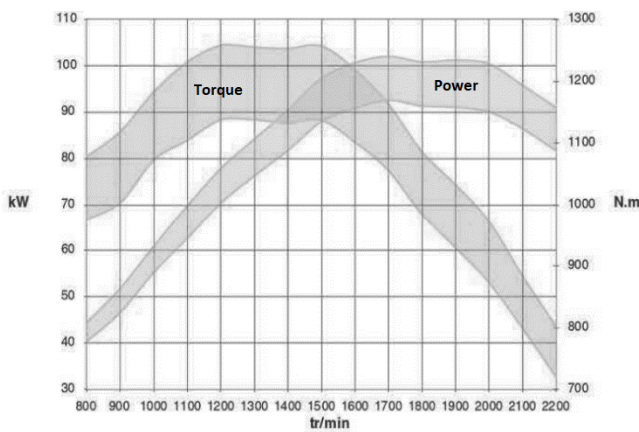


Fig. 3. Characteristics of the combustion engine of the tractor CLAAS Arion 610 [12]

When driving with the use of the electric drive, the tractor is raised by means of hydraulic cylinders to a height where the tires lose contact with the track rails. The entire weight of the tractor rests on the driving rollers of the rail running gear. With a tractor weight of ~10 tons and a roller-rail friction coefficient of 0.3–0.35, a tractive force of 30 to 35 kN can be achieved. At this stage of the concept, the traction capabilities of the tractor were not used due to the limited power of the installed electric motors due to their large dimensions.

The assumed technical and operational parameters of the tractor were:

- maximum total weight of the road-rail tractor – 10200 kg,
- the main drive system of the tractor to use on the tracks – internal combustion engine,
- supplementary drive system for driving the tractor on tracks – electric motor,
- powering electric motors – a set of lithium-ion batteries,

- battery charging – external or generator ~ 3.0 kW,
- maximum tractive force of the conventional drive – 55 kN,
- maximum tractive force of the electric drive – 15 kN,
- supply voltage of the electric motors – 400 V, 50 Hz,
- total power of electric motors – 18.4 kW (2 motors at 9.2 kW),
- energy storage systems capacity – 20 kWh,
- weight of the attached rolling stock – max 250 tons,
- maximum working time in electric driving mode ~1.0 h.

3. The energy storage system

The diesel-electric hybrid drive is characterized by cyclic recharges and discharges of the battery. The nominal battery charge (SOC) is approximately 50% (Fig. 4). The use of Ni-MH batteries means that their charge/discharge level is not too high – it is in the range of 40–60%. The use of Li-Ion batteries allows for much higher threshold values: up to 80% SOC when charging and down to about 20% when discharged. If the typical range for a battery is 25–75% SOC, this means that the capacity of the battery used must be twice as large as the intended capacity [1].

Due to the above, it was decided to build a new custom device using the available existing lithium-iron-phosphate (LiFePO4) batteries.

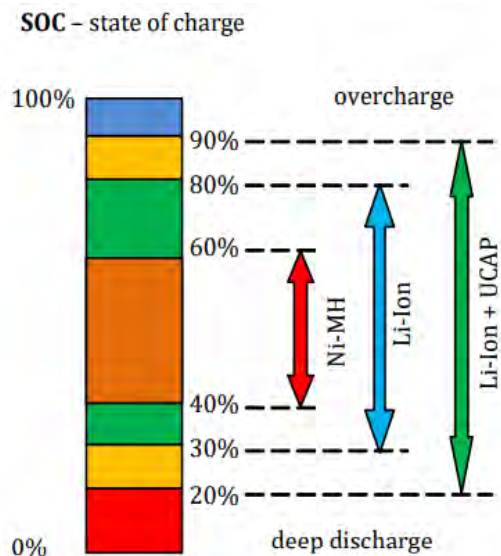


Fig. 4. Conditions for charging and discharging typical battery systems in hybrid drive systems [1]

The energy storage system was placed on the roof of the tractor cab due to the sufficiently large mounting surface of the frame attached to the brackets welded to the cab supporting pillars. The battery system with dimensions of approx. 2000 × 1600 × 400 mm holds 784 batteries with dimensions of 38 × 146 mm each (Fig. 5).

Thus a container with the following parameters was obtained:

- total storage capacity ~25 kWh,
- assumed usable energy of the battery system ~20 kWh,
- total mass of the cells – 260 kg,

A single battery and its discharge characteristics were shown in Fig. 6.

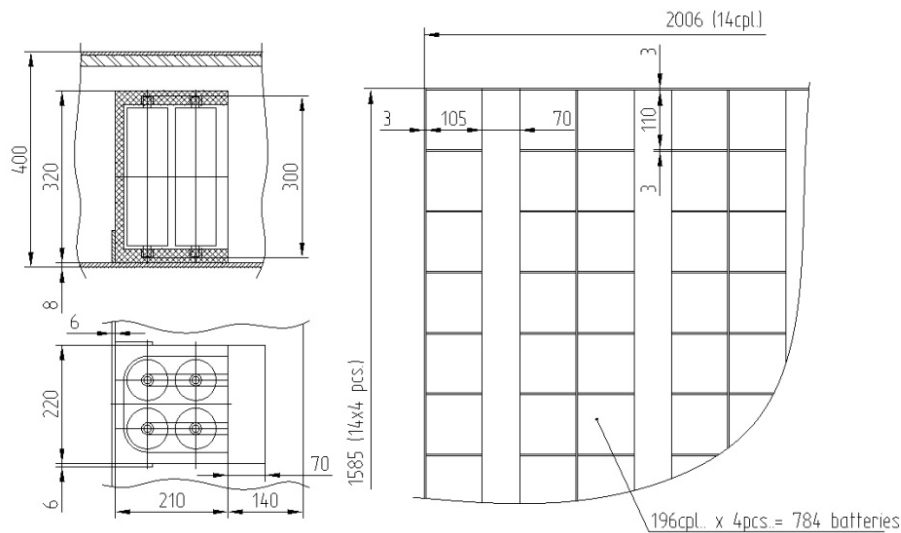


Fig. 5. Energy storage system schematic

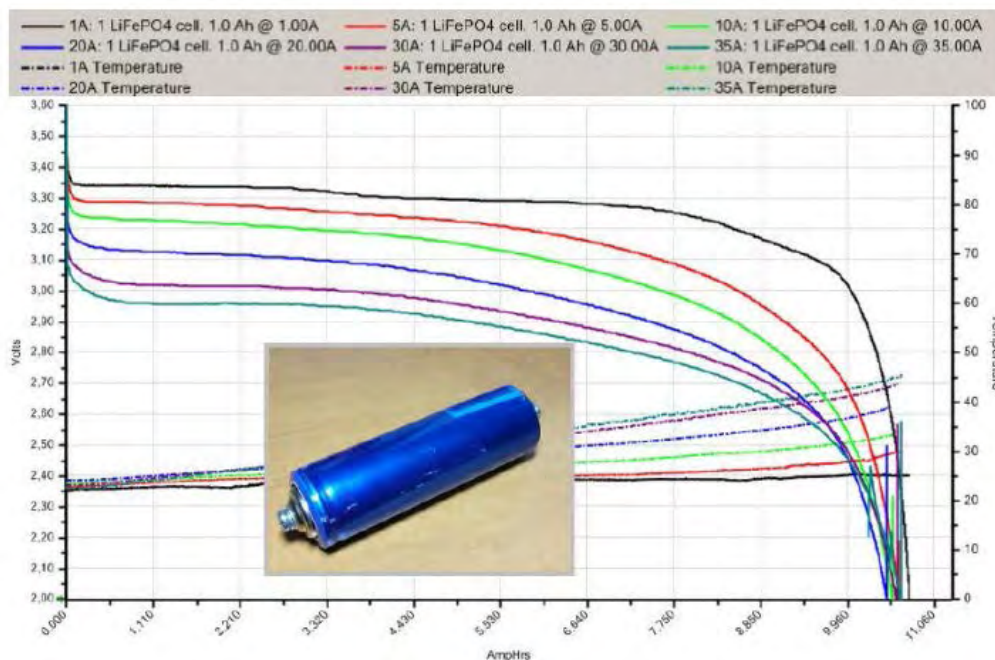


Fig. 6. A single battery cell and its discharge characteristics [11]

Characteristics of a single battery cell:

- voltage – 3.2 V
 - capacity – 10 Ah
 - internal resistance <math>< 6 \text{ m}\Omega</math>
 - charging voltage – 3.65 V ± 0.05 V
 - energy density – 105 Wh/kg
 - technology – lithium-iron-phosphate (LiFePO₄)
 - maximum discharge voltage – 2.5 V–2.0 V
 - standard charging current – 0.5 C (5 A)
 - standard charging time – 2 h
 - maximum constant charging current – 2 C (20 A)
 - standard discharge current – 1 C (10 A)
 - maximum continuous discharge current – 3 C (30 A)
 - pulse discharge current – 10 C (100 A)
 - operating temperature range:
 - charging 0–45°C
 - discharging –20°C–65°C
 - screw connections – M6 at "+" and "-"
 - dimensions – 38 × 146 mm (with M6 screws)
 - mass – 330 g
 - lifespan – over 2000 cycles (80% of capacity when charging with 1 C current)
 - possibility of combining into larger systems
- Advantages of presented battery cells:
- long lifespan
 - no memory effect
 - low passive-discharge
 - high "peak" power
 - high energy density
 - high storage capacity with high charge and discharge currents.

4. Rail axle assembly

The vehicle is equipped with two sets of rail axles installed at the front and the rear of the tractor. In diesel driving mode, the role of the rail axles is to guide the vehicle along the track by means of guide rollers mounted at the

ends of the axle. The vehicle drives and brakes using the tractor tires resting on the rail heads of the track.

In the electric drive mode, the tractor drives and brakes using the guide rollers coupled with an asynchronous electric motor. An example of a drive solution for the rail axle rollers was shown in Fig. 7.

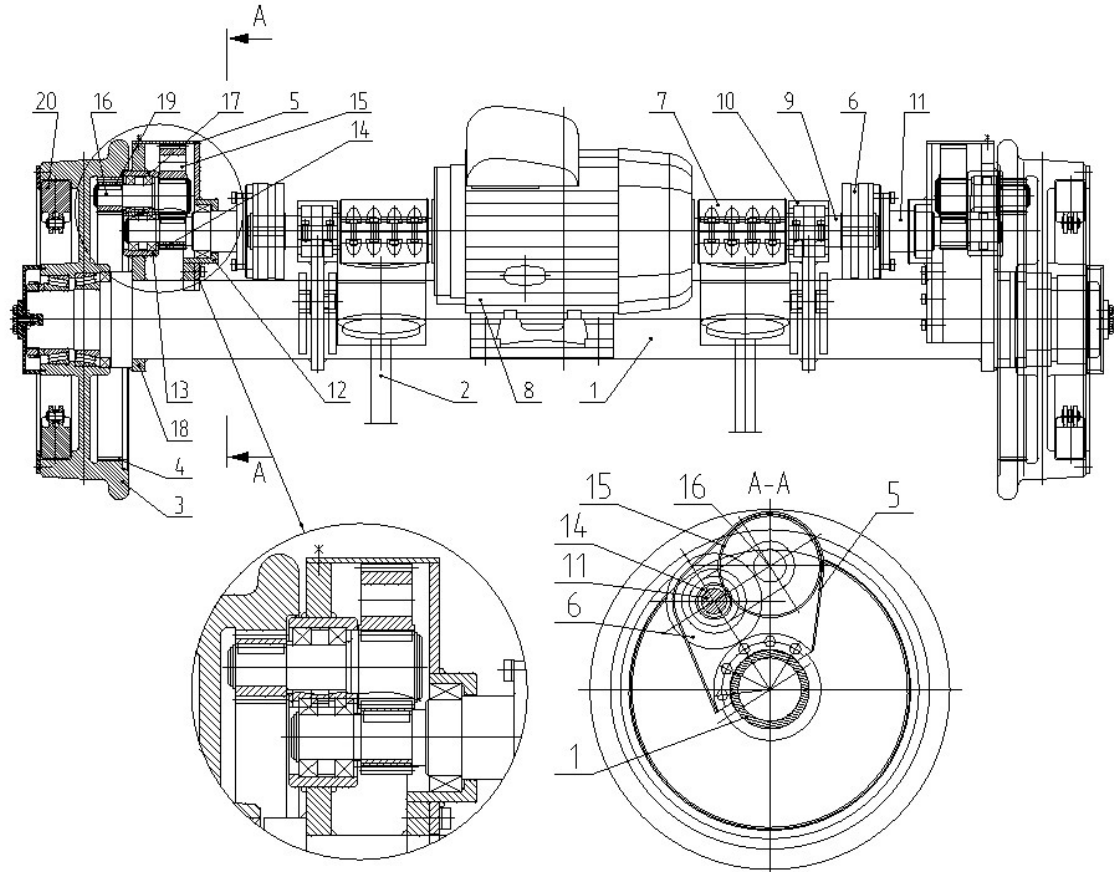


Fig. 7. Rail axle assembly with a double reduction gearbox

The axle assembly consists of the following components:

- axle **1** with rocker arms **2**
- guide rollers **3** with toothed ring **4**
- gear **5**
- electromagnetic clutch **6**
- split muff coupling **7**
- asynchronous motor **8**
- brake pad **20**.

The asynchronous motor **8** is installed in the middle part of the axle **1**. The motor has a drive shaft that extends to both sides of the motor. The shaft **9** of one part of the electromagnetic clutch **6** is connected to the drive shaft of the motor by a split muff coupling **7**. The shaft **9** is mounted in the housing **10** attached to the axle **1**. The other part of the clutch **6** is mounted on the shaft **11**, mounted in the sleeves **12** and **13**. The shaft **11** has a small toothed wheel **14** connected with the larger toothed wheel **15**, which is attached to the shaft **16** mounted on a bearing in the housing **17** welded to the bracket **18**, which is then mounted on the axle **1**. At the other end of the shaft **16** there is a small toothed

wheel **19**, which cooperates with the toothed ring **4** made in the guide roller **3**.

The gear ratio between guide rollers **3** and the toothed wheel **19** is 8.6. The gear ratio of the gear **5** is 3.1. The overall ratio between the revolutions of the motor and the revolutions of the guide rollers is $26.66 \approx 27$.

The previously developed solutions of the rail axle roller drive concept [6] were limited to the use of one toothed gear with a gear ratio of 8.6. In this case, at the nominal motor speed of 1420 rpm, the vehicle would be moving at a speed of ~ 15 km/h. In shunting traffic, the speed of 3–5 km/h is safe. Thus, an additional toothed transmission was used to reduce the theoretical speed of the vehicle to ~ 5 km/h. When designing the additional gear **5**, it was assumed that the gear housing would fit within the outer contour of the guide roller. The consequence of this assumption is the necessity to make an appropriate depression or bend of the axle **1** at the point of motor mounting to the axle **1**. The drive solution shown in Fig. 8 does not have this disadvantage.

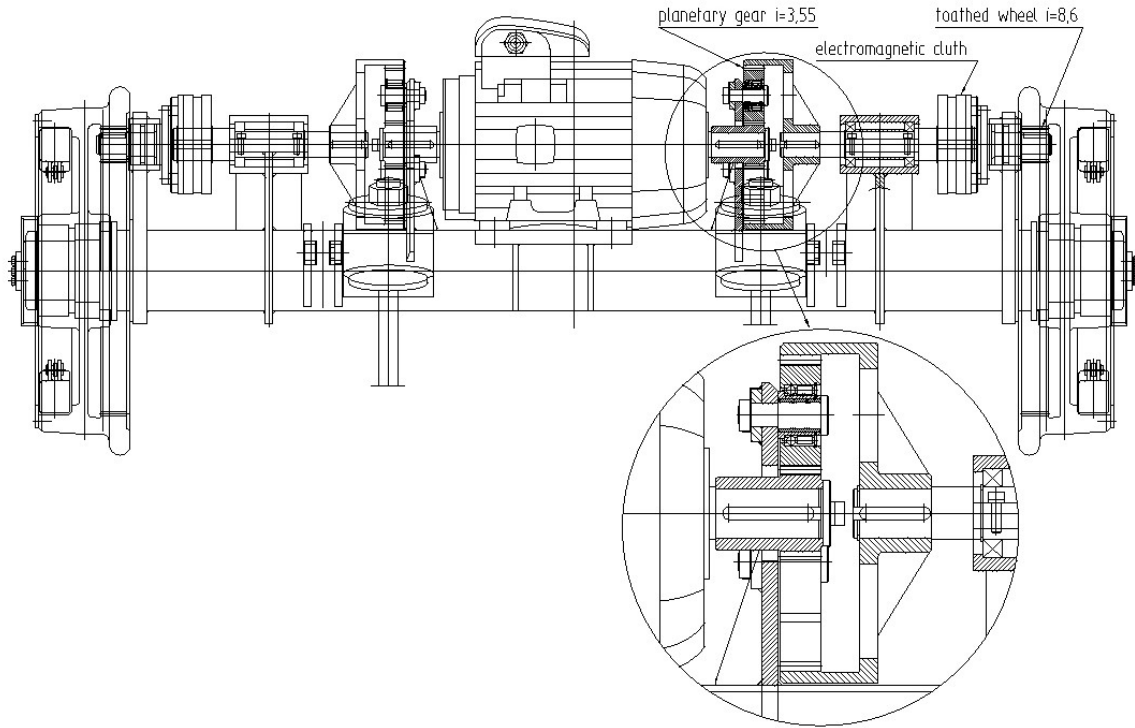


Fig. 8. Rail axle assembly with a planetary gear

Figure 8 provides an alternative solution using a planetary gear. In this guide roller drive concept, the drive shafts were arranged in one axis, which significantly simplifies the design of the drive system. A gear ratio of 3.55 was obtained in the planetary gear. The limitation of increasing the gear ratio is the distance of the shaft axis from the outer contour of the rail axle.

The electric motor used in the project was an asynchronous, three-phase motor with a double-sided shaft, type DELPHI 132MB-4-(IMB3) from the Italian company MOTIVE S.r.l (Fig. 9).

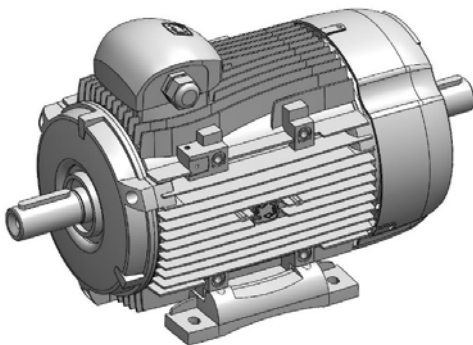


Fig. 9. DELPHI 132 MB-4-(IMB3) electric motor [13]

The technical parameters of the motor are as follows:

- motor power – 9.2 kW
- nominal motor speed – 1420 rpm
- torque at nominal rpm – 61.6 Nm
- number of poles – 4
- motor mass – 55 kg
- guide rollers torque:

$$M_K = 61.6 \cdot 30.55 = 1880 \frac{\text{Nm}}{\text{axle}} \quad (2)$$

- roller speed:

$$n_K = \frac{1420}{30.55} = 46.5 \text{ rpm} \quad (3)$$

- roller rotational speed:

$$\omega_K = \frac{n_K}{60} \cdot 2\pi = 4.9 \frac{\text{rad}}{\text{s}} \quad (4)$$

- roller linear speed

$$\begin{aligned} V_K &= R_K \cdot \omega_K = 0.25 \text{ m} \cdot 4.9 \frac{\text{rad}}{\text{s}} = \\ &= 1.22 \frac{\text{m}}{\text{s}} \cdot 3.6 = 4.3 \frac{\text{km}}{\text{h}} \end{aligned} \quad (5)$$

- torque on the rollers of one rail axle:

$$F_K = \frac{M_K}{R_K} = \frac{1880 \text{ Nm}}{0.25 \text{ m}} = 7520 \text{ N} \approx 7.5 \frac{\text{kN}}{\text{axle}} \quad (6)$$

- tractor pulling force:

$$F_c = 7.5 \cdot 2 \approx 15 \text{ kN} \quad (7)$$

In the analyzed example, the planetary gear ratio $i = 3.55$ was used. By increasing the gear ratio, e.g. to $i = 4$ the tractive force can be increased to a value of $F \approx 20 \text{ kN}$.

Conclusions

The results of analyzes of the energy storage system selection and two concepts of the guide roller assemblies of the rail drive system were presented.

The surface of the tractor cab roof and the strength of the load-bearing pillars allows for mounting one layer of the energy storage system weighing ~260 kg with a battery

capacity ~20 kWh. The obtained energy capacity of the storage system allows for continuous operation in electric driving mode for 1–1.5 hour. It is possible to install additional energy storage units of smaller dimensions, e.g. on the front supporting structure of the pull-buffer system. This makes it reasonably possible to increase the energy capacity of the tractor battery system.

Two drive system concepts for the tractor rail axle guide rollers were presented. A drive system with a planetary gear was selected for further analysis, with a proposal to increase the gear ratio to $i \approx 4$ in order to obtain a higher torque on the guide rollers.

The conducted analyzes used standard, cheap, low-speed asynchronous motors available on the market with

a power of 9.2 kW, which allow obtaining a tractive force of ~15 kN.

In order to use the full traction capabilities of the tractor in the driving mode using the electric drive (~30 kN of tractive force), it was necessary to search for an motor with greater rated power, which would achieve more than a twofold increase in torque on the rail axle guide rollers. In Poland, research is being carried out on the design of specialized motors for use in electric vehicle drives. The experience of manufacturing companies should be fully leveraged by establishing cooperation in further research works, such as between Łukasiewicz – KOMEL.

The design solution used in the preliminary project draft was submitted for patent protection.

Nomenclature

F force
M torque
n speed

V linear speed
 ω rotational speed

Bibliography

- [1] ANDRZEJEWSKI, M., PIELECHA, I., MERKISZ, J. et al. Modern drive systems of rail vehicles. *Combustion Engines*. 2019, **178**(3), 76-81. <https://doi.org/10.19206/CE-2019-314>.
- [2] BIAŁAS, A., ROSSA, R. Napęd elektryczny E-KIT dla miejskiego samochodu osobowego. *Napędy i sterowanie*. 2014, **9**.
- [3] BRYK, K., ŁUKASZEWSKI, K., MEDWID, M. Symulacyjne badania bezpieczeństwa ruchu ciągnika szynowo-drogowego CLAAS ARION 620. *Międzynarodowa Konferencja Naukowa TRANSPORT XXI WIEKU*. Arłamów 2016.
- [4] DĄBALA, K., DUDZIŃSKI, J. Napęd bezpośredni w pojazdach samochodowych – przegląd konstrukcji. *Praca Instytutu Elektrotechniki*. 2012, **260**.
- [5] MEDWID, M. Hybrydowe pojazdy kolejowo-drogowe zaprojektowane i wytwarzane w Polsce. *Technika Transportu Szynowego*. 2005, **7-8**.
- [6] MEDWID, M., DASZKIEWICZ, P., CZERWIŃSKI, J. et al. Rail-road tractor with diesel-electric drive. *Rail Vehicles*. 2019, **3**.
- [7] MEDWID, M., JAKUSZKO, W., KAZIMIERCZAK, E. Structural features of the tractor selected for adaptation to the new road-rail vehicle. *Rail Vehicles*. 2017, **3**.
- [8] MEDWID, M., STAWECKI, W., CZERWIŃSKI, J. et al. Structure modeling of the CLAAS ARION 620 road-rail shunting tractor. *Rail Vehicles*. 2017, **2**.
- [9] MEDWID, M., STAWECKI, W., CZERWIŃSKI, J. et al. Multi-purpose rail-road tractor of the new generation. *Rail Vehicles*. 2016, **3**.
- [10] SINGH, K.V., BANSAL, H.O., SINGH, D. A comprehensive review on hybrid electric vehicles: architectures and components. *Journal of Modern Transportation*. 2019, **27**, 77-107. <https://doi.org/10.1007/s40534-019-0184-3>
- [11] Battery Trade Office. <https://bto.pl> access date: 2020-08-21.
- [12] CLAAS. <https://claas.pl> access date: 2020-08-17.
- [13] MOTIVE SLR. <https://motive.it> access date: 2020-08-25.

Sylwin Tomaszewski, DEng. – Łukasiewicz Research Network – Rail Vehicles Institute “TABOR” in Poznan.

e-mail: sylwin.tomaszewski@tabor.lukasiewicz.gov.pl



Prof. Marian Medwid, DSc., DEng. – Łukasiewicz Research Network – Rail Vehicles Institute “TABOR” in Poznan.

e-mail: marian.medwid@tabor.lukasiewicz.gov.pl



Maciej Andrzejewski, DEng. – Łukasiewicz Research Network – Rail Vehicles Institute “TABOR” in Poznan.

e-mail: maciej.andrzejewski@tabor.lukasiewicz.gov.pl



Maksymilian Cierniewski, MEng. – Łukasiewicz Research Network – Rail Vehicles Institute “TABOR” in Poznan.

e-mail: maksymilian.cierniewski@tabor.lukasiewicz.gov.pl



Wojciech Jakuszko, MEng. – Łukasiewicz Research Network – Rail Vehicles Institute “TABOR” in Poznan.

e-mail: wojciech.jakuszko@tabor.lukasiewicz.gov.pl



Andrzej ZIOŁKOWSKI 
 Paweł FUC 
 Piotr LIJEWSKI 
 Łukasz RYMANIAK 
 Paweł DASZKIEWICZ 
 Michalina KAMIŃSKA 
 Natalia SZYMLET 
 Aleks JAGIELSKI

Analysis of exhaust emission measurements in rural conditions from heavy-duty vehicle

Road transport holds for the largest share in the freight transport sector in Europe. This work is carried out by heavy vehicles of various types. It is assumed that, in principle, transport should take place on the main road connections, such as motorways or national roads. Their share in the Polish road infrastructure is not dominant. Rural and communal roads are the most prevalent. This fact formed the basis of the exhaust emissions and fuel consumption tests of heavy vehicles in real operating conditions. A set of vehicles (truck tractor with a semi-trailer) meeting the Euro V emission norm, transporting a load of 24,800 kg, was selected for the tests. The research was carried out on a non-urban route, the test route length was 22 km. A mobile Semtech DS instrument was used, which was used to measure the exhaust emissions. Based on the obtained results, the emission characteristics were determined in relation to the operating parameters of the vehicles drive system. Road emission, specific emission and fuel consumption values were also calculated.

Key words: heavy-duty vehicle, emission test, exhaust emission

1. Introduction

Road transport has been observed to have the dominant position in the structure of land cargo transport in the European Union countries for many years. In 2017, 85% of all goods were transported using motor vehicles, and only 11.7% by rail. The share of inland waterway transport accounted for only 0.3% [8]. Such a configuration of the structure of cargo transport is the result of a number of factors. The most important one of them is the ability to deliver goods directly from the sender to the recipient only using one mode of transport. Currently, this is possible only with the use of road transport. This is difficult in other transport sectors because the rail and water infrastructure is not as extensive as road infrastructure. In most cases it is still necessary to also use motor vehicles to transport goods even when choosing a railroad or inland waterway as the main mode of transport. In this case, the most effective type of transport is intermodal transport using a single container unit throughout – like a car semi-trailer, container etc. This eliminates the need to unload and load the cargo itself, which extends the time and raises the transport cost.

Due to the successive increase in the number of transported goods with the use of motor vehicles in most European countries, there is a problem with the capacity of the main thoroughfares and the road network in smaller towns, which results in the increase of road congestion. It also indirectly results from the location of industrial and logistic centers often located far from the main road arteries.

The traffic intensity reduces the efficiency of transport services (extending the time and increasing the cost of moving cargo) as well as having a negative impact on the natural environment – through the emission of harmful exhaust components from motor vehicles. In countries with developed road and logistics infrastructure, this problem is not as significant as in the case of countries such as

Poland, where this infrastructure is undergoing its quickest development stage in the current decades. According to the Transport Activity Results in 2017 report prepared by the Central Statistical Office [8] in Poland in 2017, a total of 2 036 267 thousand tons of cargo were transported overall, of which up to 1 747 266 thousand tons, accounting for 85%, were transported using motor vehicles. Most of these transport activities took place in the country – the share of this type of transport reached over 80%. Therefore, it seems reasonable to assess the impact of heavy vehicles performing transport work in diversified traffic conditions, done by measuring exhaust emissions using PEMS mobile analyzers [9]. This Measurements are currently performed for various groups of vehicles [4, 7] in the field of approval and research purposes [6]. In the case of heavy-duty vehicles, the measurements are aimed at assessing the exhaust emission and fuel consumption under various operating conditions – urban driving, rural, an motorway [5, 9].

2. Research methodology

2.1. Test route selection criteria

Road infrastructure in Poland consists of national, provincial, county and communal roads. In 2017, its total length was 422 302 km, of which the largest share of 58% were municipal roads (Table 1).

Table 1. Polish road infrastructure between 2016–2017 [8]

| Road categories | Hard Surface roads | | Unsurfaced roads | |
|-----------------|--------------------|---------|------------------|---------|
| | 2016 | 2017 | 2016 | 2017 |
| National | 19 388 | 19 410 | 0.1 | 0.1 |
| Regional | 28 920 | 29 083 | 43 | 41 |
| District | 124 944 | 124 673 | 10 275 | 10 029 |
| Communal | 246 983 | 249 135 | 115 604 | 112 588 |

The smallest share in the road infrastructure that did not exceed 5% was made up by national roads. Based on this

information, it can be concluded that the national road transport of goods runs mostly along the so-called second category roads. This is also due to the location of industrial centers, which are mostly located in small and medium towns along roads of this category.

The current tendency for the development of the industrial and logistics network is to build leading centers in locations referred to as industrial districts that are close to the main thoroughfares [1]. Taking into account current trends in transport problems, eg. flow and organization of traffic for various scenarios in national transport system is used programs for modelling this issues [2, 3]. The above facts were the main factor determining the choice of the test route on which emission measurements in real traffic conditions were made. The route used for research began in the industrial district of the city of Koło, where the largest industrial plants are located, and where several dozen heavy vehicles are handled daily (Fig. 1). This district is located by the provincial road no. 270, which is also a transit route for motor vehicles with a permissible total weight over 3 500 kg by the city of Koło. This route ends at the intersection with the national road No. 92 and passes into the provincial road No. 473. Both of these roads were included into the test route chosen by the authors, which ended at the A2 motorway interchange "Dąbie". The length of the route was 22 km, of which driving in urban conditions was 10%. The remaining part of the route was in extra-urban driving conditions.



Fig. 1. The test route used in the on-road emission test of a heavy-duty vehicle [10]

2.2. Research object

For the research, the authors used heavy-duty truck (road tractors with semi-trailers) loaded with a cargo of 24,800 kg (Fig. 2). The object had a V8 412 kW (560 KM) Euro V engine (Table 2). Vehicle was fitted with an automatic transmission of the 12 + 1 configuration. Vehicle was also fitted with a driver monitoring system. The system, by a continuous analysis of signals from a series of sensors, provides real time hints and, upon end of trip, generates a report on the driving style.

The hints and the evaluation are presented on a display and have 4 categories: driving uphill, predicting, braking and gear shifts. The idea behind the system is to continuously improve the driving skills in terms of fuel consump-

tion and proper use of modern solutions such as: automatic transmission, retarder or EBS (Electronic Braking System).



Fig. 2. The heavy-duty vehicle prepared to emission test

Table 2. Characteristics of vehicles used for the tests

| Parameter | Value |
|----------------------------------|------------------------|
| Engine | |
| Displacement | 15.6 dm ³ |
| Number of cylinders/arrangement/ | 8/V8 |
| Maximum power output | 412 kW @ 1900 rpm |
| Maximum torque | 2700 N·m@1000–1400 rpm |
| Unit power output index | 10.3 kW/t |
| Emission standard | Euro V |
| Exhaust gas aftertreatment | SCR |
| Vehicle and cargo | |
| Transmission | Automatic 12+1 |
| Driver support system | SDS |
| Tractor axle configuration | 4 × 2 |
| Curb weight including trailer | 15 200 kg |
| Cargo weight | 24,800 kg |
| Type of cargo | Steel |
| Type of trailer | Canopy |

2.3. Test equipment

The Semtech DS mobile measuring device (Fig. 3) from the PEMS group was used to measure exhaust emission and fuel consumption and measured the following parameters:

- a) concentrations of CO₂, HC (hydrocarbons), THC (total hydrocarbons) and O₂ (oxygen),
- b) flue gas mass flow rate, temperature and pressure of exhaust gases,
- c) temperature, pressure and humidity of the ambient air,
- d) the speed and location of the vehicle,
- e) basic parameters of the combustion engine operation recorded from the vehicle's on-board diagnostic system.

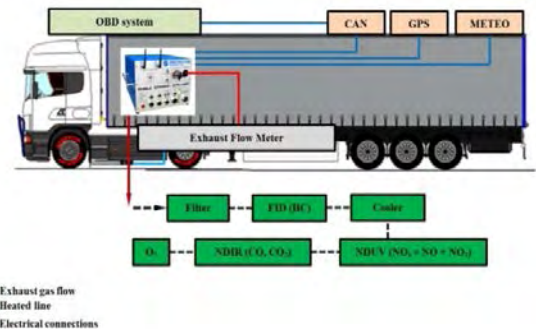


Fig. 3. The Semtech DS work schematic

Semtech DS is one of the first compact systems for the measurement of exhaust emissions in real operating conditions of vehicles. It consists of a central analyzer unit, a flow meter for measuring the exhaust mass flow rate, as well as temperature and pressure of exhaust gases. A sample of exhaust gases from the exhaust system is supplied to the central analyzer unit through a heated elastic pipe, which maintains the temperature of 191°C. This is to prevent the condensation of hydrocarbon fractions on the walls of the pipe .

3. Test results – analysis and discussion

Analyzing the characteristics of the heavy vehicle operating time share determined in the speed and acceleration intervals, the vehicle dynamics when travelling the selected route was found to be low, which is confirmed by the highest rate of acceleration from 0–0.6 m/s² representing 94% of total operating time (Fig. 4). During the tests, the vehicle moved at a speed of 0–24 m/s (0–86 km/h), with the largest share of speeds recorded in the range of 16–24 m/s (58–86 km/h). The vehicle obtained an average speed of 54 km/h on the route. Such a heavy vehicle traffic profile is characteristic for navigating the so-called second category roads, because they often run through villages and small towns with speed limits. This confirms the obtained significant share of the (0–16 m/s> speed range reaching 43%. When driving on motorways and expressways, heavy vehicles obtain higher average speeds.

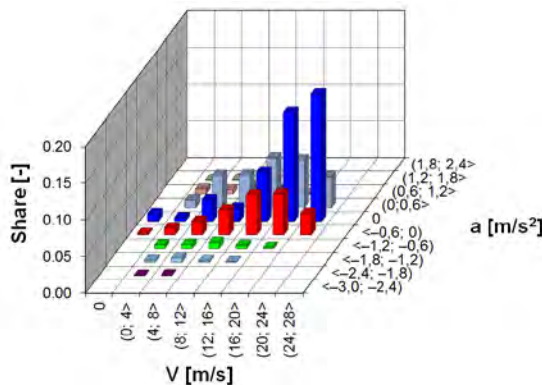


Fig. 4. Characteristics of the operating time share in the ranges of vehicle speed and acceleration

Referring the road conditions when conducting measurements to the heavy-vehicle engine operation characteristics confirms the presented thesis that the journey was characterized by a small variation in acceleration. This is mainly due to the engine running in a narrow range of crankshaft rotational speed – the largest share accounted for the engine speed of 1200 rpm and reached 62% (Fig. 5). At this speed, the engine operated mainly in the medium load range of 1200–2000 N·m. These types of engine operating parameters can be defined as an approximate load characteristic, in the scope of which the engine obtains lower specific fuel consumption than in other operating points.

The CO, CO₂ and NO_x emissions intensity were measured in the conducted road tests of a heavy vehicle. The HC emissions were intensity not measured, as earlier studies showed that in the case of heavy vehicles meeting the Euro V standard and higher, HC emissions are negligible. The

highest values of CO emission intensity were registered in the urban part of the test drive (Fig. 6a). It was caused mainly by high acceleration variability of the heavy vehicle due to the shape of road infrastructure. In the extra-urban part, the drive was characterized by smaller changes in speed, which translated into lower CO emission intensity. This was especially visible in the 600–1180 seconds of drive duration range. In terms of the general engine characteristics, the highest values of CO emission intensity occurred at the maximum torque of 2400–2800 N·m in the engine speed range of 1000–1600 rpm (Fig. 6b).

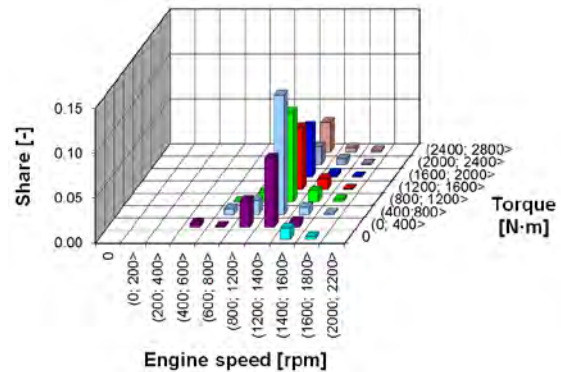


Fig. 5. Characteristics of the operating time share in the ranges of engine speed and load

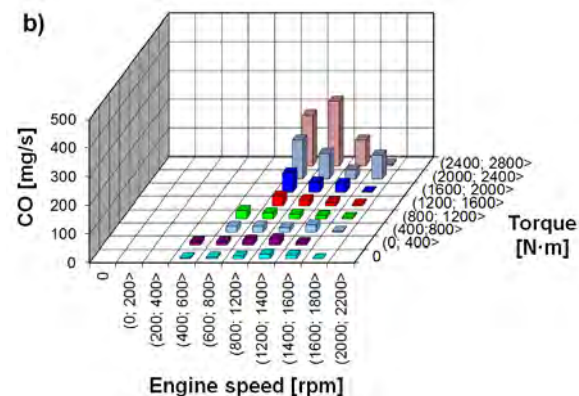
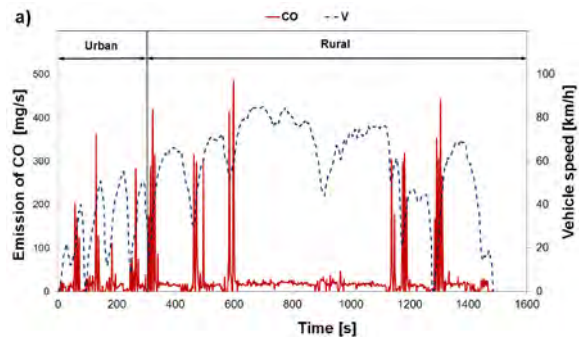


Fig. 6. The emission intensity of CO with vehicle speed (a) and emission intensity in engine speed and load intervals (b)

The NO_x emission intensity characteristic was similar to the CO emission – the intensity increased with increasing vehicle speed (Fig. 7). In the urban part, the average NO_x emission intensity value was 50.7 mg/s, which compared to the rural section is an increase of 50%. It should also be

noted that the test was started with the engine being in a stabilized thermal condition (coolant temperature was 80°C), which eliminated any impact that the engine warm-up phase could have on the SCR (*Selective Catalytic Reduction*) conversion rate which is responsible for NO_x reduction. NO_x reduction reactions in the SCR catalytic system are preceded by the injection of 32.5% of urea into the outlet system, from which the ammonia constituting the reducer is formed.

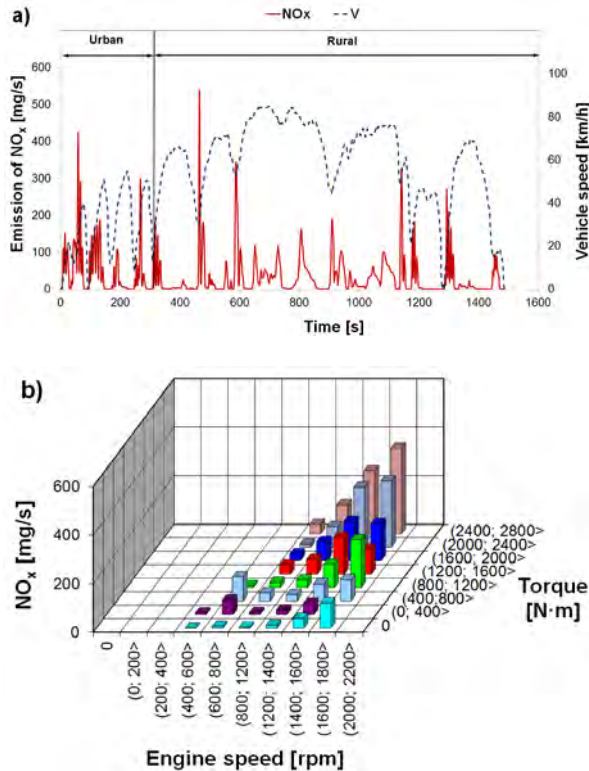


Fig. 7. The emission intensity of NO_x with vehicle speed (a) and emission intensity in engine speed and load intervals (b)

This injection takes place only when the exhaust gas temperature is greater than 200°C and the NO_x concentration exceeds 500 ppm. From this it follows that the main factor determining the intensity of NO_x emissions during road tests was a relatively large proportion of the heavy vehicle starting to move after being stationary. This translated into higher crankshaft speed values and higher engine load – in the range 1600–2800 Nm at 1400–1600 rpm. The highest NO_x emission intensities were recorded in these combustion engine operating points.

In the case of CO₂ emission intensity, its increase, related to the acceleration of the vehicle, was also recorded (Fig. 8a). CO₂ emission is representative of the fuel consumption, so in sections where CO₂ emission reaches maximum values the obtained fuel consumption is greatest. For a travelling heavy vehicle the highest fuel consumption occurs when accelerating, where the engine generates increased torque compared to when driving at a constant speed. The measurements carried out mirrored the relation described above (Fig. 8b). The highest values of CO₂ emission intensity were obtained when the engine was operating under maximum load.

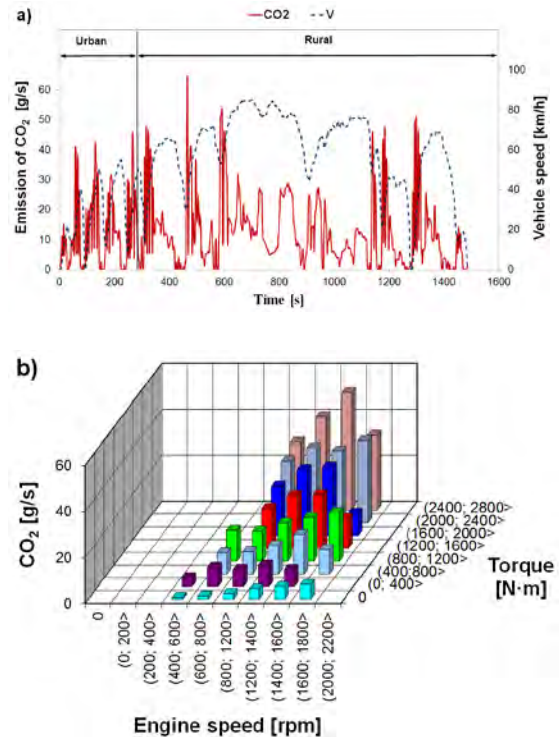


Fig. 8. The emission intensity of CO₂ with vehicle speed (a) and emission intensity in engine speed and load intervals (b)

4. Conclusion

Based on the measured values of exhaust emission intensity, vehicle speed and the registered combustion engine operating parameters of the tested vehicle the road and specific emissions of CO, NO_x, CO were determined as well as the fuel consumption value. The vehicle road emission values were:

- CO – 1.7 g/km;
- NO_x – 2.4 g/km;
- CO₂ – 836.9 g/km.

While the specific emission values were:

- CO – 1.3 g/kWh;
- NO_x – 1.8 g/kWh;
- CO₂ – 605.1 g/kWh.

On the test route the vehicle obtained a fuel consumption of 30.9 dm³/100 km. Based on the Authors own experience in road emission tests of heavy vehicles it was concluded, that the obtained fuel consumption on the extra-urban route was small compared to the mixed driving conditions. Previous research conducted by the authors [5] done using the same vehicle in conditions of combined urban and extra-urban driving can be used as an example. On said route the fuel consumption obtained was 37.1 dm³/100 km, which was 20% higher compared to the value for extra-urban driving conditions. Comparing the specific exhaust emission values of CO and NO_x from the test drive to the limit values defined in the Euro V norm it was concluded, that these values are below the set limit. Hence, despite the fact that the tests were performed on so-called second category roads, the test drive was characterized by small variability of vehicle acceleration values, which in turn resulted in relatively small specific emission values of CO, NO_x as well as low fuel consumption of the heavy vehicle.

Acknowledgements

The research was funded by European Union from European Regional Development Fund through the National Centre for Research and Development (Narodowe Centrum Badań i Rozwoju) – research project within the Smart

Growth Programme (contract No. POIR.04.01.02-00-0002/18).



Nomenclature

| | | | |
|------|--------------------------------------|-------|-------------------------------|
| a | acceleration | s_j | share |
| CAN | Controller Area Network | SCR | Selective Catalytic Reduction |
| EBS | Electronic Braking System | SDS | Driver Support System |
| GPS | Global Positioning System | T | torque |
| PEMS | Portable Emission Measurement System | V | velocity |

Bibliography

- [1] JACYNA, M. System Logistyczny Polski. Uwarunkowania techniczno-technologiczne komodalności transportu. *Oficyna Wydawnicza Politechniki Warszawskiej*, 2012.
- [2] JACYNA, M., MERKISZ, J. Proecological approach to modelling traffic organization in national transport system. *Archives of Transport*. 2014, **30**(2).
- [3] JACYNA-GOŁDA, I., ŻAK, J., GOŁĘBIEWSKI, P. Models of traffic flow distribution for various scenarios of the development of proecological transport system. *Archives of Transport*. 2014, **32**(4).
- [4] MERKISZ, J., DOBRZYNSKI, M., KUBIAK, K. An impact assessment of functional systems in vehicles on CO₂ emissions and fuel consumption. *MATEC Web of Conferences*. 2017, **118**.
<https://doi.org/10.1051/mateconf/201711800030>
- [5] MERKISZ, J., FUC, P., LIJEWSKI, P. et al. Impact of application type of engine in heavy-duty vehicle for CO₂, CO emission and fuel consumption. *Prace Naukowe Politechniki Warszawskiej – Transport*. 2013, **98**.
- [6] MERKISZ, J., KOZAK M., LIJEWSKI, P. et al. Exhaust emissions from heavy-duty vehicles under actual traffic conditions in the city of Poznań. *Asia Pacific Automotive Engineering Conference*. Bangkok. *SAE Technical Paper 2013-01-0119*, 2013. <https://doi.org/10.4271/2013-01-0119>
- [7] PIELECHA, J., JASINSKI, R., MAGDZIAK, A. Practicality of passenger vehicle driving emission tests according to new European Union procedures. *MATEC Web of Conferences*. 2017, **118**.
<https://doi.org/10.1051/mateconf/201711800021>
- [8] Transport – wyniki działalności w 2017 r. Główny Urząd Statystyczny. Warszawa 2018.
- [9] QUIROS, D.C., THIRUVENGADAM, A., PRADHAN, S. et al. Real-world emissions from modern heavy-duty diesel, natural gas, and hybrid diesel trucks operating along major California freight corridors. *Emission Control Science and Technology*. 2016, **2**. <https://doi.org/10.1007/s40825-016-0044-0>
- [10] <http://gpsvisualizer.com> (access 15.12.2018).

Andrzej Ziółkowski, DEng. – Faculty of Civil and Transport Engineering, Poznan University of Technology.

e-mail: andrzej.j.ziolkowski@put.poznan.pl



Paweł Daszkiewicz, DEng. – Łukasiewicz Research Network – Rail Vehicles Institute „TABOR” in Poznań.

e-mail: pawel.daszkiewicz@tabor.lukasiewicz.gov.pl



Prof. Paweł Fuć, DSc., DEng. – Faculty of Civil and Transport Engineering, Poznan University of Technology.

e-mail: pawel.fuc@put.poznan.pl



Michalina Kamińska, MEng. – Faculty of Civil and Transport Engineering, Poznan University of Technology.

e-mail: michalina.kaminska@put.poznan.pl



Prof. Piotr Lijewski, DSc., DEng. – Faculty of Civil and Transport Engineering, Poznan University of Technology.

e-mail: piotr.lijewski@put.poznan.pl



Natalia Szymlet, MEng. – Faculty of Civil and Transport Engineering, Poznan University of Technology.

e-mail: natalia.r.szymlet@doctorate.put.poznan.pl



Łukasz Rymaniak DEng. – Faculty of Civil and Transport Engineering, Poznan University of Technology.

e-mail: lukasz.rymaniak@put.poznan.pl



Aleks Jagielski, MEng. – Faculty of Civil and Transport Engineering, Poznan University of Technology.

e-mail: alexjagielski@gmail.com



The possibility of energy consumption reduction using the ECO driving mode based on the RDC test

The greenhouse effect and overall climate changes are the main reasons for developing ecological powertrain units dedicated to road vehicles. An electrical drivetrain without using conventional combustion engines fueled by hydrocarbon fuels is an effective method to significantly reduce CO₂ emissions from the fleet. It is particularly vital in 2020 emission regulations aspects, and continuously the number of vehicles increasing. In this paper battery electric drive system of a small size passenger car was analyzed in terms of two different drive modes in cooperation with two recuperative braking modes. The research was carried out with real driving condition test requirements and driving parameters recording. Based on data obtained from OBD signals, energy flow and torque distribution have been specified. In results, overall reducing energy consumption has been achieved with ECO mode compared to normal mode. Selection of the driving mode ECO has a positive impact on reducing the state of charge saving more than 5%, taking into account the whole RDC test; greater energy consumption reductions were observed in selected test areas.

Key words: electric vehicle, energy flow, regenerative braking, powertrain, driving mode

1. Introduction

The trends in the design of powertrains of road vehicles are mainly set by the changing exhaust emission legislation. It is a common knowledge that exhaust emissions have a negative impact on the natural environment and human health. Carbon dioxide, one of the main greenhouse gases (GHG) responsible for the global climatic changes, is generated, inter alia, during the combustion of hydrocarbon-based fuels in combustion engines (ICE) [28]. A significant contribution of road transport to the overall emission of GHG and the forecast of a 60% increase in the number of vehicles by 2035 compared to 2014 presented by International Organization of Motor Vehicle Manufacturers indicate the significance of the impact of this means of transport on the environment [2]. The effect is the tightening of the homologation regulations on the specific emission of CO₂ from newly registered passenger vehicles and light duty trucks in the European Union. Starting from 2020, the admissible average emission of carbon dioxide from a fleet of vehicles is 95 g/km. The excess of this limit (past 2021) will be subject to an additional fee of 95 euros multiplied by the exceeded emission and the number of newly registered vehicles [5, 10].

An effective method of reduction of the CO₂ emission from a fleet of vehicles is the application of zero-emission, particularly fuel-electric (EV) powertrains. The main group are the widely implemented battery electric vehicles (BEV) and, introduced by some of the carmakers, fuel-cell electric vehicles FCEV [38]. The experts forecast a reduction in the demand for diesel, gasoline and liquefied petroleum gas (LPG) fuels and an increased demand for electrical energy for the charging of BEV vehicles. The latter is to reach approx. 4806 GWh in 2035 in Poland, which gives a 178 times higher result compared to the 27 GWh in 2015 [19].

The current advancement of conventional powertrains allows the obtainment of an optimum point of work of

a combustion engine by applying automatic transmissions. A proper application of the powertrain hybridization may have a positive impact on the shift of the engine operating range towards the area of lower fuel consumption. The application of an electric motor in the powertrain allows energy regeneration with a simultaneous process of high voltage battery charging, which allows the operation of the vehicle in a fully electric or hybrid mode. In order to systematize the structures of cooperation of an electric motor in vehicle powertrains, designations from P0 to P4 were adopted (Fig. 1). For example P0 identifies belt-driven MGs attached to the front of the engine. A P2 with the PHEV capability actually delivers better overall efficiency in pure electric mode than the powersplit type. P4 allows the fitting of the electric motor directly in the driven axle.

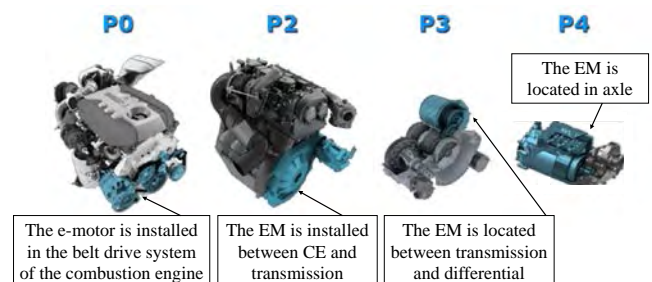


Fig. 1. Electrification of ICE-based powertrain systems [15]

In the years 2010–2019 a significant increase in the worldwide sales of electric vehicles was recorded (Fig. 2). The greatest number of electric vehicles is sold in China. The sales in the US and Europe are also significant. The number of BEV vehicles registered in Poland increased over two times from 895 in 2018 to 1677 in 2019 [26]. In multiple publications, [11, 26, 32] a further intense fleet electrification is forecasted.

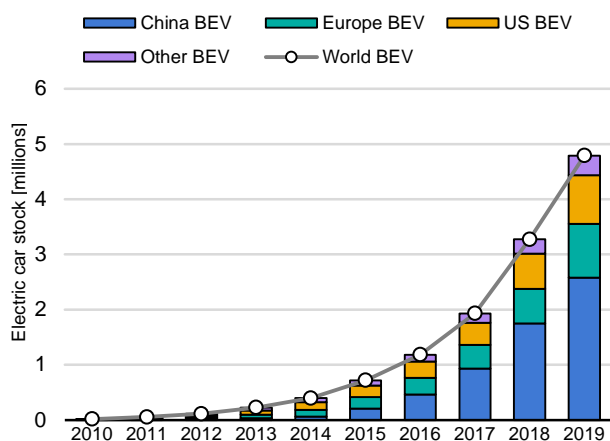


Fig. 2. World sales of Battery Electric Vehicle between 2010–2019 [27]

When considering the influence of a BEV vehicle on the environment, attention should be drawn to the source of electrical energy, which has a direct impact on the emission of carbon dioxide [37]. Burchart-Karol et al. [4] have evaluated the influence of battery charging on the natural environment going on the assumption of a constant energy consumption of 19.9 kWh/100 km by a vehicle in different EU member states. The criteria of evaluation were the emission of greenhouse gases, human health, water consumption, impact on the eco-system and depletion of natural resources. In the majority of the analyzed countries, the influence of electric vehicle charging decreased in subsequent years along with the increase in the share of renewable energy used for the charging. The battery charging had the smallest environmental impact in France, taking into account the majority of the analyzed categories, while in the case of Denmark the smallest cumulative water use was observed. The most environment-friendly source of renewable energy for the BEV vehicles was the wind energy. The performed comparative Life Cycle Assessment (LCA) for the BEV vehicles and a conventional ICEV with particular focus on utilization indicate a greater environmental impact of BEV vehicles at the stage of production. This is particularly caused by the process of production of batteries and other materials [21, 34]. An important problem in the advancement of BEV electric vehicles is the effective and ecological method of storage of electrical energy. Today, the most common material for the production of batteries is lithium, and the manufacturers estimate the life of such batteries at 6–8 years. When the battery capacity decreases by 20–30%, it is to be renewed [8, 36]. This type of batteries can be rebuilt [83], used again for other purposes such as energy storage from renewable sources [6] or recycled [7]. Given the cost of battery production reaching 35% of the final price of the vehicle, the fact of its further life is significant [36] and the assessment of the aging process is a subject of research [3, 30]. The application of batteries of lower capacity in vehicles without a significant reduction of the vehicle range is possible by the application of light materials such as aluminum and carbon fiber reinforced plastic for their production [31].

The range of a BEV vehicle depends on the battery capacity, energy consumption by the vehicle and the automo-

tive comfort systems. An efficient method of energy saving and at the same time an unparalleled advantage of electric vehicles is the possibility of energy regeneration from braking. The energy lost during braking is estimated at 50% of the energy used for the operation of the vehicle, particularly under the conditions of urban driving [20]. An important factor is also the driving style. Questionnaire-based research carried out among drivers of conventional vehicles (ICE) and EV [40] has shown a greater tendency of drivers to apply eco-driving when using an electric vehicle. This is exhibited by smoother driving with limited braking and limited hard acceleration. Such drivers are also more likely to extend the time of traveling to ensure lower energy consumption. The in-vehicle display (IVD) technologies appear quite helpful in maintaining the proper driving style.

Due to the limited range of BEV vehicles, hence the need to plan the trip, forecasting energy consumption and identification of the factors influencing this consumption is extremely important from the user's point of view. Zhichen et al. [38] used a simulation to compare the efficiency of energy recovery from a BEV vehicle. Three test routes of different average speeds were selected for comparison. The greatest amount of energy was recovered for the slowest test route (33.4%) and the smallest amount was recovered for the fastest (expressway) route. More simulations were carried out by Gao et al. [16]. They compared the influence of eco-driving for three different types of vehicles used according to their intended use. Eco-driving style was based on the reduction of frictional braking loss via appropriate speed control, avoiding unnecessary braking and, if possible, shortening the standstill time. The benefits of eco-driving using full electric powertrain reduce the energy consumption in passenger vehicles by 27%, buses 22% and heavy-duty trucks by 8% (Fig. 3). For conventional powertrains the impact of eco-driving is even greater. In the said paper, the authors also presented the significance of loss during regenerative braking. They indicate a possibly great reduction of braking in order to limit the loss.

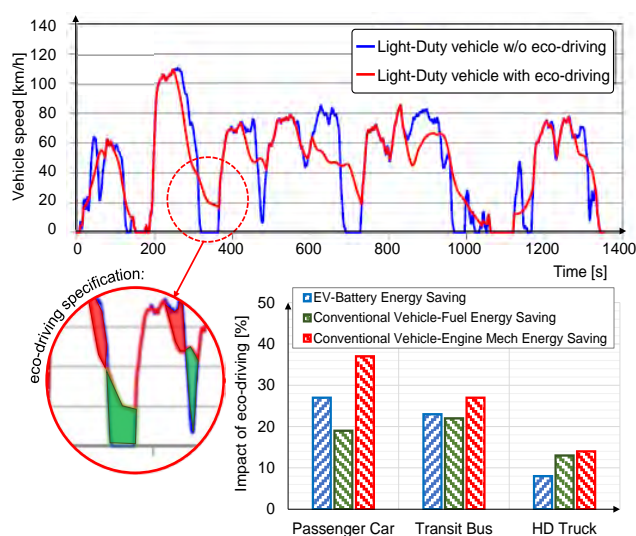


Fig. 3. Example of passenger car speed profiles with and without eco-driving applied and a comparison of the percent energy savings of the EVs and conventional vehicles resulting from eco-driving [16]

Another energy consumption test was performed on a 90 kW electric vehicle under real traffic conditions in compliance with the RDE test requirements [17]. As a result of two correctly realized test runs, an average energy consumption of 19.6 kWh was obtained. In road tests, it is important to identify the factors influencing the energy consumption (the consumption of energy by additional equipment and braking strategy). With the assistance of the developed model [1], the authors have proven a 15–40% increase in the overall energy consumption by a vehicle driven at the speed of 20 km/h and 5–15% for the average speed of 60 km/h assuming additional energy consumption on the level of 250–750 W. Additional energy consumption denotes energy consumed by climate control, interior lighting, multimedia and vehicle control. The analysis of the amount of energy recovered during braking indicates a reduction in the energy recovery along with the increasing average speed of the test run. Another aspect influencing the energy consumption is the traffic management strategy that changes the speed profiles of the vehicle [13]. The probabilistic approach analyzing four different infrastructure scenarios indicates varied energy consumption and proposes the application of the developed model in further works. Kalt et al. [29] have attempted to develop a representative driving cycle dedicated for use when designing electric powertrains. Data from a large number of EV taxis and personal vehicles were recorded with the resolution of 1 Hz. The results indicate greater acceleration values and higher average speeds than those specified by the WLTP test. It has also been confirmed that a single test cannot reflect all the cases of actual traffic operation and work points of the powertrain. When calculating the energy consumption, one must allow for the type of road. Tests performed on a chassis dynamometer according to the NEDC test requirements indicate a great significance of the arterial road [12]. Forecasting of energy consumption can be done using two paths – the offline mode based on the information pulled from vehicle systems supplemented with the information obtained in the online mode. The performed comparison of the forecast with the actual traffic conditions have rendered positive results – the difference in the energy consumption did not exceed 10% [41].

In the analyzed literature, authors draw attention to the energy consumption of a BEV vehicle directly related to its range. Predicting energy consumption based on the assessment of the vehicle energy consumption is a key factor in the further advancement of electric vehicle technology. A proper assessment should be made under actual traffic conditions, as the tests do not entirely reflect the driving dynamics. The influence of the driving dynamics on the final results is critical. In the paper, the authors attempted to analyze the energy consumption of a passenger vehicle from the A category BEV vehicle allowing for regenerative braking strategies and the available driving modes implemented by the manufacturer based on road tests performed in compliance with the RDC procedure. Similar works have been performed earlier on vehicles fitted with a hybrid drive (combustion engine-electric) [9, 14, 35].

2. Aim of the research

The aim of the performed research was the evaluation of the energy consumption of a Skoda CITIGO^e iV battery electric vehicle allowing for the actual traffic conditions and the use of different powertrain modes. The following research questions were posed: How much energy does a city electric vehicle consume during its intended operation? What economies can be expected by varying the operation of the powertrain (restricting the instantaneous power output and maximum speed of the vehicle)? The scope of the research included two test runs compliant with the RDC test procedure in urban, rural and motorway cycles. The control of the powertrain included modifying the regenerative braking strategy and activation of the eco-mode (limited energy consumption). The data from the test run were recorded in real time based on the information pulled from the vehicle CAN network by a dedicated OBD diagnostic scan tool.

The assessment of the energy flow was made in compliance with the RDC driving cycles, also used in the RDE tests. To this end, research procedure compliance analyses were performed [18, 33]. The flow of the energy ΔE was determined based on the flow of current and voltage of the battery as a result of its discharge, charge and regenerative braking:

$$\Delta E_i = \sum_{t=0}^{t=t_{\max}} U_{\text{BAT}} \cdot I_{\text{BAT}} dt \quad (3.1)$$

- discharging:

$$\Delta E_{\text{dis}} = \sum_{t=0}^{t=t_{\max}} U_{\text{BAT}} \cdot I_{\text{BAT}} dt (\text{when } \Delta E_i < 0) \quad (3.2)$$

- charging:

$$\Delta E_{\text{ch}} = \sum_{t=0}^{t=t_{\max}} U_{\text{BAT}} \cdot I_{\text{BAT}} dt \quad (3.3)$$

(when $\Delta E_i > 0$ and $M_{\text{reg}} \geq 0$)

- energy recovery (regenerative braking):

$$\Delta E_{\text{reg}} = \sum_{t=0}^{t=t_{\max}} U_{\text{BAT}} \cdot I_{\text{BAT}} dt \quad (3.4)$$

(when $\Delta E_i > 0$ and $M_{\text{reg}} < 0$)

where: U_{BAT} – voltage [V], I_{BAT} – current [A], dt – time [h], M_{reg} – braking torque [Nm].

In order to determine the individual electric powertrain operating conditions, road portions were specified where the system operated in these individual conditions. On this basis, the operating modes were divided into individual phases: driving, acceleration, standstill and braking during operation of the electric drive. The adopted criteria have been shown in Table 1.

Table 1. Vehicle motion phase criteria

| Mode | Parameters |
|-------------------------|------------------------------------|
| EV mode | $a = 0, v > 0$ |
| Acceleration EV | $a > 0, v > 0$ |
| Standstill | $v = 0$ |
| EV regenerative braking | $a < 0, v > 0, I_{\text{BAT}} > 0$ |

3. Research object

The investigations were carried out using a vehicle fitted with a ŠKODA CITIGO° iV electric drive allowing different driving modes and variable intensity of regenerative braking. The ŠKODA CITIGO° iV powertrain of the power output of 61 kW used a Li-Ion battery of the full capacity of 36.8 kWh and useable capacity 32.3 kWh. The location of the batteries has been presented in Fig. 4. The batteries are fitted in the tunnel between the seats, under the driver and passenger's seats and under the rear seats. The parameters of the investigated vehicle have been presented in Table 2.



Fig. 4. Location of the battery in the vehicle [24]

Table 2. Technical data of the analyzed powertrain fitted in Skoda CITIGO° iV [39]

| ŠKODA CITIGO° iV | |
|---------------------------|---------|
| Electric motor | |
| Max. voltage [V] | 360 |
| Max. power output [kW/KM] | 61 (82) |
| Max. torque [Nm] | 212 |
| Battery | |
| Type | Li-Ion |
| Capacity [kWh] | 32.3 |

The analyzed electric vehicle is a redesigned version of the original model fitted with a conventional combustion engine powertrain. In the original powertrain, the engineers fitted a naturally aspirated 1.0L three-cylinder indirect fuel injected (MPI) gasoline engine (Fig. 5) combined with a 5 speed automatic transmission. The electric version of CITIGO° iV is fitted with a liquid-cooled three-phase powertrain (Fig. 6) with a single electric motor of a constant gear ratio.

Figure 7 presents the performance of two types of powertrains used in the analyzed vehicle model. The electric 61 kW motor marked red and the most powerful version of the combustion engine (55 kW) are used in this car model. The main difference between the engine and the electric motor is the speed range resulting from the design differences. It is noteworthy that the comparison involved the engines only, not the entire powertrain. The powertrains differ in the way the power is transferred to the wheels. In

the case of the electric motor, a constant ratio transmission was applied while the conventional powertrain included a multi-speed manual or automatic transmission.



Fig. 5. The gasoline engine used in the conventional Skoda CITIGO° iV powertrain system [25]

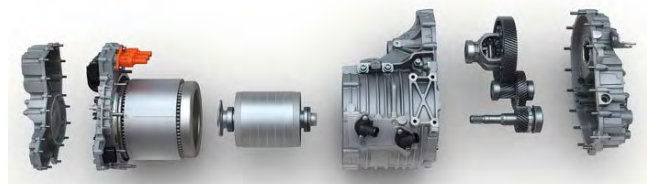


Fig. 6. Design of the Skoda Citigo° iV electric powertrain unit [23]

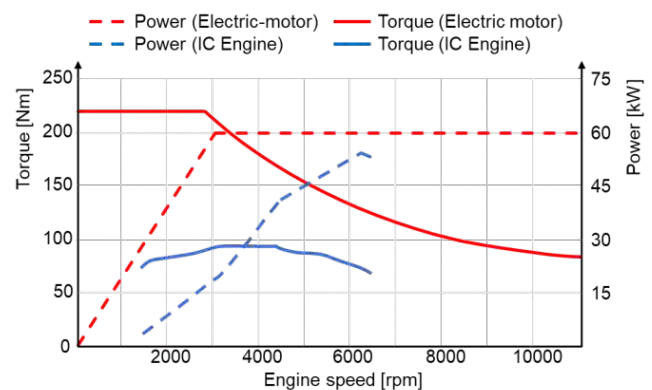


Fig. 7. Catalogue comparison of the performance of the electric motor and the internal combustion engine fitted in Skoda CITIGO° iV [39]

4. Research methodology

The investigations presented in this paper were performed experimentally based on the test runs carried out on a BEV vehicle on the predetermined route in compliance with the RDE homologation tests. The advantage of the said tests is that the cycles are defined so as to represent a real life scenario. They must take into account variable environment, road slopes, wind, traffic and different driving behaviors (Fig. 8). As per the presented range, the RDE test provides the analysis of the powertrain in its widest possible range of operation.

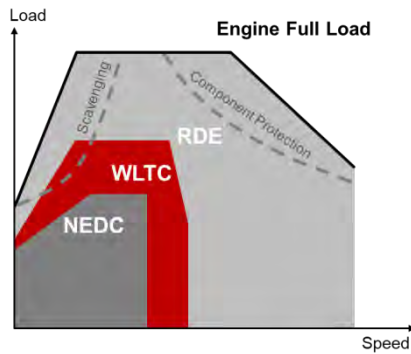


Fig. 8. Emission norm cycle operating ranges comparisons [22]

The selected route (Fig. 9) went through the city of Poznań and its surrounding areas. It covered urban, rural and motorway portions. The maximum legal speed on the latter is 140 km/h. The test route was proposed and determined following another paper by the authors [14] and its determination was not the purpose of this paper. Selected test requirements related to the course of the test run have been presented in Table 3. As per the requirements, the duration of all the test runs exceeded 90 minutes.

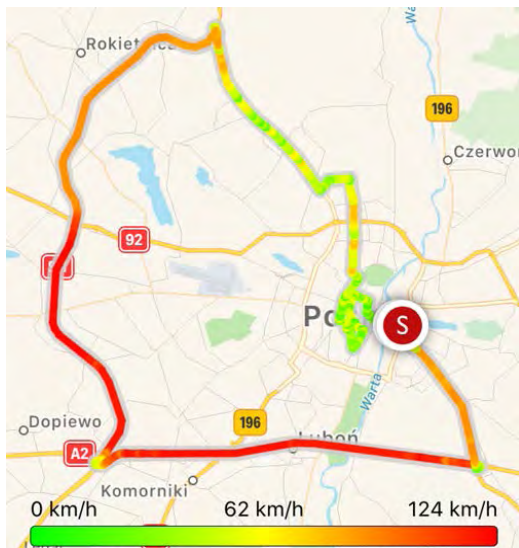


Fig. 9. Route pattern followed in the research

Table 3. Real Driving Conditions test requirements

| Selected RDE/RDC test requirements | Urban | Rural | Motorway |
|---|-----------------------------|---------------------|----------|
| Cycle repetition ($\pm 10\%$) [%] | $29 < \text{ratio} \leq 34$ | 33 | ← |
| Speed [km/h] | < 60 | $60 \leq V \leq 90$ | $V > 90$ |
| Max. speed (± 15 km/h for less than 3% of driving time) [km/h] | – | – | 145 |
| Average speed (stops included) [km/h] | $15 \leq V \leq 30$ | – | – |
| Minimum travelled distance [km] | 16 | ← | ← |
| Altitude difference (beginning/end) [m] | 100 | ← | ← |
| Maximum slope [m/100 km] | 1200 m/100 km | ← | ← |

Two runs were carried out at the same time of day, day after day in order to ensure possibly reproducible test conditions. The average ambient temperature was 22°C and ambient pressure 1015 hPa.

In the analyzed passenger car, four recuperation braking intensity levels from 1 to 4 are available (Fig. 10). Level 1 means the lowest braking intensity, Level 4, also called "B" means the biggest intensity. The electric motor automatically realizes the braking while releasing the accelerator pedal.

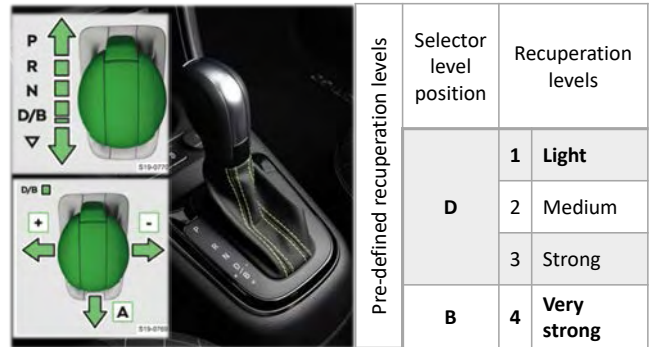


Fig. 10. Available recuperation levels (results of tests for D1 and B4 modes presented in this article) [39]

During the first test run, the vehicle operated in the NORMAL mode, which means all energy saving systems were deactivated. Additionally, the regenerative braking assistance was set to minimum (level 1). Automatic braking was minimum and the vehicle was in the sailing mode. In the consecutive test run, the ECO mode was activated with a button located in the central console (Fig. 11). In this mode, the maximum vehicle speed was restricted to 120 km/h and the maximum power output to 80%. In extreme unexpected road situations it is possible to obtain the maximum power by depressing the accelerator pedal to the floor. Additionally to the activation of the ECO system, regenerative braking was set to level B (level 4). In this mode, the vehicle automatically braked with the energy regeneration function using the electric motor as the driver retracts the foot from the accelerator pedal.



Fig. 11. The location of the ECO mode button [39]

Given the fact that the analyzed vehicle was fitted with an electric drive, precise data related to the operation of the powertrain were pulled in real time from the CAN network

through a diagnostic scan tool. Nine parameters were recorded that were used for further analysis. The course of the test route was recorded with a mobile GPS device. The view of the equipment and its arrangement has been shown in Fig. 12.



Fig. 12. Arrangement of the data acquisition equipment during the tests

4. Results and discussions

The driving cycles realized in compliance with the RDC procedures were started at the battery level SOC 100% (software readout). The test runs were performed by a single driver to avoid inconsistency in the driving style. During the test run, the vehicle speed and battery level were recorded. The results have been presented in Fig. 13.

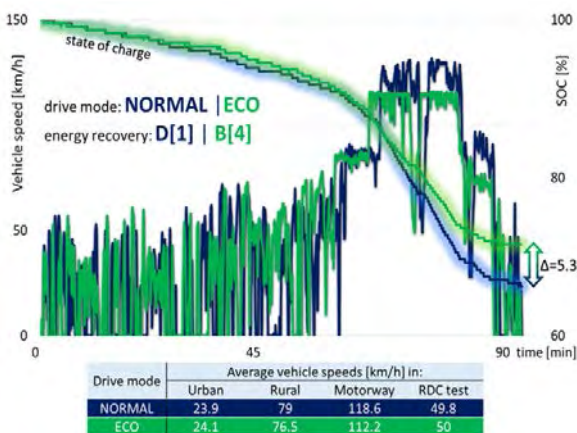


Fig. 13. Comparison of the RDC test for the performed test runs in the NORMAL and ECO modes

The tracing shows the speed profile and current SOC as a function of time. Additionally, in the table, the authors presented the average speeds in the analyzed speed intervals as divided into road portions. The beginning of the test route was the urban cycle where the vehicle speed did not exceed 60 km/h. The next one was the rural area with the speeds of 60–90 km/h and the motorway with the speed in excess of 90 km/h. The SOC decreased in time with the intensity depending on the vehicle speed. During the realization of the first part of the test, no significant difference was recorded between the NORMAL and ECO modes in the urban cycle, which results from the similar average speeds in the urban area. An increase in the average speed in the rural portion resulted in an increase in the energy consumption in the NORMAL mode. The greatest differences were observed when the vehicle operated at the high-

est speed during the test. The difference in the average speeds in this road portion was 6.5 km/h. This results from the speed restriction to 120 km/h in the ECO mode. The change in the driving mode to ECO resulted in a decrease in the battery discharge level by 5.3%. This indicates the significance of the vehicle speed on the energy consumption, particularly at high speeds. This is influenced by the vehicle motion resistance. Despite the differences in the average speeds in the analyzed portions, the final values of the average speeds for the entire tests are similar, which gives grounds for further reliable analysis.

A selective analysis of the test results allowed determining of the share of individual drive phases against distance and time (Fig. 14). A drive phase with a constant speed was distinguished when the vehicle acceleration equaled $a = 0$, change of speed where the acceleration/deceleration assumed values \pm and stoppage where the vehicle speed equaled $V = 0$ km/h. For both powertrain modes, the greatest share had the phase with the constant speed, which is particularly visible when we consider it in relation to the covered distance. The drive in the ECO mode was characterized with a smaller share of acceleration and deceleration and a greater share of driving with a constant speed. The process of energy recovery from braking and acceleration leads to loss generated during the conversion of electrical energy into mechanical one and vice versa. Limiting these phases leads to a reduction of the energy conversion loss, which reduces the energy consumption by the vehicle.

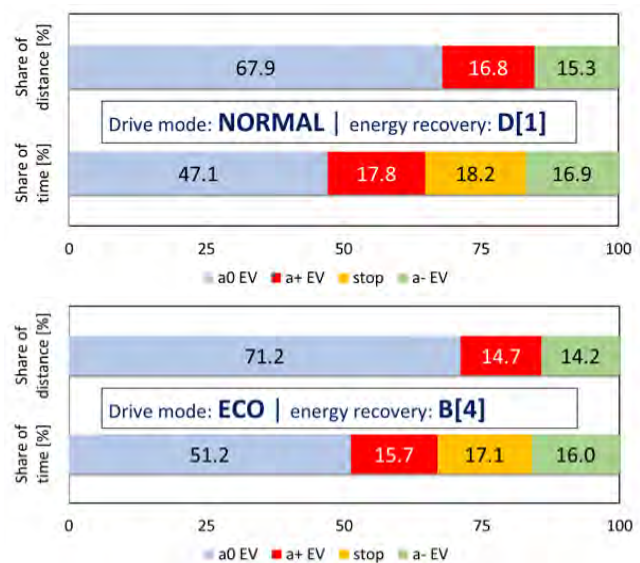


Fig. 14. Comparison of the phase motion share during the RDC test with NORMAL and ECO modes

The share of individual drive phases in time has been presented in detail in Fig. 15. When comparing both test runs, we can see differences in the distribution of the individual phases. This is related to the dynamically changing traffic conditions. In the case of road tests, these types of differences among the test runs are unavoidable and extremely valuable when further analyzed, particularly when developing energy consumption models.

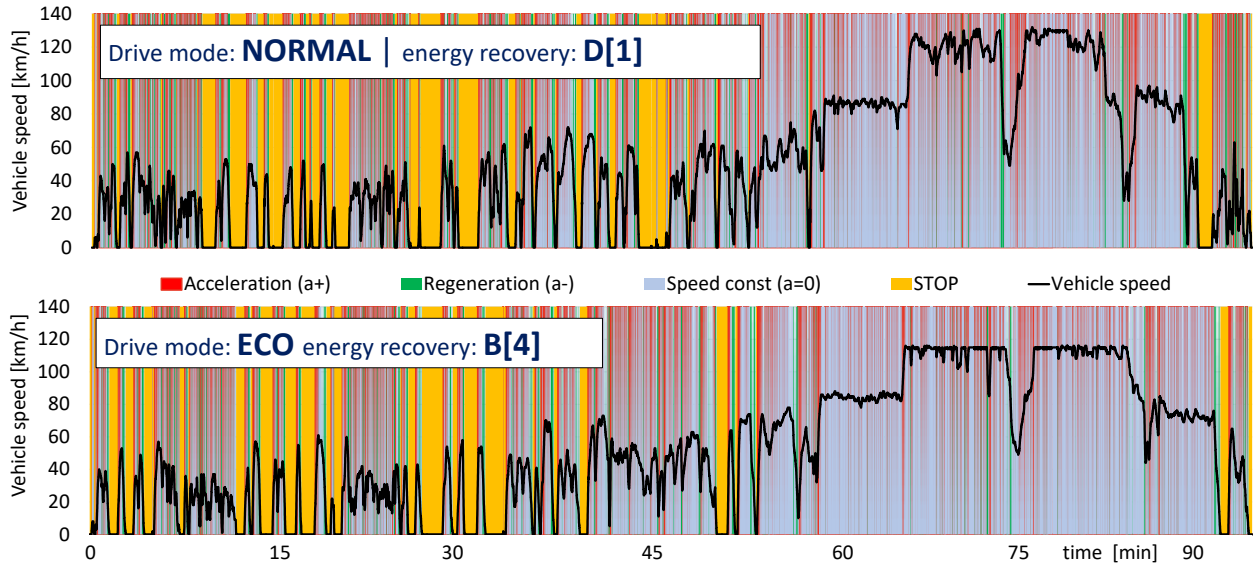


Fig. 15. Distribution of motion phases in terms of NORMAL and ECO driving modes

In EV vehicles, the flow of energy between the source and the electric machine is an extremely important aspect. In this paper, it has been determined based on the voltage and the current flowing to the motor during acceleration and from the electric motor to the battery during regenerative braking.

Figure 16 presents the flows of energy for both realized driving modes. The bar chart pertains to the collective share of a given vehicle speed in the entire test for a given speed interval against distance and time.

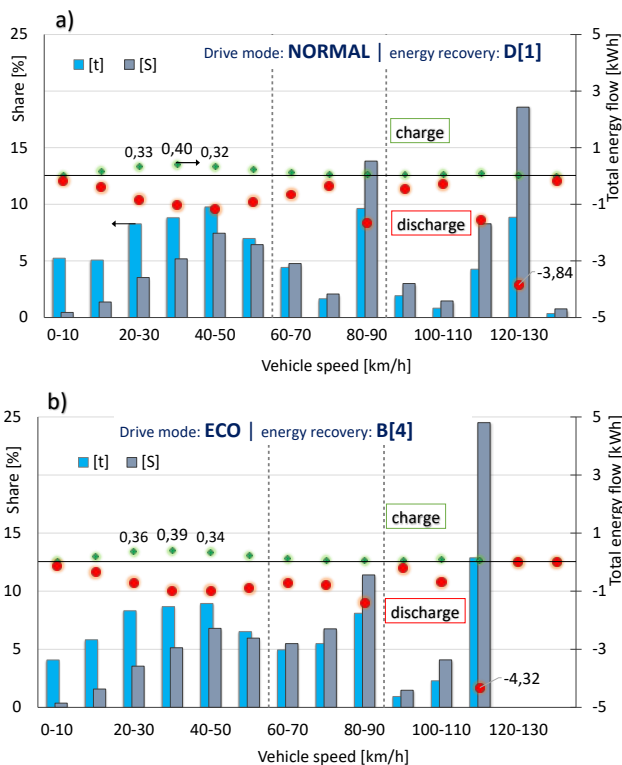


Fig. 16. Energy flow characteristic and the share of energy consumption for different speed intervals in the RDC tests; a) NORMAL D[1]; b) ECO B[4]

The marked points present the total flow of the recovered (green) and consumed (red) energy in a given speed interval. For both test runs (a, b), the same nature of changes of the energy flow was recorded. Small differences were found in values in individual speed intervals. Due to the speed restriction in the ECO mode, the greatest share in the energy consumption was observed for the speed interval of 110–120 km/h. The greatest amount of energy was recovered in the speed interval of 20–40 km/h. The amount of recovered energy in the urban speeds interval allows extending the vehicle range. However, the energy consumption in each speed interval is higher.

In Figure 17 collective values of the energy flow for each speed interval (bar chart) have been compared with the values of instantaneous energy flow (point chart). The sampling frequency of the diagnostic system was approx. 4 Hz, hence the presented results of the instantaneous maximum energy flow pertain to the energy recovery or consumption in the time of 0.25 s. In the NORMAL mode (a), which was the case when the vehicle operated at the speed exceeding 120 km/h, a maximum energy consumption greater by 1.74 kWh was obtained for the 120–130 km/h interval against the maximum total energy consumption obtained in the ECO mode (b) in the 110–120 km/h interval. In the NORMAL mode of the smallest assistance in regenerative braking, the instantaneous values of recovered energy were on a constant level between 40 and 120 km/h. In the case of the ECO mode, the activation of the regenerative braking assistance B(4), in the speed interval 80–0 km/h resulted in a lower maximum value of recovered energy. The difference may have resulted from the irregularity of the regenerative braking process. When the regenerative braking assistance is off, the driver uses the brake in the same way during each braking. If mode B is used, the vehicle mostly brakes automatically when the driver takes the foot off the gas pedal and the brake is used only in emergency situations or when the vehicle is decelerated from high speeds. It is these situations that decide about the reduction of the energy recovered during braking.

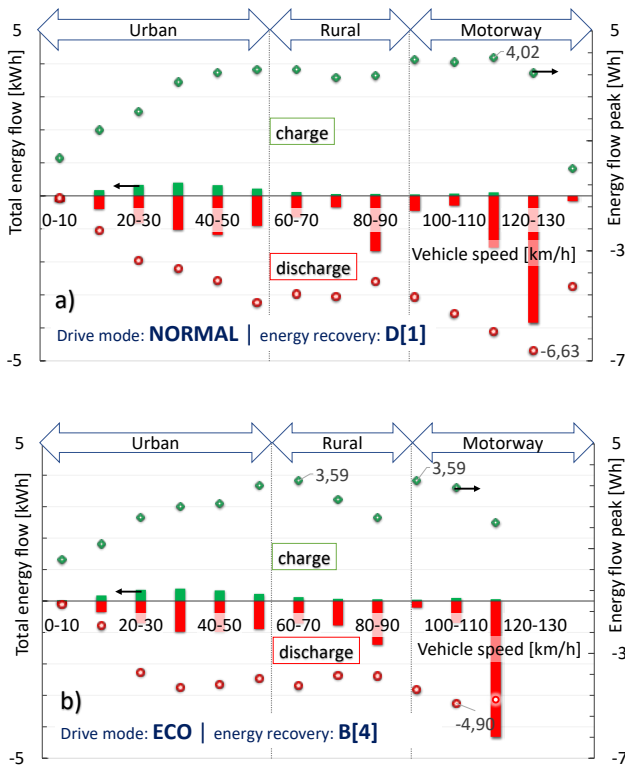


Fig. 17. Total energy flow characteristics and peak values for different speed intervals in the RDC tests; a) NORMAL D[1]; b) ECO B[4]

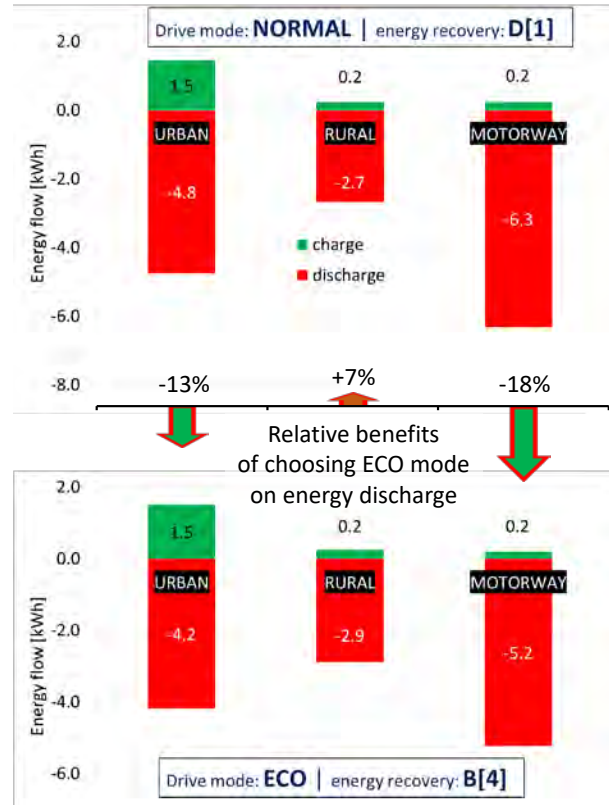


Fig. 18. Energy consumption balance in terms of different road types for Normal and ECO modes

The energy balance allowing for the type of the test road portion has been presented in Fig. 18. Irrespective of the applied driving and braking mode, the same values of recovered energy were obtained during braking in each road portion. The greatest amount of energy was recovered in the urban cycle due to the high number of brakings compared to the road portions where the traffic was smooth. The activation of the ECO mode allowed a reduction of the energy consumption by 13% in the urban cycle and 18% in the expressway cycle. An increased consumption was recorded in the rural cycle. The above, however, may have resulted from the variable traffic conditions in the RDC test. The differences may have been caused by the restricted power output when the vehicle accelerated.

A great advantage of the electric drive is the ability to generate high torque at a relatively low speed of the motor. The last stage of the research presented in the paper was the identification of the torque distribution during the road tests. Figure 19 presents the distribution of the value of torque generated for the engine speed against the experimentally created full load characteristics in a given vehicle driving mode. The chart shows the restrictions applied when activating the ECO mode (torque reduction) and the initial fluctuations attributed to the activation of the restrictions. It is noteworthy that, in the case of the analyzed vehicle, the engine speed was directly proportional to the vehicle speed. The red circles denote the share of individual torque values divided into road portions: urban, rural and motorway and their position indicates average values. This indicates the most frequent use of the torque value from the lower range of available torque values. It was observed that during the tests, the torque did not significantly exceed 150 Nm.

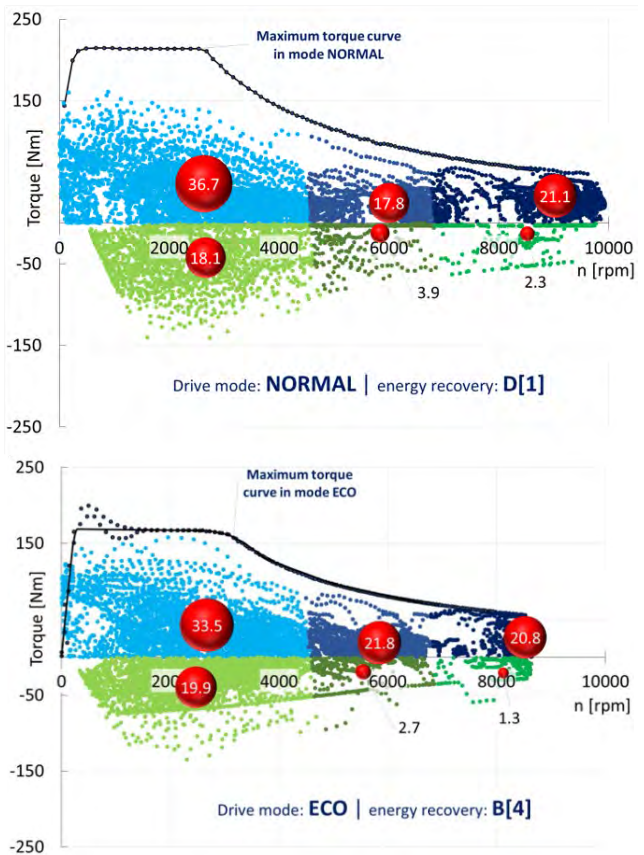


Fig. 19. The obtained torque distribution on the full load characteristic for NORMAL and ECO modes

After activation of the B mode responsible for the regenerative braking assistance, one could clearly see the restrictions of the system operation through a linear alignment of the points in the lower quadrant of the presented chart. The points outside the line indicate independent braking of the driver. When using the B mode, each release of the accelerator pedal activated energy recovery. This was particularly visible at high engine speeds. The obtained values of the braking moment were, however, much lower in the ECO mode than in the NORMAL mode when the driver applied the brake.

Conclusions

This paper presented an analysis of the influence of the energy management and change of the regenerative braking strategy on the energy consumption and behavior of a passenger BEV vehicle. The results were obtained following road tests compliant with the RDC regime. All the test runs complied with these requirements.

During the first test run, the powertrain operated in the NORMAL mode with the active regenerative braking system assistance set to minimum. The second test run was carried out in the ECO mode activated manually by pressing the 'ECO' button. Additionally, the regenerative braking system assistance was set to the B mode. This means that the vehicle braked automatically when the gas pedal was released.

The following conclusions have been drawn:

1. When analyzing the SOC during the test, the greatest differences were observed in the motorway cycle. The ECO mode reduced the drop of the SOC by 5.3%.

2. In the case of the ECO mode, the following were observed: a greater share of constant speed (by 3.3%), acceleration (by 2.1%) and deceleration (by 1.1%) against the distance identical for both tests. These results were separate for each RDC test run and reflected the road congestion.

3. The flow of energy in the electric vehicle was realized in two directions – when accelerating the energy went to the electric motor and during regenerative braking it was recuperated to the battery. For both driving modes, the greatest amount of energy was recovered in the speed interval of 20–40 km/h. Greater values of instantaneous energy recovery were obtained in the NORMAL mode (driver braking). Also, greater instantaneous energy consumption in individual speed intervals in the NORMAL mode was observed.

4. Instantaneous energy consumption for the speeds in the 120–130 km/h interval was 6.63 Wh (in the NORMAL mode) and 4.9 Wh in the 110–120 km/h interval; the reduction of the speed by 10 km/h resulted in a reduction of the instantaneous energy consumption by approx. 30%.

5. The energy balance for the ECO mode indicates a lower energy consumption by 13% and 18% in the urban and expressway portions respectively. No differences in the energy recovery between the test runs were observed.

6. Activating the ECO mode restricts the vehicle power output. When driving, the most frequently applied torque falling in the lower range of the available interval was – 50 N·m (energy regeneration) to 50 N·m (driving) – Fig. 20.

7. Activating mode B did not influence the amount of recovered energy. It only changed the strategy of its regeneration. Despite the activation of mode B, in emergency situations it was necessary to use the main brake.

Summarizing, in the NORMAL mode the vehicles consumed 10.35% more energy than when it operated in the ECO mode. Irrespective of the applied mode, the amount of recovered energy was identical. The influence of regenerative braking rendered the best results in urban driving whether or not the regenerative braking assistance was activated.

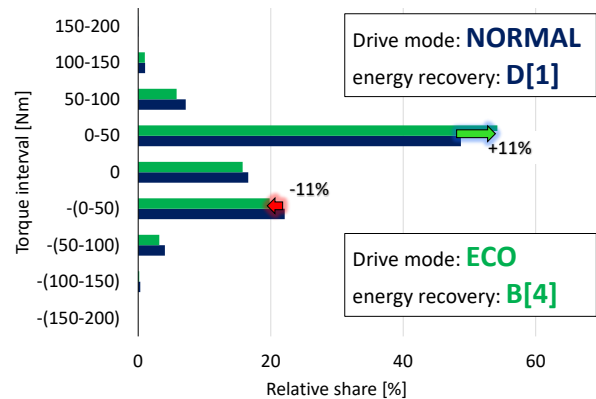


Fig. 20. Relative share of the torque interval during the RDC test for NORMAL and ECO modes

Acknowledgements

This work was supported by the Volkswagen Group Polska Sp. z o.o. and the Subvention of Polish Ministry of Higher Education, project number 0415/SBAD/0297 at Poznan University of Technology.

Nomenclature

| | |
|------|----------------------------|
| BEV | battery electric vehicle |
| CAN | controller area network |
| CE | combustion engine |
| CI | compression ignition |
| CNG | compressed natural gas |
| DI | direct injection |
| EM | electric motor |
| EV | electric vehicle |
| FCEV | fuel cell electric vehicle |
| GHG | greenhouse gas |

| | |
|-----|----------------------------|
| ICE | internal combustion engine |
| IVD | in-vehicle display |
| LCA | life cycle assessment |
| LPG | liquified petroleum gas |
| MPI | multi point injection |
| RDC | real driving conditions |
| RDE | real driving emission |
| SI | spark ignition |
| SOC | state of charge |

Bibliography

- [1] BADIN, F., LE BERR, F., BRIKI, H. et al. Evaluation of EVs energy consumption influencing factors, driving conditions, auxiliaries use, driver's aggressiveness. *2013 World Electric Vehicle Symposium and Exhibition (EVS27)*. Barcelona 2013, 1-12. <https://doi.org/10.1109/EVS.2013.6914723>
- [2] BENVENISTE, G., RALLO, H., CANALS CASALS, L., et al. Comparison of the state of lithium-sulphur and lithium-ion batteries applied to electromobility. *Journal of Environmental Management*. 2018, **226**, 1-12. <https://doi.org/10.1016/j.jenvman.2018.08.008>
- [3] BRACO, E., MARTIN, I.S., BERRUETA, A. et al. Experimental assessment of cycling ageing of lithium-ion second-life batteries from electric vehicles. *Journal of Energy Storage*. 2020, **32**, 101695. <https://doi.org/10.1016/j.est.2020.101695>
- [4] BURCHART-KOROL, D., JURSOVA, S., FOLEGA, P. et al. Life cycle impact assessment of electric vehicle battery charging in European Union countries. *Journal of Cleaner Production*. 2020, **257**, 120476. <https://doi.org/10.1016/j.jclepro.2020.120476>
- [5] CABUKOGLU, E., GEORGES, G., KUNG, L. et al. Battery electric propulsion: an option for heavy-duty vehicles? Results from a Swiss case-study. *Transportation Research Part C: Emerging Technologies*. 2018, **88**, 107-123. <https://doi.org/10.1016/j.trc.2018.01.013>
- [6] CASALS, L.C., GARCÍA, B.A., AGUESSE, F. et al. Second life of electric vehicle batteries: relation between materials degradation and environmental impact. *International Journal of Life Cycle Assessment*. **22**, 82-93, 2017. <https://doi.org/10.1007/s11367-015-0918-3>
- [7] CHANG-HEUM, J., SEUNG-TAEK, M. Efficient recycling of valuable resources from discarded lithium-ion batteries. *Journal of Power Sources*. 2019, **426**, 259-265. <https://doi.org/10.1016/j.jpowsour.2019.04.048>
- [8] CHRISTOPHERSEN, J.P. Battery test manual for electric vehicles. Revision 3. United States: 2015. <https://doi.org/10.2172/1186745>
- [9] CIEŚLIK, W., PIELECHA, I., SZĄLEK, A. Assessment of parameters of the hybrid drive system in vehicles in urban traffic conditions. *Combustion Engines*. 2015, **161**(2), 14-27.
- [10] Commission Regulation (UE) 2019/631 of 17 April 2019.
- [11] Electric Transport Revolution. <https://www.pveurope.eu/News/E-Mobility/Electric-Transport-Revolution-Set-To-Spread-Rapidly-Into-Light-and-Medium-Commercial-Vehicle-Market>
- [12] YAO, E., YANG, Z., SONG, Y. et al. Comparison of electric vehicle's energy consumption factors for different road types. *Discrete Dynamics in Nature and Society*. 2013, **2013**, 1-7. <https://doi.org/10.1155/2013/328757>
- [13] FERNANDEZ, R.A., CARABALLO, S.C., LOPEZ F.C. A probabilistic approach for determining the influence of urban traffic management policies on energy consumption and greenhouse gas emissions from a battery electric vehicle. *Journal of Cleaner Production*. 2019, **236**, 117604. <https://doi.org/10.1016/j.jclepro.2019.117604>
- [14] FLUDER, K., PIELECHA, I., CIEŚLIK, W. The impact of drive mode of a hybrid drive system on the energy flow indicators in the RDE test. *Combustion Engines*. 2018, **175**(4), 18-25. <https://doi.org/10.19206/CE-2018-403>
- [15] FRIEDL, H., FRAIDL, G., KAPUS, P. Highest efficiency and ultra low emission – internal combustion engine 4.0. *Combustion Engines*. 2020, **180**(1), 8-16. <https://doi.org/10.19206/CE-2020-102>
- [16] GAO, Z., LACLAIR, T., OU, S. et al. Evaluation of electric vehicle component performance over eco-driving cycles. *Energy*. 2019, **172**, 823-839. <https://doi.org/10.1016/j.energy.2019.02.017>
- [17] GIS, W., MERKISZ, J. The development status of electric (BEV) and hydrogen (FCEV) passenger cars park in the world and new research possibilities of these cars in real traffic conditions. *Combustion Engines*. 2019, **178**(3), 144-149. <https://doi.org/10.19206/CE-2019-325>
- [18] GIS, W., PIELECHA, J., MERKISZ, J. et al. Determining the route for the purpose light vehicles testing in Real Driving Emissions (RDE) test. *Combustion Engines*. 2019, **178**(3), 61-66. <https://doi.org/10.19206/CE-2019-311>
- [19] GIS, W., WĄSKIEWICZ, J., MENES, M. Experts forecasts on the demand for energy carriers in motor vehicle transport in Poland up to year 2035. *Combustion Engines*. 2019, **178**(3), 162-165. <https://doi.org/10.19206/CE-2019-328>
- [20] HE, L., YE, W., HE, Z. et al. A combining sliding mode control approach for electric motor anti-lock braking system of battery electric vehicle. *Control Engineering Practice*. 2020, **102**, 104520. <https://doi.org/10.1016/j.conengprac.2020.104520>
- [21] HELD, M., SCHUCKING, M. Utilization effects on battery electric vehicle life-cycle assessment: a case-driven analysis of two commercial mobility applications. *Transportation Research Part D: Transport and Environment*. 2019, **75**, 87-105. <https://doi.org/10.1016/j.trd.2019.08.005>
- [22] How to use Real Driving Emission cycles in Simcenter Amesim? <https://community.sw.siemens.com/s/article/how-to-use-real-driving-emission-cycles-in-simcenter-amesim>
- [23] <https://netcarshow.com/volkswagen/2014-e-up/>
- [24] <https://elektrowoz.pl/auta/skoda-citigoe-iv-elektryczna-skoda-na-bazie-vw-e-up-już-oficjalnie/>
- [25] <https://leasing.com/car-leasing-news/driven-skoda-fabia-se-1-0-75/>
- [26] <https://www.statista.com/statistics/1081332/poland-number-of-registered-electric-passenger-cars/>
- [27] IEA, Global EV Outlook 2020, IEA, Paris <https://www.iea.org/reports/global-ev-outlook-2020>
- [28] JEONGYONG, K., INHO, S., WOONGCHUL, C. An electric bus with a battery exchange system. *Energies*. 2015, **8**, 6806-6819. <https://doi.org/10.3390/en8076806>
- [29] KALT, S., BRENNER, L., LIENKAMP, M. Requirements for electric machine design based on operating points from real driving data in cities. *World Electric Vehicle Journal*. 2019, **10**, 60. <https://doi.org/10.3390/wevj10040060>
- [30] LI, L., LIU, Q. Study on the influence of acceleration curve on electric vehicle energy consumption and battery life. *IOP Conference Series: Earth and Environmental Science*. 2020, **512**, 012106. <https://doi.org/10.1088/1755-1315/512/1/012106>
- [31] LUK, J., KIM, H., DE KLEINE, R. et al. Impact of powertrain type on potential life cycle greenhouse gas emission reductions from a real world lightweight glider. *SAE Technical Paper 2017-01-1274*, 2017. <https://doi.org/10.4271/2017-01-1274>
- [32] MCKERRACHER, C., IZADI-NAJAFABADI, A., O'DONOVAN, A. et al. Electric vehicle outlook 2020. <https://about.bnef.com/electric-vehicle-outlook/>
- [33] MERKISZ, J., PIELECHA, J. Selected remarks about RDE test. *Combustion Engines*. 2016, **166**(3), 54-61. <https://doi.org/10.19206/CE-2016-340>
- [34] NAUMANEN, M., UUSITALO, T., HUTTUNEN-SAARI-VIRTA, E. et al. Development strategies for heavy duty electric battery vehicles: comparison between China, EU,

- Japan and USA. *Resources, Conservation & Recycling*. 2019, **151**, 104413.
<https://doi.org/10.1016/j.resconrec.2019.104413>
- [35] PIELECHA, I., CIEŚLIK, W., FLUDER, K. Analysis of energy management strategies for hybrid electric vehicles in urban driving conditions. *Combustion Engines*. 2018, **173**(2), 14-18. <https://doi.org/10.19206/CE-2018-203>
- [36] RALLO, H., BENVENISTE, G., GESTOSO, I. et al. Economic analysis of the disassembling activities to the reuse of electric vehicles Li-Ion batteries. *Resources, Conservation and Recycling*. 2020, **159**, 104785.
<https://doi.org/10.1016/j.resconrec.2020.104785>
- [37] SKEETE, J., WELLS, P., DONG, X. et al. Beyond the EVent horizon: battery waste, recycling, and sustainability in the United Kingdom electric vehicle transition. *Energy Research & Social Science*. 2020, **69**, 101581.
<https://doi.org/10.1016/j.erss.2020.101581>
- [38] SUN, Z., WEN, Z., XIN, Z. et al. Real-world driving cycles adaptability of electric vehicles. *World Electric Vehicle Journal*. 2020, **11**(1), 1-22.
<https://doi.org/10.3390/WEVJ11010019>
- [39] Training data from Volkswagen group Poland company.
- [40] WANG, G., MAKIN, K., HARMANDAYAN, A. et al. Eco-driving behaviors of electric vehicle users: a survey study. *Transportation Research Part D: Transport and Environment*. 2020, **78**, 102188.
<https://doi.org/10.1016/j.trd.2019.11.017>
- [41] WANG, J., BESSELINK, I., NIJMEIJER, H. Battery electric vehicle energy consumption prediction for a trip based on route information. *Proceedings of the Institution of Mechanical Engineers, Part D: Journal of Automobile Engineering*. 2018, **232**(11), 1528-1542.
<https://doi.org/10.1177/0954407017729938>
- [42] ZHAO, Y., YUAN, Z., JIANG, L. Regeneration and reutilization of cathode materials from spent lithium-ion batteries. *Chemical Engineering Journal*. 2020, **383**, 123089.
<https://doi.org/10.1016/j.cej.2019.123089>

Wojciech Cieślak, DEng. – Faculty of Civil and Transport Engineering, Poznan University of Technology.
e-mail: wojciech.cieslik@put.poznan.pl



Filip Szwejca, MEng. – Faculty of Civil and Transport Engineering, Poznan University of Technology.
e-mail: filip.szwejca@put.poznan.pl



Jacek Golimowski – Škoda Service Department, Volkswagen Group Polska Sp. z o.o., Poland.
e-mail: jacek.golimowski@skoda-auto.pl





Poznan University of Technology



Institute of Combustion Engines and Powertrains

POLAND, 60-965 Poznan, Piotrowo 3 street, tel. 48 61 6652207, fax. 48 61 6652204



Optical research of engine processes

Rapid Compression Machine

Constant Volume Chamber

LaVision HighSpeedStar 5

Continuum YAG solid-state laser



Hybrid, Electric and Fuel Cells vehicles

Full-hybrid powertrain test bench, energy flow research

RDC/RDE hybrid and electric powertrain research



Engine and driveline load systems

Engine test bed for testing under dynamic conditions

AVL DynoRoad 120 kW



Simulation platforms

Passanger car simulator

AS1200-6 (AutoSim AS)

Flight simulator

MotionCor5 (CKAS Mechatronics Pty Ltd)



Research on RDE (PEMS)

Gaseous exhaust emissions (CO, HC, NO_x)

Semtech DS, Ecostar (Sensors), M.O.V.E. (AVL)

Particle mass (PM) & number (PN) emissions

Micro Soot Sensor, Particle Counter (AVL),

Ecostar PM, Ecostar PN (Sensors), EEPS (TSI)

www.cel.put.poznan.pl



HYBRID

SAMOŁADUJĄCY
ELEKTRYCZNY
NAPĘD
HYBRYDOWY

NADJEŹDŹA HYBRYDOWA REWOLUCJA



Toyota **Business**
Plus

Seria silników **D-LINE Diesel** z systemem COMMON-RAIL



**Ewolucyjna
gama silników
VETUS serii D-Line
o mocy od 122 KM
do 210 KM**

www.vetus.com

VETUS Sp. z o.o. ul. Płochocińska 111, 03-044 Warszawa, Tel. 22-452 40 52, E: info@vetus.pl



Badania homologacyjne pojazdów (motocykle, samochody lekkie, samochody ciężkie) i ich silników ze względu na emisję zanieczyszczeń i moc zgodnie z regulaminami ONZ i rozporządzeniami UE.

Type-approval testing of vehicles (motorcycles, light and heavy duty vehicles) and their engines with regard to emissions and power in accordance with UN and EU regulations.

Pomiar emisji zanieczyszczeń z układów wylotowych pojazdów w rzeczywistych warunkach ruchu drogowego (RDE).

Measurement of pollutant emissions from vehicle exhaust systems in real road conditions (RDE).



Badania emisji węglowodorów z pojazdu (komora shed).

Vehicle hydrocarbon emissions tests (shed chamber).

Pomiar zużycia paliw pojazdów zasilanych różnymi rodzajami paliw (w tym testy SORT).

Measurement of fuel consumption of vehicles powered by various types of fuel (including SORT tests).



Pomiar zużycia energii i zasięgu pojazdów o napędzie elektrycznym.

Measurement of energy consumption and range of electric vehicles.

Badania stanowiskowe pojazdów oraz silników, ukierunkowane zwłaszcza na pomiar emisji zanieczyszczeń spalin.

Bench tests of vehicles and engines focused in particular on the measurement of exhaust emissions.



Badania (homologacyjne) układów zasilania pojazdów paliwem gazowym (LPG, CNG itp.).

Testing and type-approval testing of vehicle gaseous fuel systems (LPG, CNG, etc.).

Badania pojazdów w niskich temperaturach (w komorze klimatycznej).

Testing of the vehicles at low temperatures (in a climatic chamber).



Badania układów oczyszczania spalin (reaktory katalityczne, filtry cząstek stałych) przeznaczonych na rynek części zamiennych.

Tests of exhaust gas aftertreatment systems (catalytic converters, particulate filters) intended for the spare parts market.



Publisher:

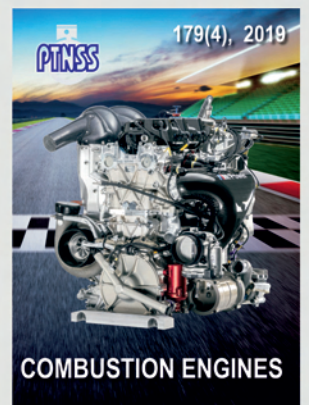
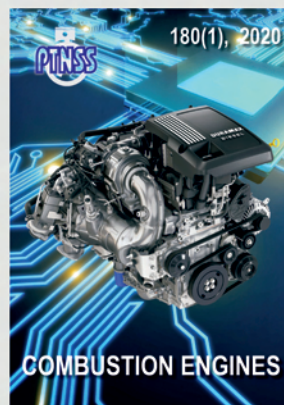
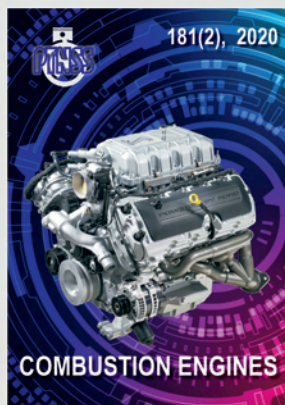
**Polish
Scientific
Society
of Combustion
Engines**



**ISSN: 2300-9896
eISSN: 2658-1442**

Combustion Engines

Polskie Towarzystwo Naukowe Silników Spalinowych



www.combustion-engines.eu